(2)

AFOSR-TR- 88-1180

BOEING

"Original contains color plates: All DTIC reproductions will be in black and white"

UNCLASSIFIED
SECURITY CLASSIFICATION OF THIS PAGE

ADA201176

REPORT DOCUMENTATION PAGE

Form Approved
OMB No. 0704-0188

1a. REPORT SECURITY CLASSIFICATION: Unclassified	1b. RESTRICTIVE MARKINGS: ~~N/A~~
2a. SECURITY CLASSIFICATION AUTHORITY: N/A	3. DISTRIBUTION/AVAILABILITY OF REPORT: ~~NONE~~ Approved for public release, distribution unlimited
2b. DECLASSIFICATION/DOWNGRADING SCHEDULE: N/A	
4. PERFORMING ORGANIZATION REPORT NUMBER(S): None	5. MONITORING ORGANIZATION REPORT NUMBER(S): AFOSR-TR- 88-1180
6a. NAME OF PERFORMING ORGANIZATION: Boeing Advanced Systems; 6b. OFFICE SYMBOL (If applicable): N/A	7a. NAME OF MONITORING ORGANIZATION: AFOSR/ Bolling AFB, DC 20332
6c. ADDRESS (City, State, and ZIP Code): P.O. Box 3703, Mail Stop 33-14 Seattle, WA 98124	7b. ADDRESS (City, State, and ZIP Code): AFOSR/ NC 410 Bolling AFB, DC 20332
8a. NAME OF FUNDING/SPONSORING ORGANIZATION: Air Force Office of Scientific Research; 8b. OFFICE SYMBOL (If applicable): ~~PKC~~ NA	9. PROCUREMENT INSTRUMENT IDENTIFICATION NUMBER: F49620-85-C-0126
8c. ADDRESS (City, State, and ZIP Code): Building 410 Bolling AFB, DC 20332	10. SOURCE OF FUNDING NUMBERS: PROGRAM ELEMENT NO. 6110?F; PROJECT NO. 2307; TASK NO A1; WORK UNIT ACCESSION NO.

11. TITLE (Include Security Classification)
Error Norm Guided Flow Analysis of Shock-Wave/Boundary-Layer Interactions

12. PERSONAL AUTHOR(S)
Mayer, David W, Forester, Clifford K, Paynter, Gerald C, and Baltar, James Y.

13a. TYPE OF REPORT	13b. TIME COVERED	14. DATE OF REPORT (Year, Month, Day)	15. PAGE COUNT
Final	FROM 1985, 8, 1 TO 1988, 7, 31	1988, 9, 30	102

16. SUPPLEMENTARY NOTATION

17. COSATI CODES			18. SUBJECT TERMS (Continue on reverse if necessary and identify by block number)
FIELD	GROUP	SUB-GROUP	Computational Fluid Dynamics, CFD, Navier-Stokes, grid generation, artificial viscosity, numerical viscosity, MacCormack, Beam-Warming, Burgers equation, accuracy.
01	01		
21	05		

19. ABSTRACT (Continue on reverse if necessary and identify by block number)

Conventional means of assessing the accuracy of Navier-Stokes analyses are difficult to implement and may not be reliable. A new approach to error assessment is being explored to address these problems. This approach uses direct measures of solution error, both as accuracy monitors and as guides to grid adjustment. The artificial diffusion ratio (ADR) is a promising error monitor. As an example, ADR was used to guide the Navier-Stokes analysis of a supersonic external compression inlet with bleed flow. ADR was useful for guiding grid selection and seemed to provide a measure of solution accuracy as well.

The algorithm dependence of ADR and the relationship between ADR and solution accuracy were explored in a follow-on study. This study investigated the algorithm and accuracy questions in two steps. First, modified equations were developed for the MacCormack explicit and Beam-Warming implicit algorithms for Burgers equation. Second, finite difference solutions were obtained (for a range of grid densities) and solution accuracy was established through comparisons with analytic solutions. This study established that ADR was useful (Continued)

20. DISTRIBUTION/AVAILABILITY OF ABSTRACT: ☒ UNCLASSIFIED/UNLIMITED ☐ SAME AS RPT. ☐ DTIC USERS	21. ABSTRACT SECURITY CLASSIFICATION: UNCLASSIFIED
22a. NAME OF RESPONSIBLE INDIVIDUAL: Dr. ~~James McMichael~~ Leonidas Sakell	22b. TELEPHONE (Include Area Code): (202) 767-4987; 22c. OFFICE SYMBOL: ~~PKC~~ NA

DD Form 1473, JUN 86 — Previous editions are obsolete. — SECURITY CLASSIFICATION OF THIS PAGE: UNCLASSIFIED

19. Abstract (continued)

as a guide for grid adjustment, that only a qualitative relationship exists between ADR and solution accuracy, and that this relationship is algorithm dependent.

The use of ADR error monitors for general purpose applications requires additional development. Further studies are recommended to improve the understanding of the relationship between solution accuracy and artificial dissipation. Work is also recommended to develop the technique through additional model equation studies and analysis comparisons with benchmark experiments.

2

ERROR NORM GUIDED FLOW ANALYSIS OF SHOCK-WAVE/BOUNDARY-LAYER INTERACTIONS

(Contract No. F49620-85-C-0126)

Final Report
for period
1 August 1985 through 31 July 1988

Prepared for

Air Force Office of Scientific Research
Building 410, Room A223
Bolling Air Force Base
Washington, D.C. 20332

Prepared by

Program Manager: Gerald C. Paynter

Principal Investigator: Clifford K. Forester

Co-Investigators:
David W. Mayer
James Y. Baltar

"Original contains color plates: All DTIC reproductions will be in black and white."

Boeing Advanced Systems
Propulsion Technology Staff
PO Box 3703, Mail Stop 33-14
Seattle, Wa 98124
(206) 241-4403

TABLE OF CONTENTS

"Original contains color plates: All DTIC reproductions will be in black and white"

LIST OF SYMBOLS

a	speed of sound
ADR	artificial diffusion ratio
b	a free parameter
c	a free parameter
CFL	Courant, Friedrich, Lewy number
E	$F - \mu \frac{\partial u}{\partial x}$
F	$cu + \frac{bu^2}{2}$
P	pressure
S	artificial dissipation flux
t	time coordinate
u	x direction velocity
x	x direction coordinate
Δ	step size
ε	a constant or nonphysical source term due to truncation, convergence and roundoff errors
μ	fluid viscosity

Superscripts

n	time plane index
*	intermediate value (results from the predictor step)

Subscripts

a	artificial diffusion coefficient
F	u momentum ADR
G	v momentum ADR
H	energy ADR
i	x direction grid index
R	mass density ADR
t	total or stagnation condition
∞	freestream condition

LIST OF FIGURES

1. INTRODUCTION

This report has been organized into six main sections. Section 1 introduces and discusses the purpose of this report, the research objectives, and pertinent background material. Sections 2 through 4, discuss the sources of computational flow analysis error, suggest a procedure (developed during the course of this investigation) for monitoring and locating these errors, and demonstrate the error monitor procedure for a configuration of engineering interest.

The contract investigation raised several issues regarding the usage and generality of the error monitor. These issues were addressed in a research effort conducted using Boeing Advanced Systems (BAS) Independent Research and Development (IRAD) funds. The results of these research studies are summarized in Section 5 and are included in their entirety in the Appendices.

The last section, Section 6, summarizes the status of the research. Significant accomplishments, conclusions, and recommendations are enumerated in this section.

The reader with limited time may wish to review the Introduction and Research Status sections first (Sections 1 and 6). Sections 2 through 5 provide a more detailed discussion. The Appendices contain the detailed technical information useful as a starting point for further investigations of the error monitors and procedures discussed in the body of this report.

1.1 Purpose of Final Report

This report summarizes the results of work performed under the contract titled "Error Norm Guided Flow Analysis of Shock-Wave/Boundary-Layer Interactions" contract number F49620-85-C-0126 and a related follow-on IRAD study. Previous reports by Forester (1986, 2/87, and 8/87) have documented preliminary results and progress of the contract effort. Pertinent information from these documents is also summarized in this, the final contract report. The purpose of the contract was to develop a grid selection and smoothing level guide for accurately applying Navier-Stokes (NS) analysis to flow fields of engineering interest. The guide indicates grid resolution problems and is computed from data readily available in NS solutions. The grid guide was formatted for graphical output. An inlet design with a shock control aperture was chosen to demonstrate the concept.

The contract results were encouraging, but raised several questions on the usage and generality of the grid selection guide. These questions included the usefulness of the guide for algorithms other than the MacCormack explicit (used for the contract study), the relationship between the guide and solution

accuracy, and the usefulness of the guide for a wide range of grid levels. A follow-on IRAD study was conducted to address these questions. In the follow-on study, additional grid refinement work was performed, the generality of the error monitor and extensions to other algorithms were investigated, and the relationship between the error monitor magnitude and truncation error levels was studied.

1.2 Research Objectives

The overall contract objective was to explore grid adjustment guides for improving the accuracy of flow field analyses. To accomplish this the following specific objectives were identified:

- o Develop and evaluate error norms as guides to grid selection and smoothing level.
- o Define and implement these error norms in a two-dimensional (2D) NS code.
- o Demonstrate and evaluate error norm usage with a NS analysis of a 2D inlet.

This work was accomplished using MacCormack's explicit predictor-corrector method with explicitly added numerical smoothing.

1.3 Background

Computational fluid dynamic (CFD) tools are needed to provide flow field properties for the design of aircraft components. For three-dimensional analyses, Paynter and Chen, and Anderson have made considerable progress. Three dimensional CFD analyses are currently used in the selection and design of test configurations and full-scale configurations. Analysis also enhances the degree of integration of the propulsion system with flight controls, aircraft aerodynamics, and structural requirements. The proper integration of these elements is the key to high performance aircraft design.

When CFD is used to provide flow properties for a flow domain of interest, algebraic approximations to the NS equations (or a subset) are solved for the values of the dependent variables at each point on a grid of points distributed through the domain. Available computer speed and storage limit the number of points at which the algebraic approximations to the NS equations (Finite difference equations or FDEs) can be solved (for a given analysis domain). Details of the flow in the domain are unknown prior to obtaining a solution, and local regions with high gradients in flow properties (such as shocks or shear layers) can occur and be of critical importance to the performance of an aircraft component. A coarse grid in a region of high local flow gradient

can inadequately resolve these gradients and result in a high local solution error, manifested as an oscillation in flow properties near the high gradient region (dispersive error). Dispersive error can be controlled to some degree at least through the use of artificial dissipation (smoothing) in regions of high flow gradient and coarse mesh. The selection of a grid point distribution and smoothing levels to achieve a desired level of solution accuracy are recognized as major problems in the use of CFD for aircraft design support.

Flow field solution accuracy is a strong function of grid density, grid placement and smoothing levels. Methods are needed for controlling solution errors due to grid and for selecting numerical smoothing levels. In general, simple and reliable grid and smoothing criteria are unavailable although criteria have been developed for specific algorithms and flow conditions. The present effort explores criteria that may be more generally useful for guiding grid adjustment and setting smoothing levels.

Work completed during an earlier contract (titled "Error Norm Guided Flow Analysis", contract number F49620-84C-0037) was summarized in a symposium paper and presentation (Forester and Strom, 1985). These results dramatically illustrated the sensitivity of solution results to grid placement and density. Solutions were obtained for supersonic flow over an axisymmetric conical afterbody with a blunt base containing a centered propulsive jet. Comparisons were made between computed and experimental results for base pressure, separation length, afterbody pressure distribution, and flow field structure. The numerical solutions were found to be sensitive to the computational grid structure and the turbulence model. Error norms were applied to aid the detection of inappropriate grid choices. The best results were obtained with adaptive grids that tracked both shear layers (i.e., due to the internal and the external flow) and a turbulence model based on the local flow features. The results of this work suggested that artificial dissipation as defined for the MacCormack explicit algorithm could be used as a guide to grid placement.

A variety of error norms were explored during the early phases of this contract (Forester, 1986, 2/87, and 8/87). This early work identified ADR (discussed in this report) as a viable error monitor.

2. ERROR SOURCES AND SMOOTHING

When a computational fluid dynamic (CFD) analysis is performed the objective is to solve a set of partial differential equations (PDE) such that

$$PDE = 0 \qquad (1)$$

Since most PDEs are too complex to be solved exactly it is necessary to solve an approximation to the PDE. A common approach is to solve a set of finite difference equations (FDE) such that

$$FDE = 0 \tag{2}$$

but

$$PDE = FDE + \varepsilon \tag{3}$$

Where ε represents nonphysical source terms due to truncation, residual and roundoff errors. This implies that the equations actually being solved are

$$PDE = \varepsilon \tag{4}$$

Comparing Equation 1 with Equation 4 it is apparent that the resulting solution (obtained by solving FDE = 0) contains errors that are grid, convergence and machine dependent.

The flow field equations and their boundary conditions are precise, exact and continuous. The process of numerically simulating these equations is not precise, exact or continuous. Numerical solutions of these field equations involve solving equations which have additional properties that are not contained by or related to the continuous equations. These additional properties are characteristic of the algebraic structure (i.e., FDEs) used to model the continuous equations.

These additional spurious properties have been catagorized as dispersive and dissipative behavior in the solutions. Examples of spurious behavior are nonphysical mass sources and sinks; negative density or temperature; and the decay of entropy or increases in available total pressure. Dispersive errors result in nonphysical oscillations or ringing in the solution to the system of equations. Dissipative behavior is manifested by poor acuity of steep gradients or by damped peak amplitudes of dependent variables or their derived quantities. The combined effect of dispersive and dissipative errors is often called diffusion error. All numerical algorithms whether finite difference, finite volume or finite element, have a truncation error and thus an intrinsic diffusion unique to a particular algorithm. In addition, artificial dissipation is often explicitly added to an algorithm either to achieve solution stability or to minimize undesirable dispersive errors near regions of high gradients in flow properties. The combined effect of the intrinsic diffusion and the explicitly added artificial dissipation is referred to, in this report, as artificial diffusion.

If the numerical solution is dispersive near a high gradient region of the flow the effect of increasing the viscosity is to reduce or eliminate (i.e., smooth) the local oscillations in the solution. Conversely, reducing the viscosity accentuates the oscillations. The dispersive numerical error is counteracted by

the viscous dissipation (i.e., has an opposite effect on the flow solution). Since the source term on the right hand side of Equation 4 typically varies (both in magnitude and sign) from point-to-point throughout the solution domain, judicious addition of numerical viscosity (or dissipation) in the vicinity of the high gradient region will reduce or eliminate the dispersive error. In effect the source term implied by Equation 4 is locally reduced or eliminated.

There is a difference in the magnitude of smoothing requirements between linear and nonlinear regions of the flow analysis domain. For example, regions of the flow featuring shocks (nonlinear) require enormous smoothing levels. Since shock-like discontinuities abound in large numbers during the early stages of the convergence process, high levels of smoothing are required in most of the flow analysis domain.

As the converged solution is approached, the smoothing levels must be low except in shock regions and poorly resolved flow regions that behave like discontinuities. These regions require locally higher smoothing to avoid unacceptable dispersive errors. Locally higher smoothing can however be an unacceptable dissipative error. Complexity is inherent in the widely varying demands for smoothing during the convergence process.

Artificial diffusion can smooth, stabilize and enhance the convergence characteristics of NS solution algorithms such as the MacCormack predictor-corrector scheme. This is done by constructing a smoothing flux that is added explicitly to the raw flux in the predictor-corrector cycles. The impact on the solution accuracy of this smoothing operator, relative to grid and residual effects, has not been well defined for the NS equations. Model equation studies from the follow-on investigation suggest that improvements in solution accuracy can be obtained with this type of smoother.

The present study was aimed at investigating a variety of error monitors including artificial dissipation to direct the analysis process for achieving "good" grids -- those grids giving solutions suitable for engineering application. Care was taken to insure that the solutions were well converged and that roundoff error was negligible. Therefore, the solution errors discussed in this report are dominated by the truncation (i.e, grid dependent) errors. The contract and follow-on studies were focused on truncation error and smoothing effects (relative to the truncation error).

3. ERROR MONITORS

During the contract new approaches to streamline and simplify the process of selecting an analysis grid were explored. Measures of solution error were investigated, including total pressure error and the artificial diffusion ratio defined in the

following paragraphs. Cross-correlation of these, plus other error measures such as local and global conservation error, have been examined to single out the best guides for selecting grid and smoothing levels.

Many methods have been used to select the local level of artificial dissipation or smoothing used to minimize dispersive errors in a flow solution. These methods range in complexity from a global increase in the bulk viscosity to flux corrected transport (Oran and Boris, 1987). The MacCormack (1975) smoother (described in section 3.1 below) senses two grid interval solution oscillations (usually a dispersive error effect). The artificial dissipation level is set at a "high" value if a dispersive error effect is present. Because the MacCormack smoother is designed to sense dispersive error, it can also be used as a guide to grid adjustment.

Artificial smoothing (MacCormack method) and its effect on the solution accuracy were examined in this study. Truncation error is usually the dominant error source. The artificial diffusion is monitored and utilized to select grid densities that ensure accuracy of the analysis process. It is shown that the artificial diffusion is large on inadequate or coarse grid solutions where flow gradients are large. This information is used to adjust grid density until the artificial diffusion is minimized and an accurate solution is obtained.

A measure of the artificial diffusion is the ratio of the explicit smoothing flux (computed with a MacCormack smoother) to the total flux through computational cell faces. This ratio is called the artificial diffusion ratio (ADR). By definition, this ratio should be insignificant everywhere in the flow analysis domain except in high gradient regions where the mesh is too coarse. For example, shock waves and shear layers must have low levels of artificial smoothing or small values of ADR relative to the peak values of ADR. Coarse grid simulations lead to the treatment of each of these continuous regions as singularities.

An ADR can be generated for each dependent variable of the compressible time-averaged Navier-Stokes equations. The dependent variables (in 2D) are two components of momentum, total energy and mass density. These dependent variables result in four artificial diffusion ratios -- ADR_F, ADR_G, ADR_H and ADR_R, respectively. A composite of these individual error monitors may be constructed by averaging the individual error monitors. All error measures are normalized to achieve peak values not exceeding unity.

The error measures that have been explored for the contract are defined in the next section. Finite difference expressions are used for this purpose.

3.1 Mathematical Definition

The concept of error analysis for numerical approximations of the NS equations can be illustrated using a model equation called the Burgers equation. The generalized Burgers equation may be written in a form consistent with the usual representation of the NS equations as follows:

$$\frac{\partial U}{\partial t} + \frac{\partial E}{\partial x} = 0 \tag{5}$$

where

$$U = u, \quad E = F - \mu \frac{\partial u}{\partial x}, \quad F = cu + \frac{bu^2}{2} \tag{6}$$

u is the velocity, μ is the fluid viscosity, and c and b are free parameters. Note that if b = 0, the linearized Burgers equation results and if c = 0 and b = 1, the nonlinear Burgers equation is obtained. If μ = 0 the equation is inviscid and if b = 0 and μ = 0 the familiar wave equation is recovered.

The finite-difference expression for MacCormack's explicit predictor-corrector method with a "product" smoother is given by (Anderson et al., 1984).

$$U_i^* = U_i^n - \frac{\Delta t}{\Delta x}\left[(E_{i+1}^n - E_i^n) - (S_{i+1}^n - S_i^n)\right] \tag{7}$$

$$U_i^{n+1} = \frac{1}{2}\left\{U_i^n + U_i^* - \frac{\Delta t}{\Delta x}\left[(E_i^* - E_{i-1}^*) - (S_i^* - S_{i-1}^*)\right]\right\} \tag{8}$$

where S represents the artificial dissipation flux at a point. For the NS equations S is defined as

$$S_i^n = \varepsilon\,(|u_i^n| + a_i^n)\,\frac{|P_{i+1}^n - 2P_i^n + P_{i-1}^n|}{(P_{i+1}^n + 2P_i^n + P_{i-1}^n)}\,(U_i^n - U_{i-1}^n) \tag{9}$$

$$S_i^* = \varepsilon\,(|u_i^*| + a_i^*)\,\frac{|P_{i+1}^* - 2P_i^* + P_{i-1}^*|}{(P_{i+1}^* + 2P_i^* + P_{i-1}^*)}\,(U_{i+1}^* - U_i^*) \tag{10}$$

and $0 \leq \varepsilon \leq 0.5$

Note that when solving Burgers equation, the pressure, P, is not a dependent variable and the speed of sound, a, is not a solution parameter. Therefore, for Burgers equation, velocity is used in place of pressure and the wave speed, c, is used in place of "a" in the definition of the artificial dissipation flux.

An additive artificial viscosity is thus defined as

$$\mu_{a,i} = \varepsilon\ (\Delta x)\ r\ |u_{i+1} - 2u_i + u_{i-1}| \tag{11}$$

where $$r = \frac{(|u_i| + c)}{(u_{i+1} + 2u_i + u_{i-1})} \tag{12}$$

The Δx is included in the definition of the artificial viscosity so that $S = \mu_a\ \partial u/\partial x$ and is comparable to the viscous term $\mu\ \partial u/\partial x$ contained in E. Also note that the sign on the smoothing terms in Equations 7 and 8 have been selected so that they have the same sign as the viscous term in E. This smoother is triggered by oscillations in a numerical solution (a third order or dispersive effect). A monatonic variation of u over the i-1 to i+1 grid interval results in a low value of $\mu_{a,i}$. A two grid interval oscillation in u results in a high value of $\mu_{a,i}$. With an appropriate setting for ε the dissipation added by the smoother will damp the third order dispersion error.

The artificial diffusion ratio, ADR, is defined as follows:

$$ADR = \frac{|(S^n_{i+1} - S^n_i)|}{|(E^n_{i+1} - E^n_i)| + |(S^n_{i+1} - S^n_i)|} \tag{13}$$

Note that the magnitude of the added artificial smoothing term is compared with the $\partial E/\partial x$ term such that ADR must range between 0 and 1. This definition is for the predictor step. A similar definition may be expressed for the corrector step, but studies have shown that both definitions have essentially the same characteristics. ADR based on the predictor step was used for the present effort.

The ADR may be defined similarly for the continuity equation, the two components of the momentum equation, and for the energy equation. These quantities are called ADR_R, ADR_F, ADR_G, and ADR_E, respectively.

3.2 Minimizing Errors

The equations of the previous section constitute a system of unknowns whose range is determined by the number and distribution of grid points. The number of grid points is chosen rather arbitrarily until data is available on the truncation error. Once this data exists, a systematic procedure for minimizing the error using grid refinement may be followed. It is usually desirable to distribute the grid so that the truncation error is approximately uniform over the grid (using ADR as a guide).

Once the grid distribution is arrived at, the accuracy of the numerical approximation can be increased by increasing the number of grid points. If this is done, a correlation emerges between the truncation error and ADR. It is this correlation which is critical to the viability of ADR as a useful error monitor.

4. TEST PROBLEM

To test the error monitors, an analysis problem was required. It was desirable to select this problem to achieve accurate computational solutions at a reasonable cost. High quality test data was also needed so that comparisons could be made between the computed and measured results. The inlet/aperture flow field test problem was selected because the test data was of high quality and because the geometry was two-dimensional. Two-dimensional NS solutions on a number of grids were feasible for the inlet within the available computer budget.

4.1 Geometry and Flow

A supersonic inlet throat region geometry and the flow physics associated with an external compression inlet with throat bleed flow is illustrated in Figure 1. The inlet/aperture approach flow, parallel to the centerbody ramp, is at the throat design Mach number of 1.28. The bulk of the flow in the streamtube spanning the gap between the cowl lip and ramp crown is captured by the inlet.

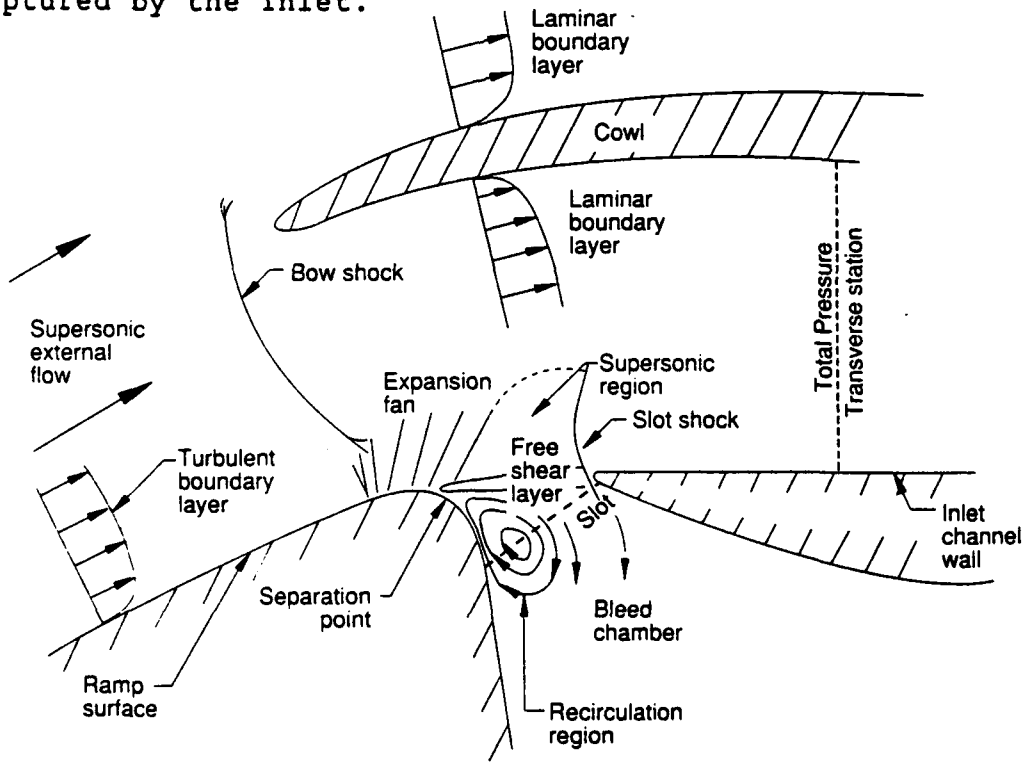

Figure 1. Inlet-Aperture Flow Field Features

Some spillage flow may occur at the cowl lip, depending on the engine face flow and the bleed slot flow requirements. The cowl generates a shock wave that is positioned upstream of the lip and impinges on the ramp boundary layer downstream, but near the crown of the ramp. The ramp shock-wave/boundary-layer interaction is stabilized in this position by bleeding flow into a slot opening in the ramp. This slot is downstream of the crown of the ramp. The crown of the ramp generates an expansion fan which locally accelerates the flow to a higher Mach number ($\simeq$ 1.7) before the flow arrives at the slot opening. These flow physics generate a complex interaction of the cowl shock wave, ramp boundary layer and the ramp crown expansion fan. These interactions produce a free shear layer across the slot opening which has strong viscous generated transverse velocity gradients and strong local inviscid transverse velocity gradients in the supersonic tongue. Further, this flow region is strongly influenced by the slot geometry and amount of bleed flow. These flow and geometry features generate higher gradients in flow properties in the longitudinal direction. The locations of these longitudinal contortions are dictated by the downstream lip of the slot opening. This lip produces a strong shock wave ($M_1 \simeq$ 1.7) in the slot region. It is a stronger shock than the cowl shock with high local curvature. This curvature adjusts the flow field in the neighborhood of the slot opening so that the resultant flow downstream of the slot opening is subsonic to match the static pressure of the remaining flow captured by the inlet.

The slot shock and the shear layer interaction are sensitive to the supersonic flow originating from the ramp crown. Flow solutions near the slot were very sensitive to solution error. Incomplete Prandtl-Meyer expansion in the numerical solution dramatically reduces slot shock strength, and in the extreme case, produces no slot lip shock. Over-expansion in the solution leads to misdirecting the slot free-shear layer to the slot lip. Either of these mismatches lead to incorrect slot pressure, either too high or too low respectively. In turn, the slot flow entrance separation point is affected dramatically by the pressure in the bleed flow opening. The nature of the recirculation flow field impinging upon the bleed entrance free shear layer is subject to change according to the separation point which induces feedback upon the bleed entrance pressure. Experimental results for the inlet were thought to be sensitive to experimentally undefined boundary conditions.

Turbulence in the bleed entrance and in the bleed cavity affect the flow pressure at the bleed entrance. The ratio of the length of the bleed flow opening and the thickness of the free shear layer, plus the pressure gradient in the free shear layer, influence the structure of the turbulence in the bleed cavity and in the free shear layer. Favorable pressure gradients accelerate the wall boundary layer at the crown of the ramp. Mixing zone intensity is excited by adverse pressure gradients which prevail between the bleed cavity and the supersonic flow regions.

Feedback between the turbulence and the pressure field can cause unsteadiness or instability of the flow at the bleed slot entrance. The intensity of the mixing can be damped or amplified by the unsteadiness. The mixing process may include at least five types of flow:

1) nearly laminar flow of the wall boundary layer at the ramp crown and downstream of the separation point,

2) transition to steady flow mixing between the fully developed supersonic flow and the bleed cavity flow field,

3) possible vigorous flow mixing between the established bleed flow opening free shear layer and the bleed cavity flow field,

4) possible resonance phenomena of the free shear layer and the bleed cavity flow field, and

5) fully developed mixing in boundary and free shear layers.

The occurrence of these types of flow phenomena depends upon flow transition phenomena. Model scale inlets and full scale inlets can have large differences in the location and streamwise extent of transition. For the model scale inlet, examined in the present study, only flow types 1, 2 and 5 have been identified. Numerical experiments indicate that only type 5 flow dominates the wall boundary layers and free shear layers.

4.2 Computational Approach

The computational approach in the present study is an extension of the work of Peery and Forester. It uses a conservation-based body-fitted adaptive grid model of the thin-shear-layer formulation of the compressible, Reynolds-averaged, Navier-Stokes equations together with mass and energy conservation equations.

Control of the residual errors is achieved, by an artificial time relaxation approach with a constant CFL criteria. Steady state is achieved by asymptotic time relaxation. Truncation errors are reduced through the use of solutions on varying grid densities and varying grid distributions. The formulation of (a) the governing thin-shear-layer equations, (b) the finite volume explicit predictor-corrector finite difference algorithm, (c) the boundary conditions, (d) the two-layer algebraic turbulence model with its associated wall functions, and (e) the mesh generator and the adaptive mesh mover are detailed by Campbell and Forester (1985) and the associated references. The procedure for design application of this code is given by Campbell et al. (1984).

The computer program allows three coupled computational regions. In the present study, computational region one (see

Figure 2) is the slot cavity flow region, region two is the ramp/cowl/engine-face flow region, and region three is the region above the cowl. The grid blocks have point and slope continuity at each interface. This simplifies the boundary condition treatment needed at the surface of grid blocks. Freestream boundary conditions are specified on the left side of regions two and three. The grid is body-fitted to the ramp, slot, and cowl. As shown in Figure 2, the length scales of the grid intervals vary widely over the analysis domain. The smallest grid intervals are generally located in critical regions as follows:

- o boundary layers,
- o free shear layers,
- o rapid compression/expansion regions,
- o shocks, and
- o stagnation regions.

To simplify the notation for grid size definition, grid sizes are defined by a cluster of numbers separated by commas. The numbers between the commas are the interval counts in x by y directions of the grid in region 1, region 2 and region 3, respectively. The grid sizes employed are (10x5, 27x17, 22x12), (21x10, 54x34, 44x24), and (42x18, 106x66, 46x26). These three grid sizes are labeled coarse, medium and fine, respectively. The influence of grid on resolution is considered relative to accuracy produced by pairs of grids (coarse/medium, coarse/fine, medium/fine.) Only the coarse and fine grid results are shown.

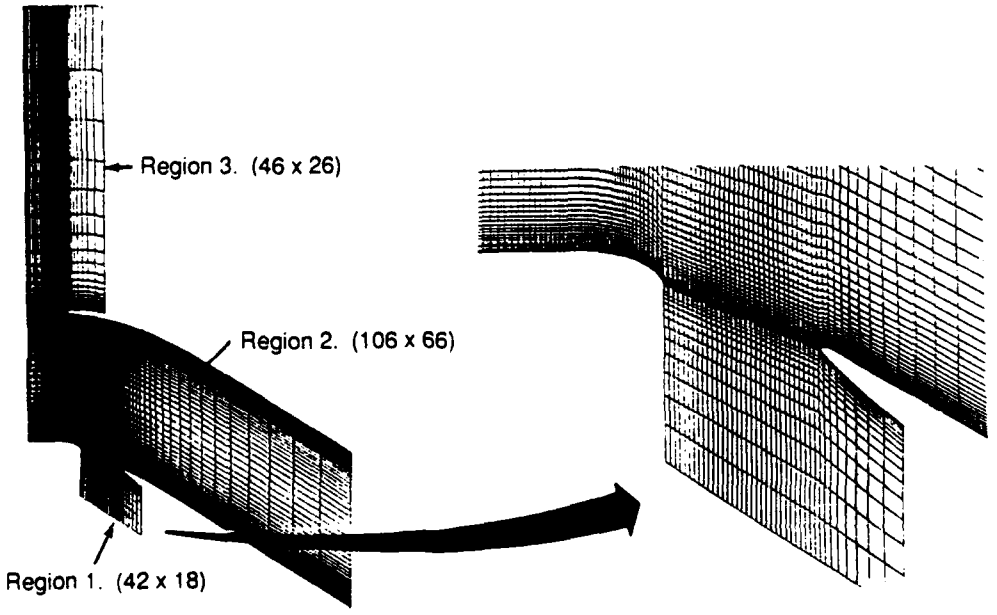

Figure 2. Fine Grid

4.3 Computational Results

Many parameters could be studied to explore error norm guides. The parameters selected for this study were the total pressure, artificial diffusion ratio, and Mach number. All of these parameters except for the artificial diffusion ratio are traditional parameters for error assessment. The artificial diffusion ratio is shown in conjunction with the Mach contours and does not replace these because physical features simply are not revealed by the artificial diffusion ratio. In fact, the artificial diffusion ratio should be void of physical features except near shocks. Mach contours show physical features including shocks.

Figures 3 through 7 relate solution accuracy to smoothing coefficient level and to grid placement through test data comparisons. Figure 1 shows the traverse station for the total pressure ratio, $P_t/P_{t\infty}$, in the throat region of the inlet. Figure 3 shows the improvement in the total pressure with respect to grid refinement and with respect to reducing the artificial smoothing.

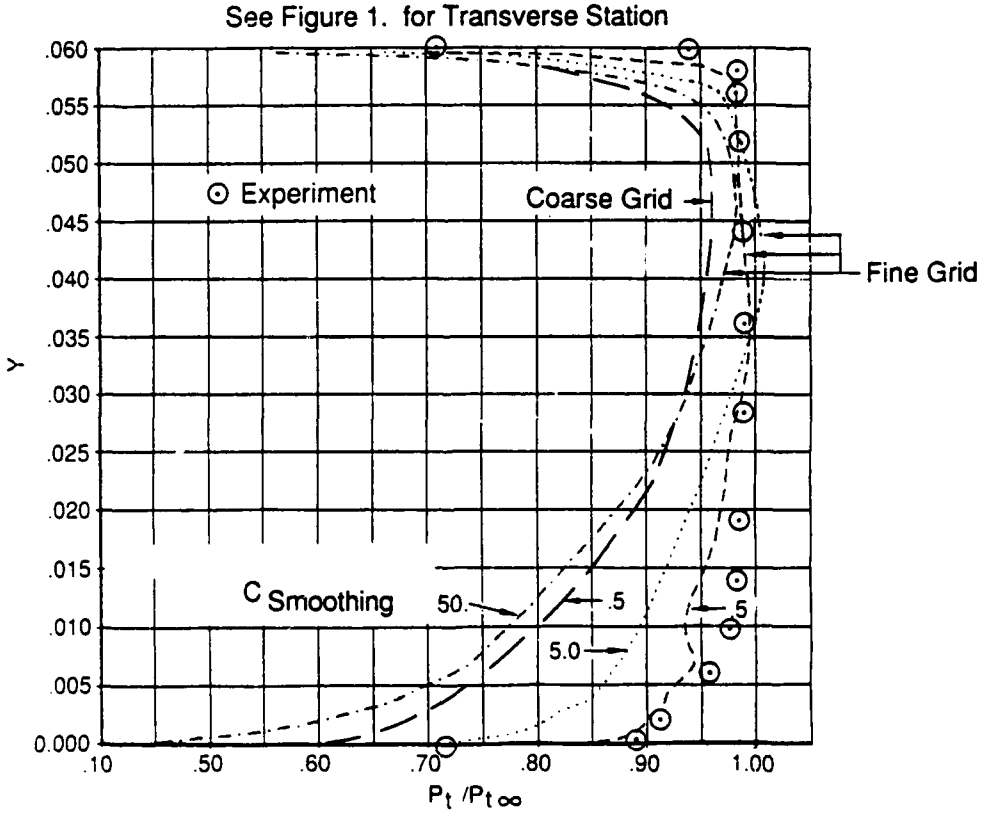

Figure 3. Total Pressure Ratio in Throat Region

Note that the degradation of the total pressure results from excessive smoothing or from too coarse a grid. Also note that the results improve with respect to grid refinement even with abnormally high smoothing coefficients. Ultimately grid refinement is the critical issue. However, the efficiency of using a particular grid is improved by setting smoothing coefficients near the stability limit, rather than to maximize convergence. Further examples of this behavior are now discussed.

Figures 4 through 7 are comparisons of solution results for selected grids and smoothing coefficients. Figures 4 and 5 show the effect of smoothing level on ADR for coarse, and fine grids, respectively. Figures 6, 7, and 8 are Mach number contours. Figures 4 and 5, and Figures 6 and 7 show the effect of grid density. Comparison of Figures 4 and 5 with Figures 6 and 7 show that ADR rises sharply with increased smoothing levels and with increased grid coarseness. Note that when ADR is above 0.01 (except for shocks where ADR should be about 0.01), too high a smoothing level or too coarse a grid is indicated. In these regions, the grid must be refined or the smoothing level must be reduced.

It is possible to generate a composite effect of all of these error sources on a particular grid. The grid used for this purpose is shown in Figure 2. Figure 8 shows an example of Mach number contours for the aperture region. Note the agreement between the shadowgraph of the flow field for an experimental test of this inlet and the predicted result for the same flow field (Figure 8).

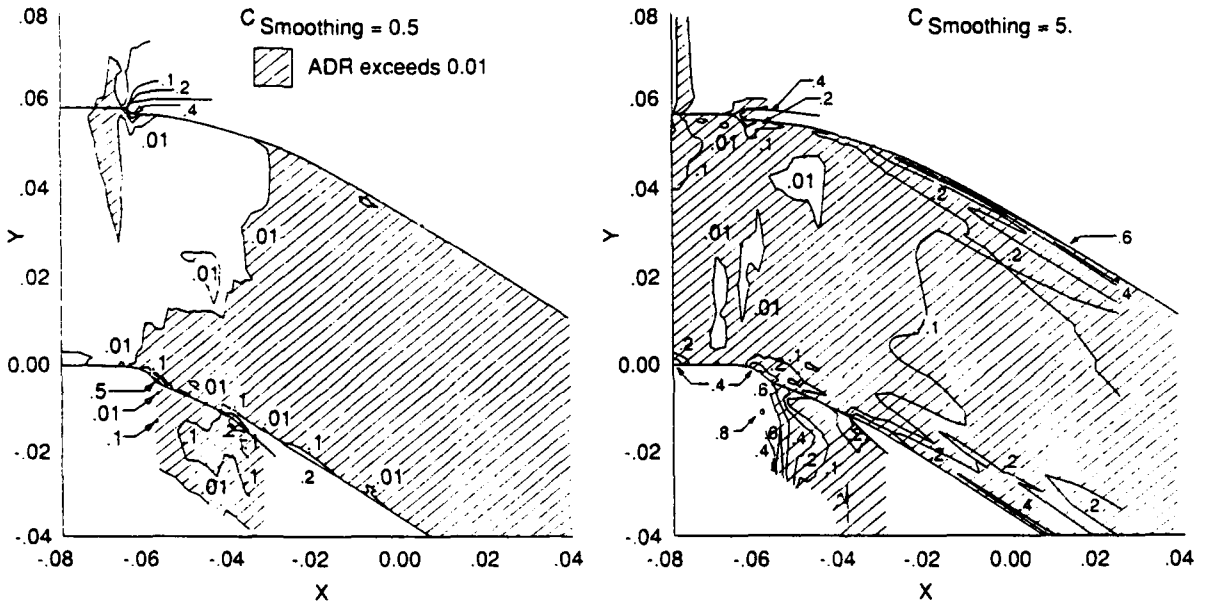

Figure 4. Coarse Grid Artifical Diffusion Ratio Contours

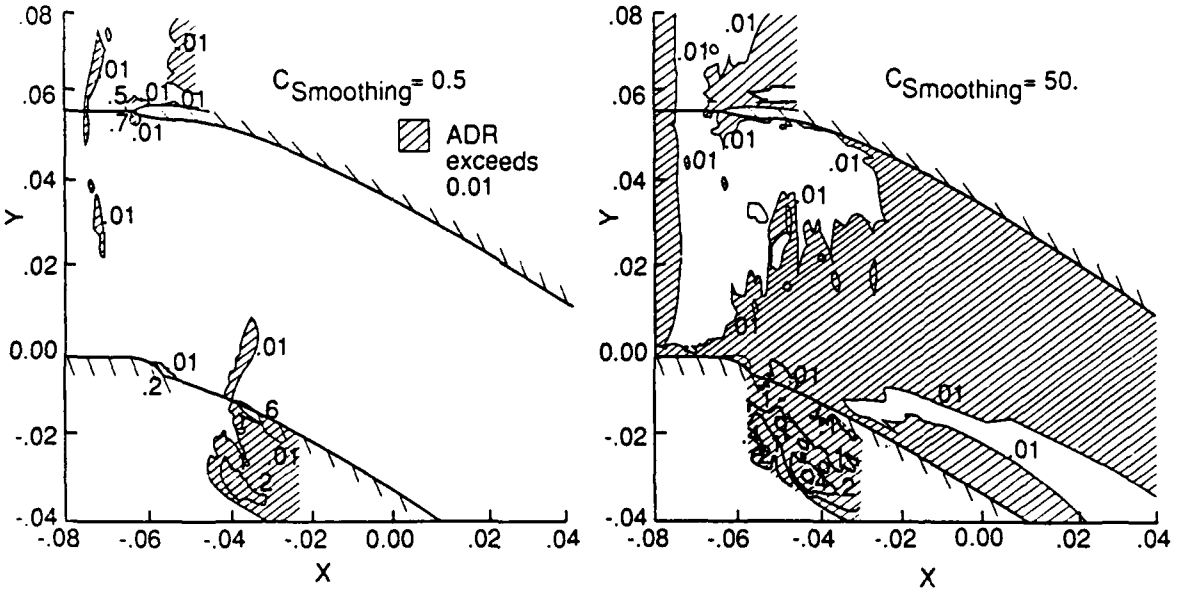

Figure 5. Fine Grid Artifical Diffusion Ratio Contours

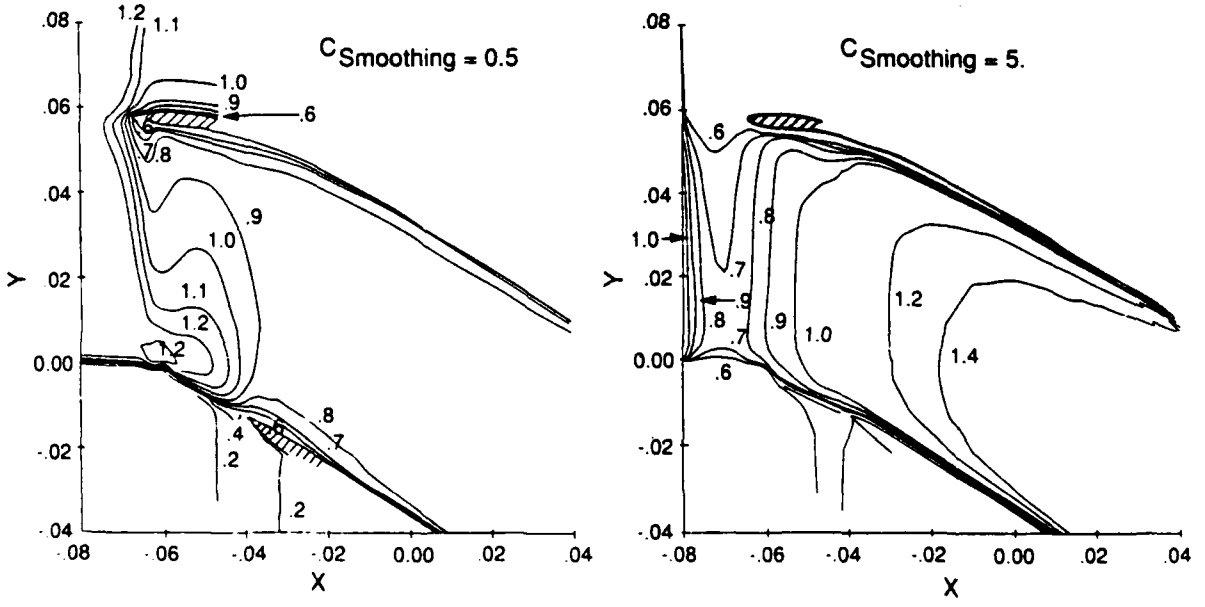

Figure 6. Coarse Grid Mach Contours

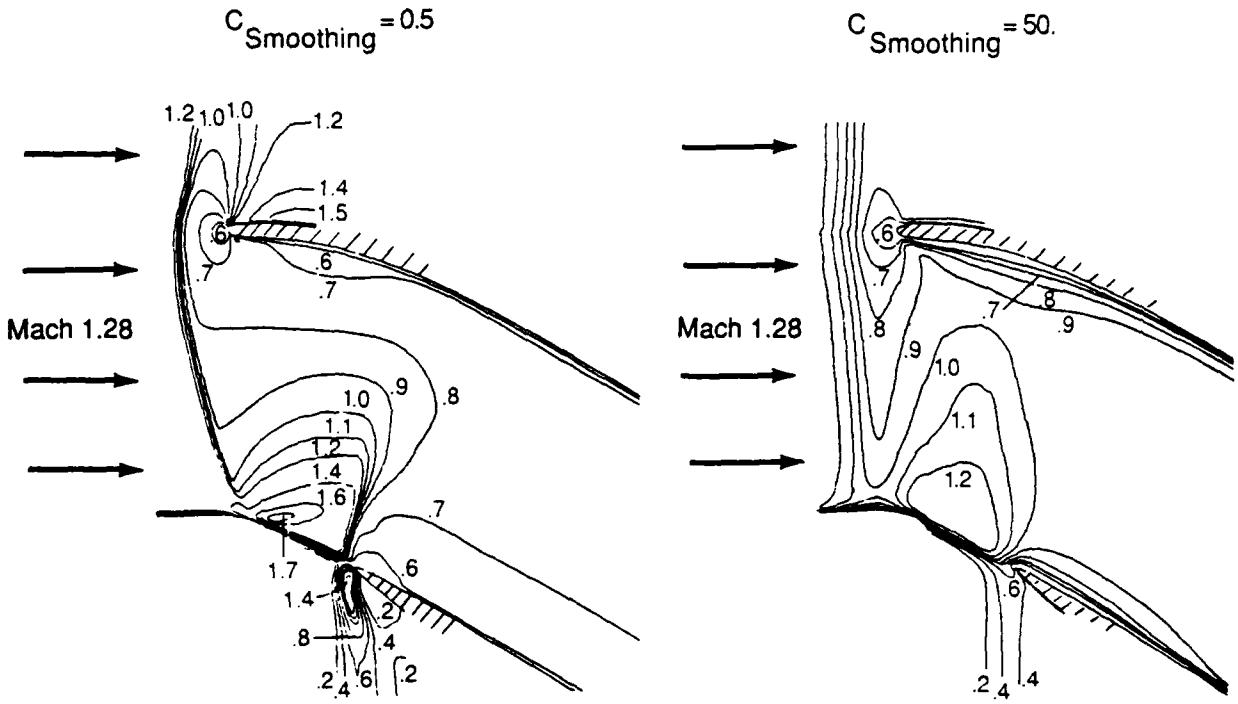

Figure 7. Fine Grid Mach Contour

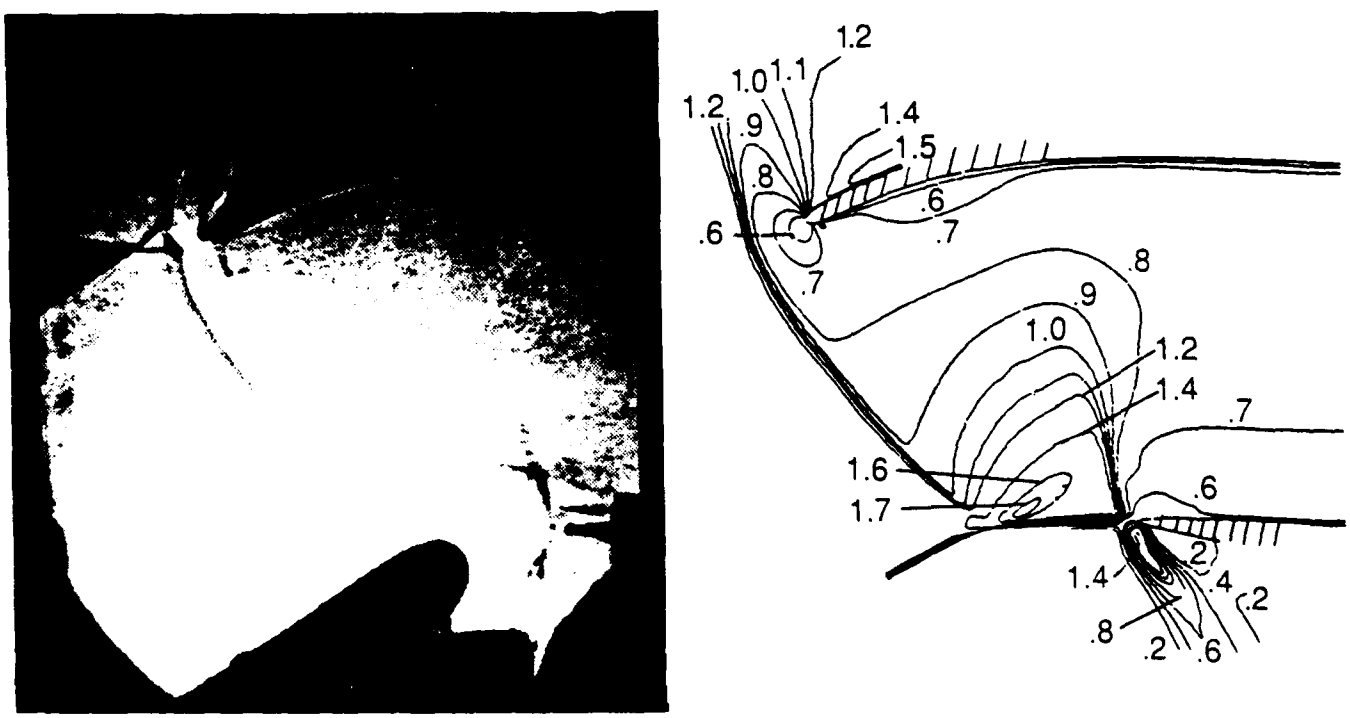

Shadow Graph

Predicted Mach Contours

Figure 8. Comparison of Experiment with Analysis

5. RELATED RESEARCH

Because of the promising nature of the contract results, a follow-on study was conducted to address several remaining questions. The follow-on study was performed with BAS IRAD funds. In particular, the questions addressed were as follows:

- Does the directionality of ADR (i.e., the u and v momentum ADR, ADR_F and ADR_G) provide guidance to the direction of the required grid refinement?
- Since the previous results indicate some error still exists between the predicted and measured total pressures, can grid refinements, that achieve the suggested ADR levels, reduce this error?
- Is ADR useful for algorithms other than the MacCormack explicit algorithms studied thus far? Specifically, is ADR useful for the Beam-Warming algorithm used in the popular ARC NS codes (Pulliam, 1984) and the PARC NS codes (Cooper, 1987)?
- What is the relationship between ADR magnitude and the solution error magnitude?
- Can ADR be used with algorithms that use intrinsically added smoothing such as the MacCormack implicit algorithm (MacCormack, 1985)?

The usefulness of ADR to guide grid adjustment in a grid direction (directionality) and the question of whether grid adjustment for the inlet problem to reduce local ADR levels would improve agreement between the computed and measured flow properties were addressed by continuing the contract study approach - application of the NS analysis to the inlet test problem. Work and results from this are reported in Section 5.1 below. The usefulness of ADR for other algorithms and the relationship between ADR and solution accuracy, were addressed through model equation studies using Burgers equation as an analog to the NS equations. Work and results from this are reported in Section 5.2.

5.1 ADR Directionality and Grid Refinement

Additional grid refinement work was performed for the test case, discussed in Section 4.3, using BAS IRAD funds (Baltar, 1988). Details of this study are included in Appendix A and are summarized in this section. The ADR measures were used to guide this grid refinement study.

During the contract effort ADR was identified as a useful parameter for guiding grid refinement and establishing solution accuracy. The objective of the IRAD effort summarized in Appendix A was to investigate if ADR is a useful guide for localized grid refinement of a complex flow field analysis. Improvement in flow prediction was evaluated by comparing the calculated total pressure with experimentally measured total pressure in the throat region. Regions of high ADR were shown to be reduced in size when more mesh was added in the direction normal to the gradient or in a way to reduce the cell aspect ratio of the mesh. The agreement between computed and experimentally measured total pressure profiles improved about 2% when the recommended levels of ADR were achieved throughout the computed flow field. The remaining disagreement could be caused by improper ADR thresholds, improper geometry resolution, or by experimental uncertainties. Preliminary results from investigation into the use of ADR to determine the direction of the required grid refinement were promising but additional study is needed.

During the course of this study a valuable graphical technique for using ADR to guide grid refinement was developed. Figure 9 is a representative ADR_E contour plot. Note the three color bands. Since ADR thresholds of 0.01 and 0.001 were being evaluated the color bands represent regions where the ADR is greater than 0.01 (the red band), between 0.01 and 0.001 (the yellow band), and less than 0.001 (the green band). The procedure for using these plots is to refine the grid in the red and yellow regions first. The green regions were assumed to have an adequate grid density. Once the majority of the flow domain had relatively low ADR values (illustrated by the large green region in Figure 9) the agreement with the data was good. As shown in Figure 10, the agreement between the predicted and measured total pressures in the throat region are within 2% and for much of the traverse the agreement is nearly perfect. Also note the crispness of the shock definitions in the Mach contour plot.

5.2 Model Equation Studies

Two problems were evident with continuation of the contract approach addressing the usefulness of ADR for other algorithms and establishing the relationship between solution error and ADR. First, exploring the usefulness of ADR with other algorithms was too complex to be practical (in the context of the short term follow-on study) using solutions of the NS equations. Second, establishing the level of accuracy of solutions to the NS equations is difficult because analytic solutions do not exist for cases of interest. Use of experimental results to represent an analytic (exact) solution to the NS equations is dangerous because of experimental uncertainties.

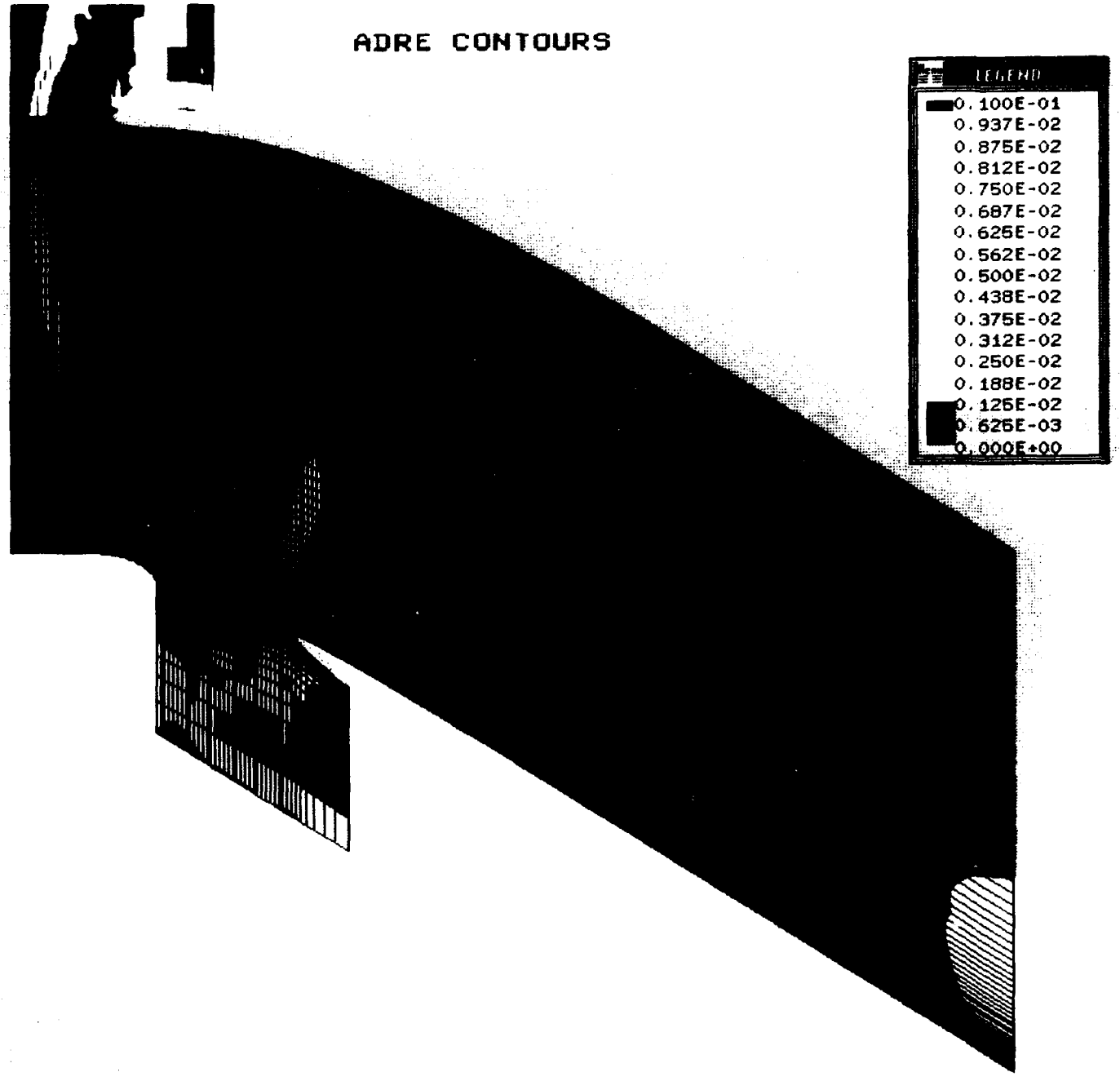

Figure 9. Case 2 – 90 Y-Direction Cells with X-Direction Refinement

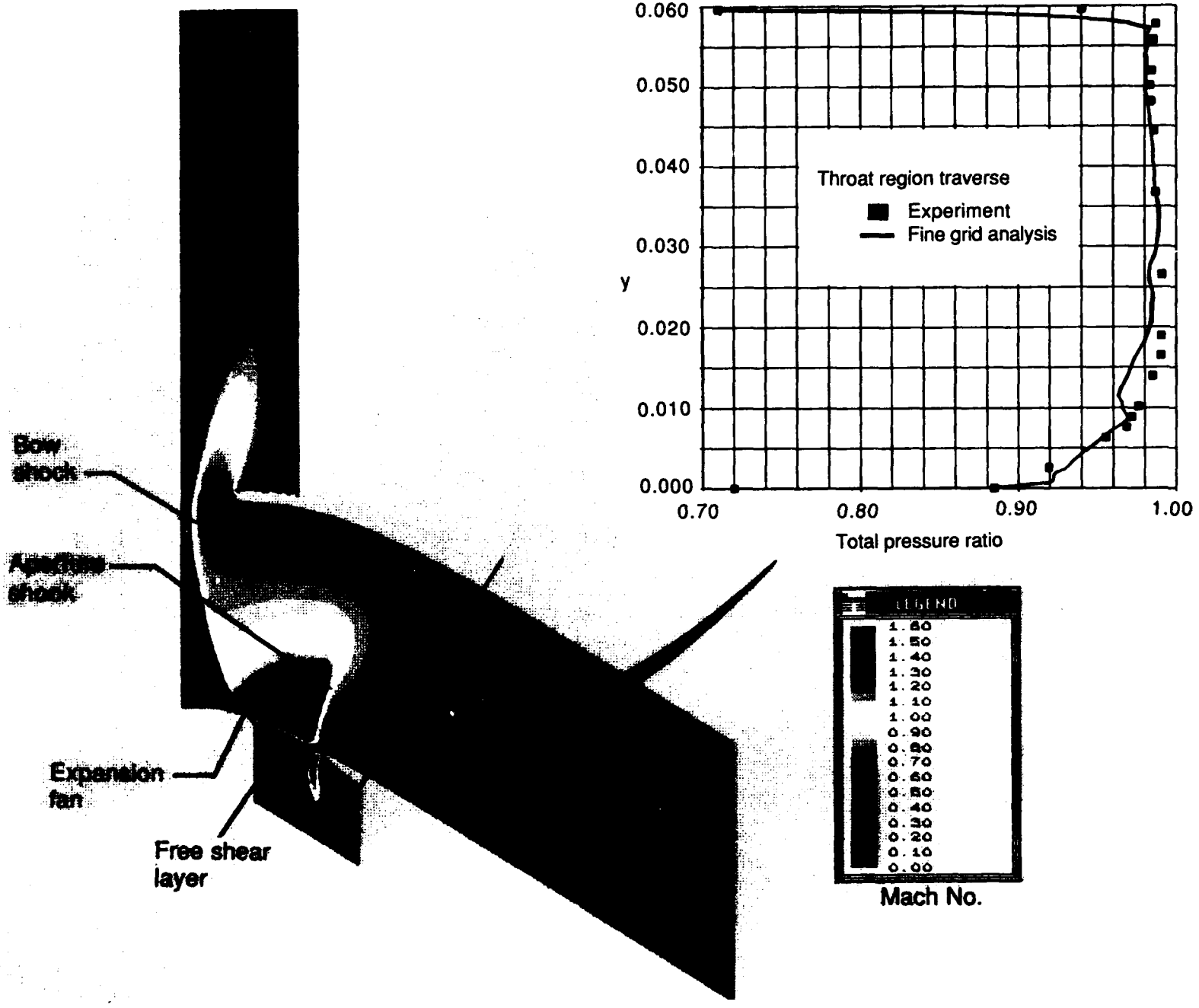

Figure 10. Inlet-Aperture Analysis: Mach Number Contours and Total Pressure Profile

The approach selected for the follow-on study was as follows:

- o Use Burgers equation as a simple analog of the NS equations.
- o Solve Burgers equation using the MacCormack and the Beam-Warming algorithms both with and without artificial dissipation modeling.
- o Establish the accuracy levels of the numerical solutions through comparisons between analytic and numerical results.
- o Complete modified equation analyses of the MacCormack and Beam-Warming FDE approximations to Burgers equation to address why ADR might be a measure of solution accuracy.

The advantages of this approach are that Burgers equation is recognized as an analog to the NS equations, analytic solutions are available to Burgers equation so that the accuracy of the numerical solutions can be established without ambiguity, the MacCormack and Beam-Warming algorithms are currently the most popular explicit and implicit methods, and programming the two methods is simple enough to be practical within the timeframe of a short study. Further, while a successful result with ADR in the follow-on study doesn't guarantee the success of using ADR with the NS equations, failure would make success with the NS equations improbable. Success here is defined as establishing a relationship between ADR and solution error and demonstrating the usefulness of ADR for the Beam-Warming and MacCormack algorithms.

5.2.1 Model Equation Analysis

Using Burgers equation as an analog to the NS equations, modified equations were developed for the linear viscous Burgers equation for both the MacCormack explicit method (used for the present contract work) and the Beam-Warming implicit method (used in other popular NS codes such as ARC and PARC). The details of this portion of the follow-on IRAD study (Paynter, 1988) are included in Appendix B and are summarized below.

The modified equation is the finite difference expression written as a sum of the partial differential equation and the truncation error with the lead time derivative terms in the truncation error replaced by spatial derivatives through a manipulation of this equation. Modified equations were developed for the linear viscous Burgers equation for both the MacCormack explicit and the Beam-Warming implicit algorithms. It was found that the lead truncation error term with the MacCormack algorithm is dispersive and that the lead term with the Beam-Warming algorithm is dissipative.

The artificial diffusion is in effect a source term added to the PDE being solved. The magnitude of the source term is at least a qualitative measure of the dispersive solution error. Because of the non-linear nature of the flow equations, a quantitative relationship between solution error and ADR was not established. A quantitative relationship between solution error and ADR would be algorithm and problem dependent due to the differences in the lead terms of the truncation error from algorithm to algorithm. This is supported by the computed results of Section 5.2.2. The artificial diffusion should be less useful for algorithms with high intrinsic dissipation since ADR is insensitive to intrinsic dissipation effects. It seems clear that a quantitative relationship between artificial diffusion and solution accuracy would be algorithm and problem dependent.

5.2.2 ADR as a Measure of Error Magnitude

Comparisons between analytic and CFD solutions of Burgers equation for a range of grids for the Beam-Warming and MacCormack algorithms were studied as part of the follow-on IRAD study (Mayer, 1988). The details of this are reported in Appendix C and the results summarized below.

- o solution accuracy is not simply related to ADR thresholds,
- o ADR is useful for defining grid regions that require refinement, and
- o ADR is less useful in defining regions of high grid error for the Briley-McDonald algorithm (which is equivalent to the Beam-Warming algorithm when applied to Burgers equation) than for the MacCormack explicit algorithm.

The computer program developed for this follow-on study (Appendix D) could be readily adapted for other algorithms, including those with intrinsic dissipation. Modified equation analyses could be performed to define the lead truncation error terms for other algorithms and model equations. Analytic solutions could be used to directly evaluate these error terms. A detailed study of these error terms relative to the definition of ADR should provide valuable insight and guidance to using ADR for assessing solution accuracy.

6. RESEARCH STATUS

Several significant accomplishments and conclusions have resulted from the contract effort and associated Boeing Advanced Systems (BAS) independent research and development (IRAD) funded

research. In addition, the promising results from the current work suggests additional research to develop the error monitor, the artificial diffusion ratio (ADR), into a tool useful for general purpose CFD applications. These accomplishments, conclusions and recommendations are discussed in the following sections.

6.1 Significant Accomplishments

The solutions of the flow field in the aperture region of an external compression inlet with bleed and spillage flow by Navier-Stokes analysis were obtained on a variety of grids and a new approach was explored to guide grid adjustment. Measures of numerical errors in the analysis process were explored including ADR for mass, energy, and momentum. Correlation of these error measures show that ADR provides guidance for grid and smoothing level selection. The application of ADR leads to a grid choice that yields an adequate solution to the flow field. Comparison of this solution with experimental data shows good agreement. The promising contract results led to a follow-on IRAD study to further explore the usefulness of ADR as a guide to grid adjustment.

In the follow-on study, the usefulness of ADR was further explored for the inlet test problem on a variety of grids. The applicability of ADR to other algorithms and the relationship between ADR and solution accuracy were explored in model equation studies. The inlet studies resulted in a new procedure for graphical display of the ADR data and some work toward establishing the usefulness of ADR to guide grid adjustment in a given direction.

Modified equations were developed for the linear viscous Burgers equation for both the MacCormack explicit and the Beam-Warming implicit algorithms. This development clearly illustrates the nature of the lead truncation error terms for these algorithms. The nature of these terms indicate how ADR detects solution errors for MacCormack's explicit method. In addition, the mathematical development of these terms makes it feasible to directly evaluate the magnitude of these errors for test problems that have analytic solutions.

Analytic and CFD solutions on a range of grids were obtained for the viscous Burgers equations for both the Beam-Warming and MacCormack implicit algorithms. Comparisons between the analytic and CFD results were useful in establishing the relationship between solution accuracy and ADR for a given algorithm. The computer program written for the model equation studies could be easily extended for the study of other algorithms.

6.2 Conclusions

The major conclusions drawn from the research are as follows:

- The use of ADR to pinpoint grid problems has been demonstrated. Regions of the flow where the grid is too coarse to accurately capture gradients results in noise or ringing in the solution. This noise is dispersive in nature, and when using a MacCormack smoother, results in correspondingly high values of ADR. Therefore, regions of the flow that have relatively high levels of ADR are candidates for further grid refinement.

- Solution accuracy is improved and the high ADR values are reduced by performing localized grid refinement based on the location of high ADR values.

- ADR thresholds as direct measures of solution accuracy have not been established. There does exist a correlation between ADR and solution accuracy, but the correlation is more complex than a simple one-to-one relationship. Achieving a given level of ADR does not guarantee a given accuracy level. This relationship is thought to be algorithm and problem dependent.

- ADR does not pinpoint regions of grid error as well for the Briley-McDonald method (comparable to the Beam-Warming method for the 1D Burgers equation). The regions of high ADR cover a greater extent than the regions of relatively high solution error. This means that ADR for the Briley-McDonald method exaggerates the extent of regions that require grid refinement.

- The lead truncation error term is dispersive for the MacCormack algorithm and is dissipative for the Beam-Warming algorithm. In addition, an intrinsic third order dispersive error term exists for the Beam-Warming algorithm.

- The artificial dissipation acts as a source term added to the partial differential equation being solved. For algorithms with high dispersive error the artificial dissipation is a qualitative measure of solution accuracy.

- Artificial dissipation is less useful for algorithms with high intrinsic dissipation.

- A quantitative relationship between artificial dissipation and solution accuracy is algorithm and problem dependent.

6.3 Recommendations

Further work is recommended for demonstrating the utility of ADR as follows:

- The results of the modified equation analysis of the MacCormack explicit and the Beam-Warming implicit algorithms (Paynter, 1988, Appendix B) makes it feasible to directly evaluate the lead truncation error terms for an analytic solution. A detailed study of these terms relative to the present (or alternate) definitions of ADR should provide valuable insight and guidance to using ADR for assessing the solution accuracy of these algorithms.

- The extension to solution algorithms that use intrinsic smoothing (i.e., not added explicitly) has not been demonstrated. The computer program written for the present study (Appendix D) may be readily adapted to explore the use of ADR for these and other algorithms.

- Additional test problems should be investigated to evaluate the use of ADR (for algorithms studied with the above methods) for flows with different flow field characteristics (i.e., flow separation, without shocks, inviscid, laminar, etc.). These test problems should be performed for configurations with high quality experimental data suitable for CFD validation.

- The utility of ADR should be tested for other design analyses of aircraft components (both model scale and full scale).

REFERENCES

Anderson, BH, "Three-Dimensional Viscous Design Methodology for Advanced Technology Aircraft Supersonic Inlet Systems," NASA TM-83558, January 1984.

Anderson, DA, Tannehill, JC, and Pletcher, RH, "Computational Fluid Mechanics and Heat Transfer," Hemisphere Publishing Company, 1984.

Baldwin, BS, RW MacCormack, and GS Deiwert, "Numerical Techniques for the Solution of the Compressible Navier-Stokes Equations and Implementation of Turbulence Models," NASA Ames Research Report, 1977.

Baltar, JY, "Artificial Diffusion Ratio (ADR) Guided Grid Refinement Study," Boeing Advanced Systems Coordination Sheet number L-7150-88-JYB-012, August 15, 1988. (Summarized in Appendix A).

Campbell, AF and CK Forester, "Evaluation of a Method for Analyzing the Aperture Region of Two-Dimensional External Compression Inlets," AIAA-85-3072, October 1985.

Campbell, AF, J Syberg, CK Forester, "Design Study of an External Compression Inlet Using a Finite Difference Two-Dimensional Navier-Stokes Code," AIAA-84-1275, June 1984.

Cooper, GK, "The PARC Code: Theory and Usage," Arnold Engineering Development Center, Report No. AEDC-TR-87-24, October 1987.

Forester, CK (Principal Investigator), "Error Norm Guided Flow Analysis of Shock-Wave/Boundary-Layer Interactions," Air Force Office of Scientific Research, Contract No. F49620-85C-0126, 1985.

Forester, CK and Tjonneland, E, "New Guide for Accurate Navier-Stokes Solution of Two-Dimensional External Compression Inlet With Bleed," 16th International Council of the Aeronautical Sciences Congress, Jerusalem, Israel, August 28 through September 2, 1988.

Forester, CK, "Error Norm Guided Flow Analysis," prepared for Air Force Office of Scientific Research, contract number F49620-84-C-0037, April 1985.

Forester, CK, "Error Norm Guided Flow Analysis of Blunt Base Rocket Nozzle Flow Field," Boeing document number D180-28954-2, prepared for the Air Force Office of Scientific Research, contract number F49620-85-C-0126, August, 1986

Forester, CK, "Error Norm Guided Flow Analysis: Inlet/Aperture Problem Identification," Boeing document number D180-28954-3, prepared for the Air Force Office of Scientific Research, contract number F49620-85-C-0126, February, 1987.

Forester, CK, "Error Norm Guided Flow Analysis of Inlet/Aperture Flow Field," Boeing document number D180-28954-4, prepared for the Air force Office of Scientific Research, contract number F49620-85-C-0126, August, 1987.

MacCormack, RW, "Current Status of Numerical Solutions of the Navier-Stokes Equations," American Institute of Aeronautics and Astronautics Paper No. 85-0032, 1985.

MacCormack, RW and BS Baldwin, "A Numerical Method for Solving the Navier-Stokes Equation with Application to Shock-Boundary Layer Interactions," AIAA Paper 75-1, January 1975.

Mayer, DW, "Evaluation of the Artificial Diffusion Ratio Through Numerical Solutions to Burgers Equation," Boeing Advanced Systems Coordination Sheet number PROP-7150-88-DWM-014, August 17, 1988. (Summarized in Appendix C).

McDonough, JM, "A Class of Model Problems for Testing Compressible Navier-Stokes Solvers," AIAA paper 88-3645, presented at the 1st National Fluid dynamics Congress, Cincinnati, Ohio, July, 1988.

Oran, ES and JP Boris, "Numerical Simulation of Reactive Flow", Elsevier Science Publishing Co., NY, 1987.

Paynter, GC, CK Forester and E Tjonneland, "CFD for Engine-Airframe Integration," Journal of Engineering for Gas Turbines and Power, Vol. 109, April 1987.

Paynter, GC and HC Chen, "Progress Toward the Analysis of Supersonic Inlet Flows," AIAA-83-1371, June 1983.

Paynter, GC, "Modified Equation Analyses for Spatial Truncation Error Effects in Numerical Solutions of Burgers Equation," Boeing Advanced Systems Coordination Sheet number L-7150-88-GCP-015, August 22, 1988. (Summaried in Appendix B).

Peery, KM and CK Forester, "Numerical Simulation of Multistream Nozzle Flows," AIAA Journal, Vol 18, No. 9, September 1980, pp. 1088-1093.

Pulliam, TH, "Euler and Thin Layer Navier-Stokes Codes: ARC2D, ARC3D," Notes for Computational Fluid Dynamics User's Workshop, Tullahoma, Tennessee, March 12-16, 1984.

CHRONOLOGICAL LIST OF WRITTEN PUBLICATIONS IN TECHNICAL JOURNALS

Forester, CK and I Strom, "Navier-Stokes and Experimental Modeling of Blunt-Base Rocket Nozzle Flow," in Turbulent Shear-Layer/Shock-Wave Interactions, International Union of Theoretical and Applied Mechanics Symposium, Palaiseau, France, September 9-12, 1985, Ed. J. Delery, Springer-Verlag, 1986.

Forester, CK and E Tjonneland, "New Guide for Accurate Navier-Stokes Solution of Two-Dimensional External Compression Inlet with Bleed," in ICAS Proceedings 1988, Vol. 1, Paper Number ICAS-88-2.5.1, 16th International Council of the Aeronautical Sciences Congress, Jerusalem, Israel, August 28-September 2, 1988. Distributed by the American Institute of Aeronautics and Astronautics, Washington D.C.

LIST OF PERSONNEL ASSOCIATED WITH RESEARCH EFFORT

Baltar, James Y. Co-Investigator. Specialist Engineer, Boeing Advanced Systems, Propulsion Technology Computational Fluid Dynamics Group. MSME, 1980, Georgia Institute of Technology, Thesis Title: An Investigation of Coal Particle Reaction with the Sodium D Line Reversal Technique. BSME, 1976, Georgia Institute of Technology.

Forester, Clifford K. Principal Investigator. Senior Specialist Engineer, Boeing Advanced systems, Propulsion Technology Computational Fluid Dynamics Group. MSME, 1969, University of Washington. BSME, 1958, Montana State College. He has more than 24 years of experience in computational fluid dynamics and he has developed new research codes for 2D Navier-Stokes and 3D full potential flow analysis. As principal investigator on the Apollo 13 oxygen tank redesign and flight certification program he was recognized by a special NASA commendation for advancing the state-of-the-art in cryogenic analysis. He is a member of Tau Beta Pi (the national engineering honor society).

Mayer, David W. Co-Investigator. Senior Specialist Engineer, Boeing Advanced Systems, lead engineer of the Propulsion Technology Computational Fluid Dynamics Group. MSME, 1977, University of Washington, Thesis Title: Turbulent Supersonic Boundary Layer Flow in an Adverse Pressure Gradient Including the Effects of Mass Bleed. BSME Magna Cum Laude, 1975, University of Washington. He is a member of the American Institute of Aeronautics and Astronautics, the American Society of Mechanical Engineers, and Tau Beta Pi (the national engineering honor society). He is a licensed Professional Engineer (Washington State) and has authored or co-authored 23 technical publications.

Paynter, Dr. Gerald C. Program Manager. Principal Engineer, Boeing Advanced Systems, lead engineer of the Hypersonic Computational Fluid Dynamics Group (1987 to present). Lead engineer of the Propulsion Technology Computational Fluid Dynamics Group (1975-1985). He has worked on fluid dynamic problems associated with a number of Boeing aircraft projects. These include the inlet design for the V-22 tilt-rotor aircraft, jet noise suppression devices for the 727, shock-wave/boundary-layer interaction modeling for the supersonic transport, and an inflight thrust reverser for the YC-14. He is an Associate Fellow of the American Institute of Aeronautics and Astronautics (AIAA), a member of the AIAA Fluid Dynamics Technical Committee, and has authored or co-authored more than 40 technical publications.

Tjonneland, Elling. Chief Engineer, Boeing Advanced Systems Propulsion Technology Staff. MSME, University of Washington. He has extensive management and engineering experience in advanced propulsion technology, including experimental and analytical supersonic inlet design.

APPENDIX A:
Artificial Diffusion Ratio (ADR) Guided Grid Refinement Study

by
JY Baltar

1. Summary

Forester and Tjonneland (1988) identified the artificial diffusion ratio (ADR) as a useful parameter for guiding grid refinement and establishing solution accuracy. Global grid refinement and artificial viscosity levels were studied in their paper. The objective of this appendix is to investigate if ADR is a useful guide for localized grid refinement of a complex flow field analysis. Improvement in flow prediction is evaluated by comparing the calculated total pressure with experimentally measured total pressure in the throat region. Regions of high ADR are shown to be reduced in size when more mesh is added in the direction normal to the gradient or in a way to reduce the cell aspect ratio of the mesh. The agreement between computed and experimentally measured total pressure profiles improved about 2% when the recommended levels of ADR were achieved throughout the computed flow field. The disagreement that remains may be caused by improper ADR thresholds, improper geometry resolution, or by experimental uncertainties. Preliminary investigation into the use of ADR to determine the direction of the required grid refinement looks promising but more study is needed.

2. Introduction

This appendix documents the work performed using ADR to guide a grid refinement study on the inlet-aperture problem analyzed by Campbell and Forester (1985). The previous work (performed by PS Hertel of Boeing Computer Services and CK Forester) studied the changes in ADR during global grid refinement and artificial viscosity level studies on this inlet flow field. The results were reported by Forester and Tjonneland (1988).

The geometry and flow field features for the inlet-aperture case analyzed are shown schematically in Figure A-1. The approach flow parallel to the ramp surface is at a Mach number of 1.28. A cowl shock wave is established which impinges on the ramp boundary layer near the crown of the ramp. The ramp boundary-layer/shock-wave interaction is stabilized in this position by bleeding flow into a slot opening in the ramp. The crown of the ramp generates an expansion fan which locally accelerates the flow before the flow arrives at the slot opening. The downstream lip of the bleed slot opening produces a strong shock wave so that the resultant flow downstream of the slot is subsonic to match the static pressure of the remaining flow captured by the inlet. This highly complex flow region with normal shocks, rapid expansions, and strong shear layers presents a challenging problem for CFD analysis.

A new approach was introduced by Forester and Tjonneland (1988) to aid in guiding grid refinement studies. The parameter used to guide the grid refinement is ADR. ADR is defined as the ratio of the artificial smoothing flux to the total flux through computational cell faces. Values of ADR of 0.01 or less in shock waves and values of ADR of 0.001 or less for smooth flow regions were recommended by Forester (1987). The goals of this study were to 1) achieve the recommended levels by locally adding grid points where the ADR was high to see if the computed flow solution could be brought into agreement with experiment; and 2) to determine if the directionality of ADR could be used to guide the x- versus y-direction grid refinement. Improvement in flow prediction was evaluated by comparing the calculated total pressure with experimentally measured total pressure in the throat region. Since experimental uncertainties exist, perfect agreement with the *data was not expected. The data does provide* valuable indications of grid related errors.

As described by Forester and Tjonneland (1988), ADR can be generated for each dependent variable of the flow equations that are solved by the CFD code. For this study, the ADR for the energy equation and the two momentum equations were calculated and analyzed to determine if they could be used to determine where and in which direction the grid needed refinement. These ratios were labeled ADR_E (energy), ADR_F (streamwise momentum) and ADR_G (normal momentum) after the standard names for the flux vectors in the 2D Navier-Stokes equations.

3. Results and Discussion

Figure A-2 shows a color contour plot of ADR for the energy equation (ADR_E) with the grid overlayed. This data is from the final fine grid/low smoothing result shown by Forester and Tjonneland (1988). This case will be called the Reference Case for the remainder of this discussion. Table A-1 gives some pertinent information about this case and about the other cases discussed in this appendix. In Figure A-2, the areas in which ADR_E is above the threshold of 0.01 are colored red while the regions in which ADR_E is between 0.001 and 0.01 are colored yellow. The regions of the flow field which are below the threshold of 0.001 are colored green. This color scheme is used throughout this appendix since both ADR thresholds may be shown on one plot. The ADR_F and ADR_G color contour plots for this case are shown in Figures A-3 and A-4.

Figure A-5 shows a plot of the total pressure profile from this CFD solution compared with the experimentally measured values. The total pressure measuring plane is about 0.012 meters or 12 nodes downstream of the bleed slot lip and is perpendicular to the wall of the constant area section of the duct (see Figure A-1). The agreement between the CFD prediction and experiment is fair considering the complexity of the flow field. However, several regions of the flow indicate a need for improvement to accurately predict the local total pressure. Notably, the region between 0.0075 and 0.03 meters from the lower wall (which is strongly influenced by the expansion-fan/shock-wave interaction) shows a disagreement of as much as 4%.

During this study, several refinements were made to the grid that is shown in Figure A-2. Since the 0.01 threshold regions for the Reference Case (Figures A-3 and A-4) were larger for ADR_G than for ADR_F, the initial grid refinements were made by adding more mesh in the y-direction (normal to the flow). This was accomplished while holding the near wall cell height constant so the maximum cell height at the center of the duct was reduced significantly. For this grid refinement, 24 cells were added in the y-direction in two steps for a total of 90. The results for this case (Case 1a) are shown in Figures A-6, A-7 and A-8. Figures A-6 and A-7 show that the 0.01 threshold regions in the cowl and slot shocks were almost removed and the 0.001 threshold regions in the smooth flow regions (particularly in the expansion from the upstream end of the bleed slot) were reduced significantly. Figure A-8 shows that the flow field total pressure profile comparison is improved so that the maximum disagreement is now less than about 2%. This improvement can be attributed to the increased resolution in the region of the expansion and the shock wave/expansion interactior. The increased resolution in this region is primarily due to the fact that the cell aspect ratio was reduced to near unity in a region with strong gradients diagonal to the mesh.

A further refinement in the y-grid, called Case 1b, brought the total number of cells in the y-direction to 132 which is double the amount used in the Reference Case. As shown in Figure A-9, the 0.001 threshold regions of ADR_E in the two shocks were reduced slightly for Case 1b, but the peak ADR values in the shocks (near the 0.01 threshold) increased slightly. The extent of the region of large disagreement in the total pressure profile was reduced as shown in Figure A-10, but the largest disagreement has increased to approximately 3%. Some noise is starting to contaminate the solution near the top wall which is indicated by the high ADR_E region and the noise in the total pressure profile. This noise is probably caused by the large cell aspect ratios in that region.

Since grid refinement in the y-direction did not eliminate the regions of high ADR and total pressure disagreement, an attempt was made to refine the grid in the streamwise (x) direction. The upstream (left) boundary was moved closer to the bow shock by reducing the mesh stretch factor to the left of the cowl lip, thereby increasing the number of points in the bow shock. Twelve equal spaced mesh points were also added just downstream (to the right) of the bleed slot lip to increase the resolution at the downstream end of the slot shock. Figure A-11 shows the ADR_E contours for this case (Case 2) with the overlayed grid. This grid includes refinement of the grid in the streamwise direction and the same y-direction grid as was used for Case 1a. As shown by the ADR_E contours, significant reductions were made in the ADR_E greater than 0.001 threshold regions downstream of the slot shock. However, a comparison of the total pressure profiles with and without the x-direction refinements (Figure A-12) shows that the agreement with the measured data is not improved significantly. Significant reductions in the noise near the upper wall did occur (indicated by the reduced ADR_E in this region) since the cell aspect ratio was decreased by the additional x-direction mesh.

The Case 1a results shown in Figures A-6 and A-7 were reviewed again since the refinements to the grid in the streamwise direction did not produce significant improvements in the total pressure profile. These ADR contour plots indicated a large region of high ADR in the bleed chamber. Therefore a run was made with the grid in the bleed chamber increased from 42 x 18 cells to 51 x 26 cells. Color contour plots from this run (Case 3) showed a significant reduction in ADR in the bleed chamber, but almost no change in ADR contours in the inlet region. The total pressure profile from this run (shown in Figure A-13 compared with Case 1a) showed some changes in the boundary layer near the lower wall, but the disagreement between y = 0.0075 and 0.03 meters did not change.

To investigate the convergence effects on ADR contours and total pressure profiles, the Reference Case was restarted and run an additional 20,000 cycles. This case (Case 4) had then completed the same number of cycles as was completed for Case 1a. A comparison of the ADR contours from the Reference Case and Case 4 showed that ADR did not change significantly with the additional cycles. However, as shown in Figure A-14, the additional 20,000 cycles has resulted in a more fully developed boundary layer profile downstream of the bleed slot thus reducing the maximum disagreement in the total pressure profile to about 3%. Figure A-15, which compares the results from Case 1a with Case 4, shows that the effect of the additional 24 y-direction cells on the total pressure profile at the same number of cycles is to reduce the maximum disagreement by about 1%. This convergence study shows that of the 2% improvement in total pressure claimed in Figure A-8, about 1% is due to the increased y-direction grid and the other 1% is due to convergence in this part of the flow field.

Examination of the ADR_E contours relative to mesh density indicated that ADR_E was high in regions where the grid was too coarse to properly resolve the gradients in the flowfield. Refinements to the grid in the direction normal to the gradients produced the greatest reductions in ADR_E. In regions of the flow field where the steep gradients are diagonal to the mesh, refinement was required to achieve cell aspect ratios close to unity. If the cell aspect ratio was near unity and ADR_E remained high, refinements to the grid were required in both directions.

A study of the change in the predicted total pressure profiles as compared to the measured total pressure profiles showed that satisfying the recommended ADR thresholds was not sufficient to guarantee an accurate solution. This is consistent with one conclusion of Appendix C which says that there is not a direct correlation between peak ADR level and solution accuracy. The disagreements that remain could also be caused by uncertainties in the experimental measurements, uncertainties in the numerical boundary conditions, or by improper geometry resolution at both ends of the bleed slot.

A comparison of the simultaneous changes in ADR_F and ADR_G for these grid changes was made. In regions of the flow field where the steep gradients were diagonal to the mesh and the cell aspect ratio was large, a high ADR_F or ADR_G would indicate that mesh refinement was needed in the direction normal

to the velocity component used to calculate ADR. For example, in the expansion region in Figure A-3, ADR_F (streamwise momentum) was high indicating that normal (y) direction mesh was needed to make the cell aspect ratio closer to unity. This effect was also seen for high ADR_G regions and streamwise direction refinements. In regions of the flow field where the gradients were aligned to the mesh, all three ADRs tended to be near the same level, so direction for grid refinement could not be inferred solely from ADR_F and ADR_G.

4. Conclusions and Recommendations

The use of ADR to guide the localized grid refinement for a very complex flow analysis has been shown in this study. The regions of the flow field where the grid was too coarse to properly resolve the flow gradients produced high values of ADR. The high ADR values were reduced and the solution accuracy improved when more mesh was added.

The use of ADR thresholds as a quantitative measure of solution accuracy has not been shown in this study. As the ADR levels were reduced to the recommended levels, the predicted total pressure profiles were brought into better agreement with the experimental results, however, some disagreement remained between the computed and measured total pressure profiles. This conclusion is consistent with the conclusion of the Appendix C study of ADR for a 1D model equation.

For this study, the experience of the CFD user was utilized to determine that the high ADR_E regions could be reduced by adding mesh in the direction normal to the gradient or in a way to reduce the cell aspect ratio. It would be advantageous to develop guidelines using ADR that could be given to novice CFD users or could be programmed into an adaptive mesh generator. The investigation into using ADR_F and ADR_G to guide the grid refinement direction showed promise, but additional research is required.

Several recommendations for continuing work on this problem are:

1) Add more x-direction mesh in the bleed-slot lip shock region. This can be accomplished with the current mesh generator but has not been performed at present due to time constraints.

2) Use an elliptic mesh generator, preferably with multi-block capability, to better define the geometry at both ends of the bleed slot and at the cowl lip.

3) Demonstrate the use of ADR on other test problems and with other codes.

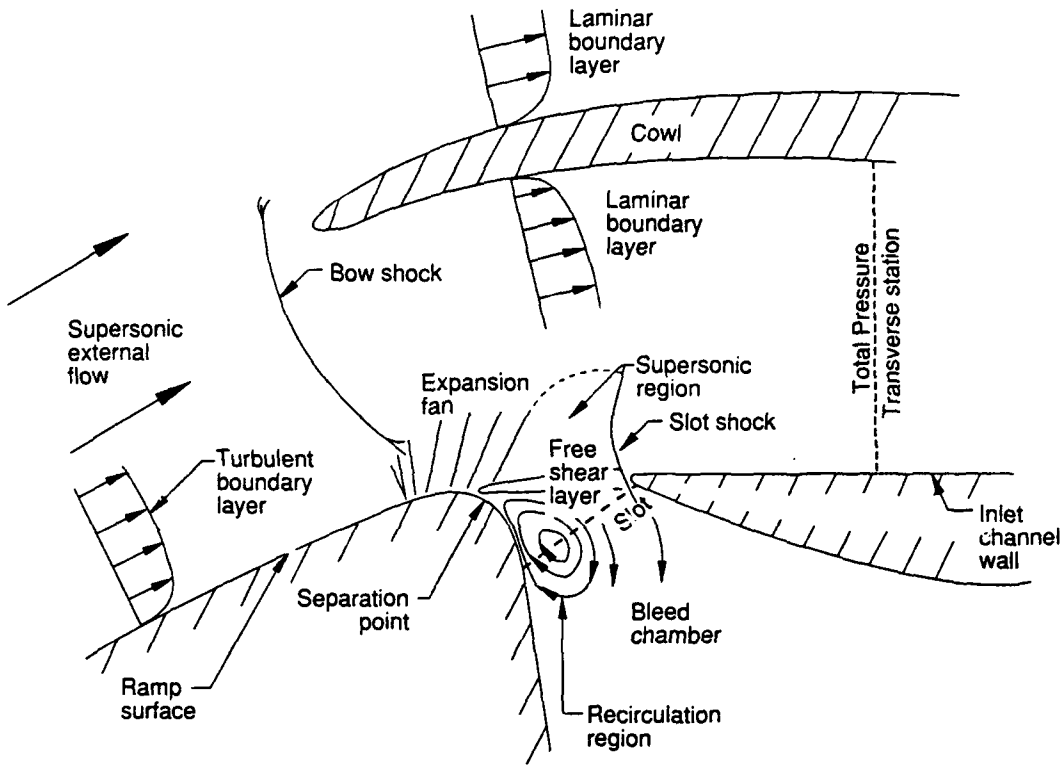

Figure A–1. Inlet-Aperture Flow Field Features

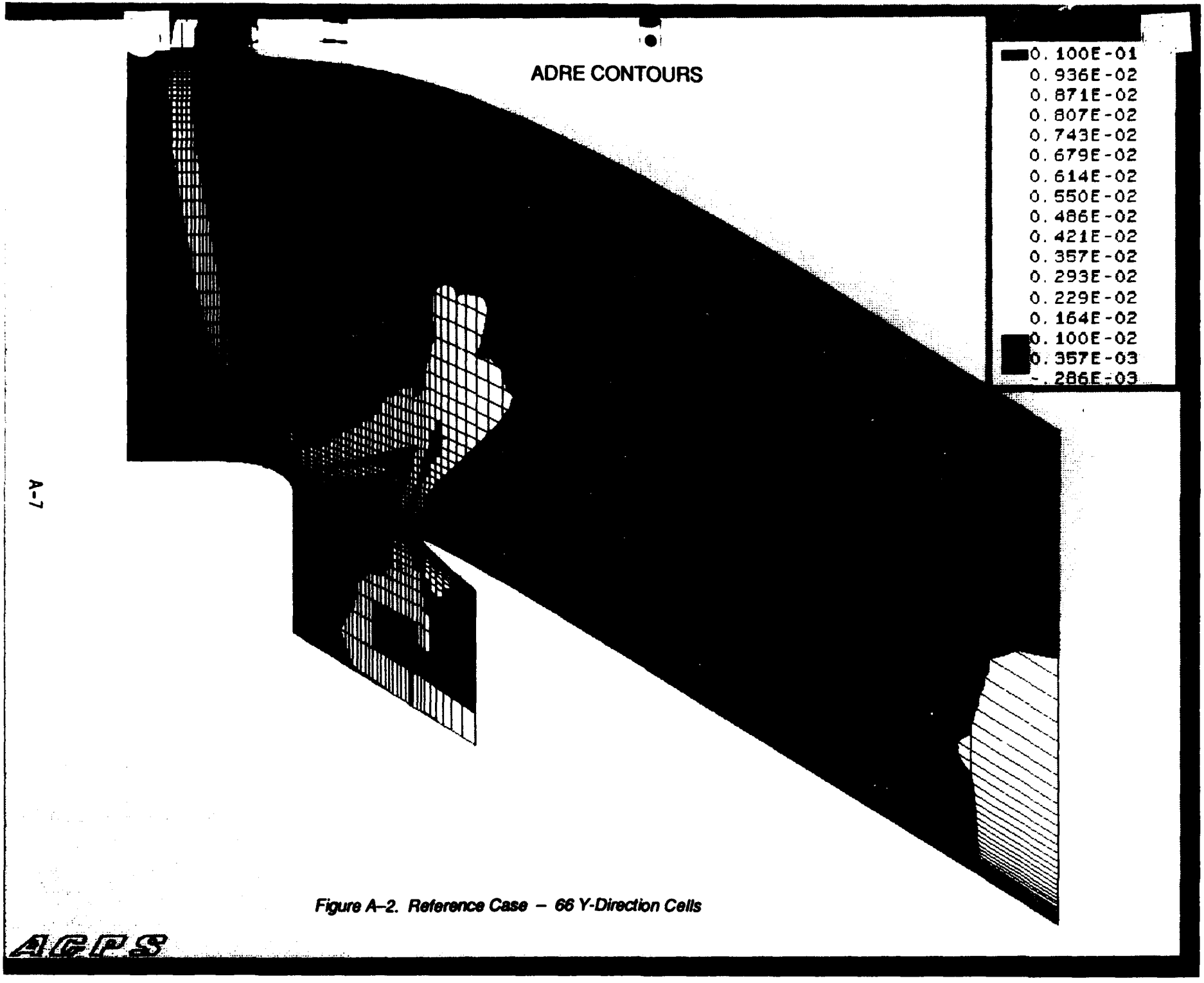

Figure A–2. Reference Case – 66 Y-Direction Cells

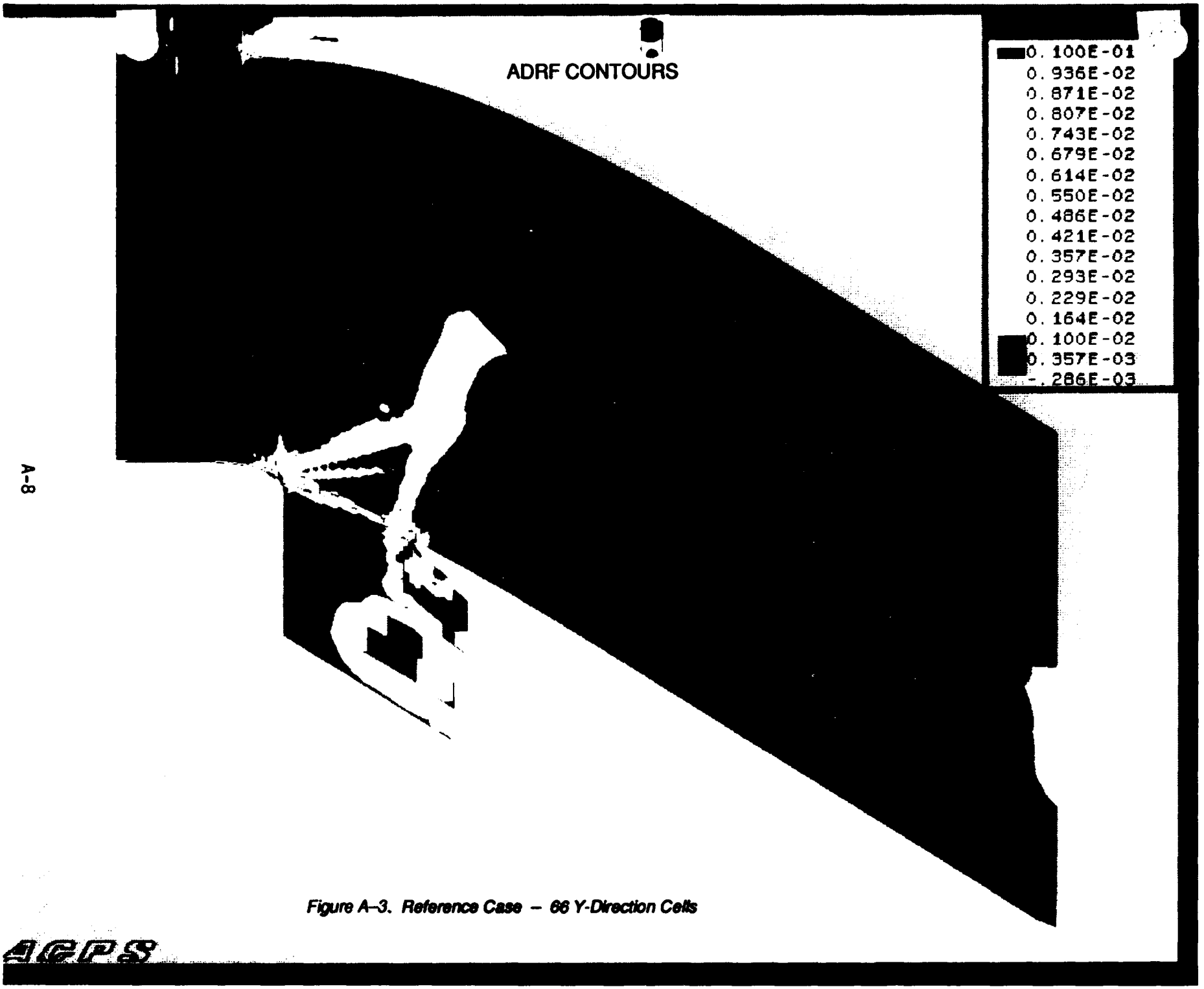

Figure A–3. Reference Case – 66 Y-Direction Cells

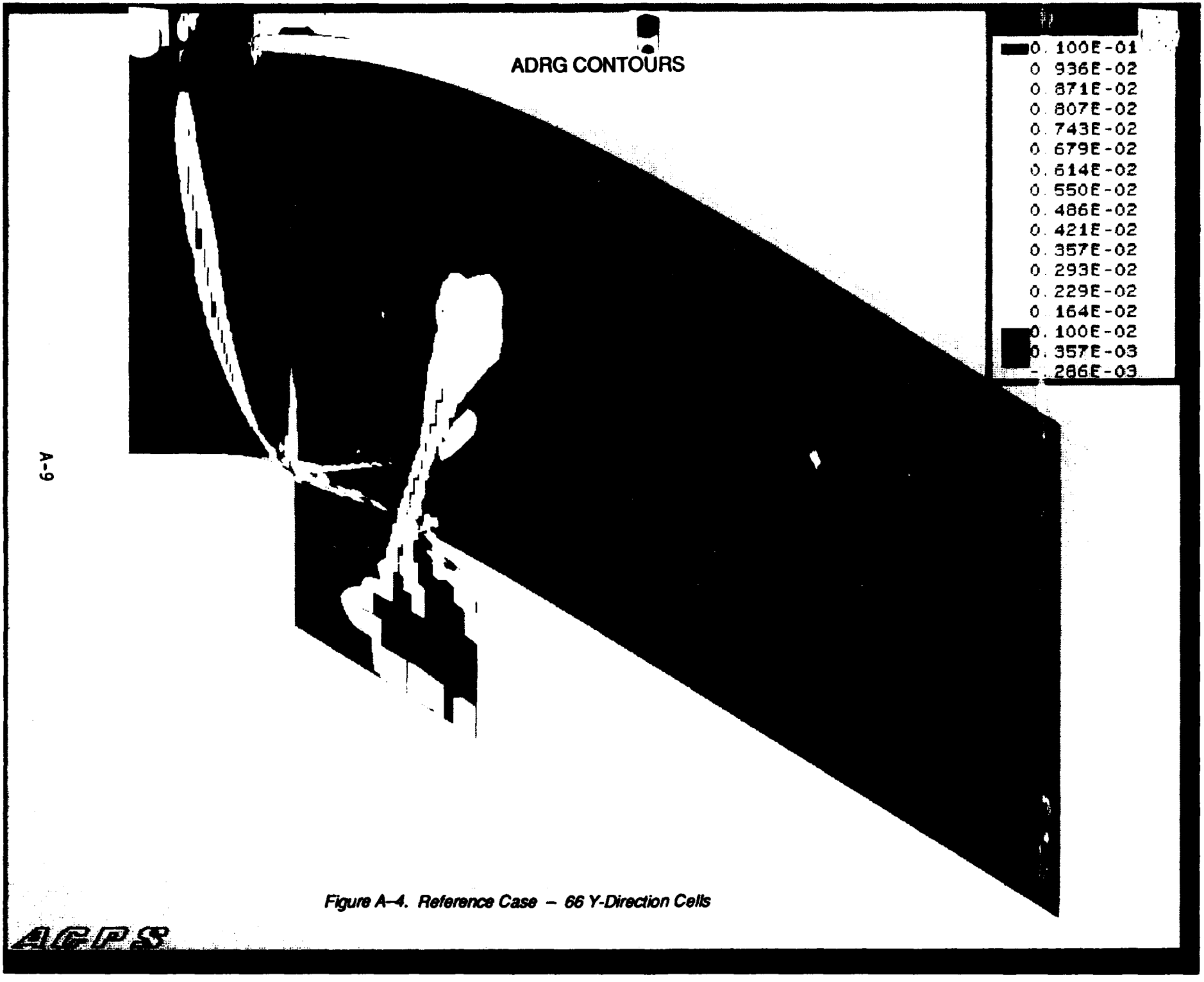

Figure A–4. Reference Case – 66 Y-Direction Cells

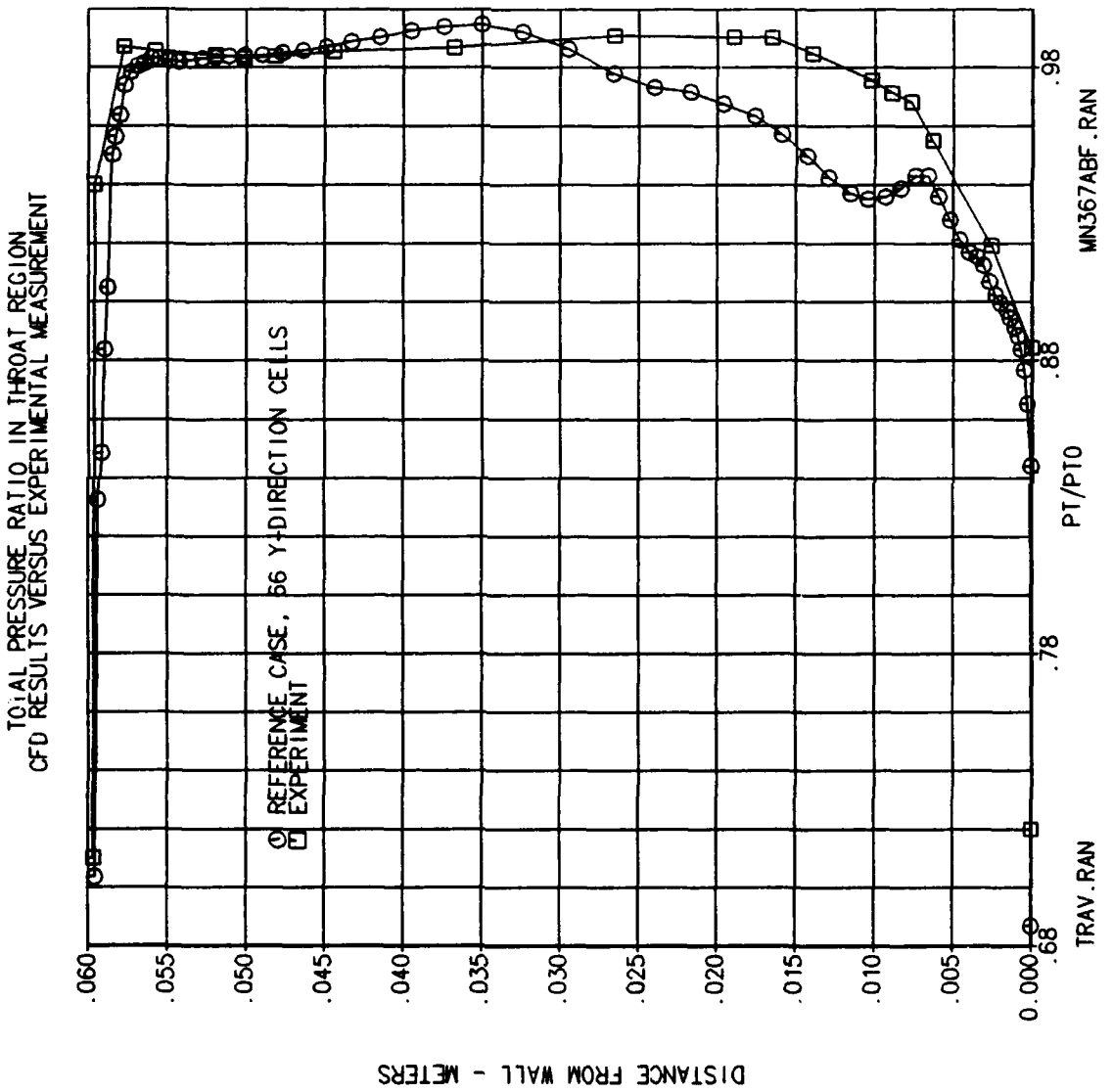

Figure A-5. Total Pressure Comparison – Reference Case vs. Experiment

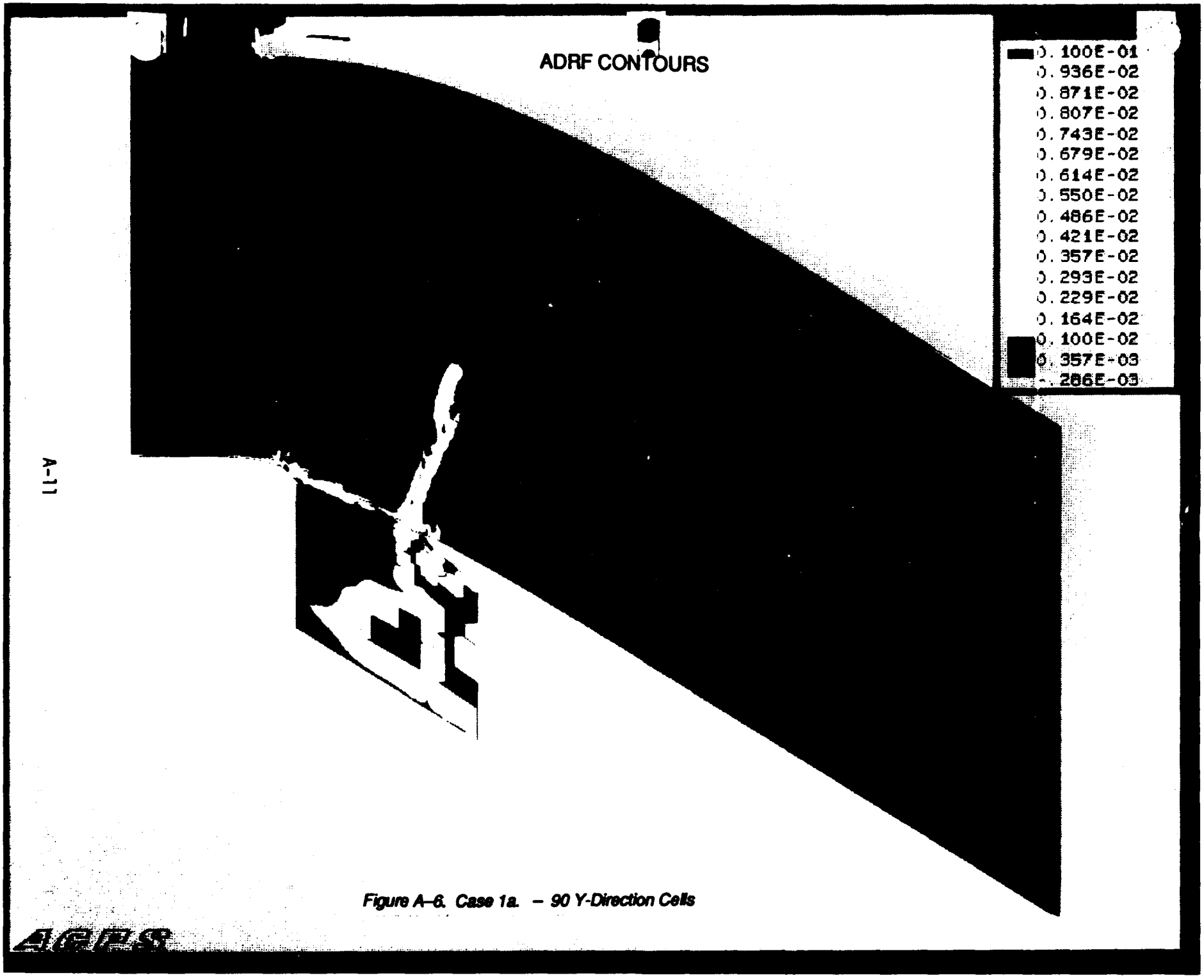

Figure A–6. Case 1a. – 90 Y-Direction Cells

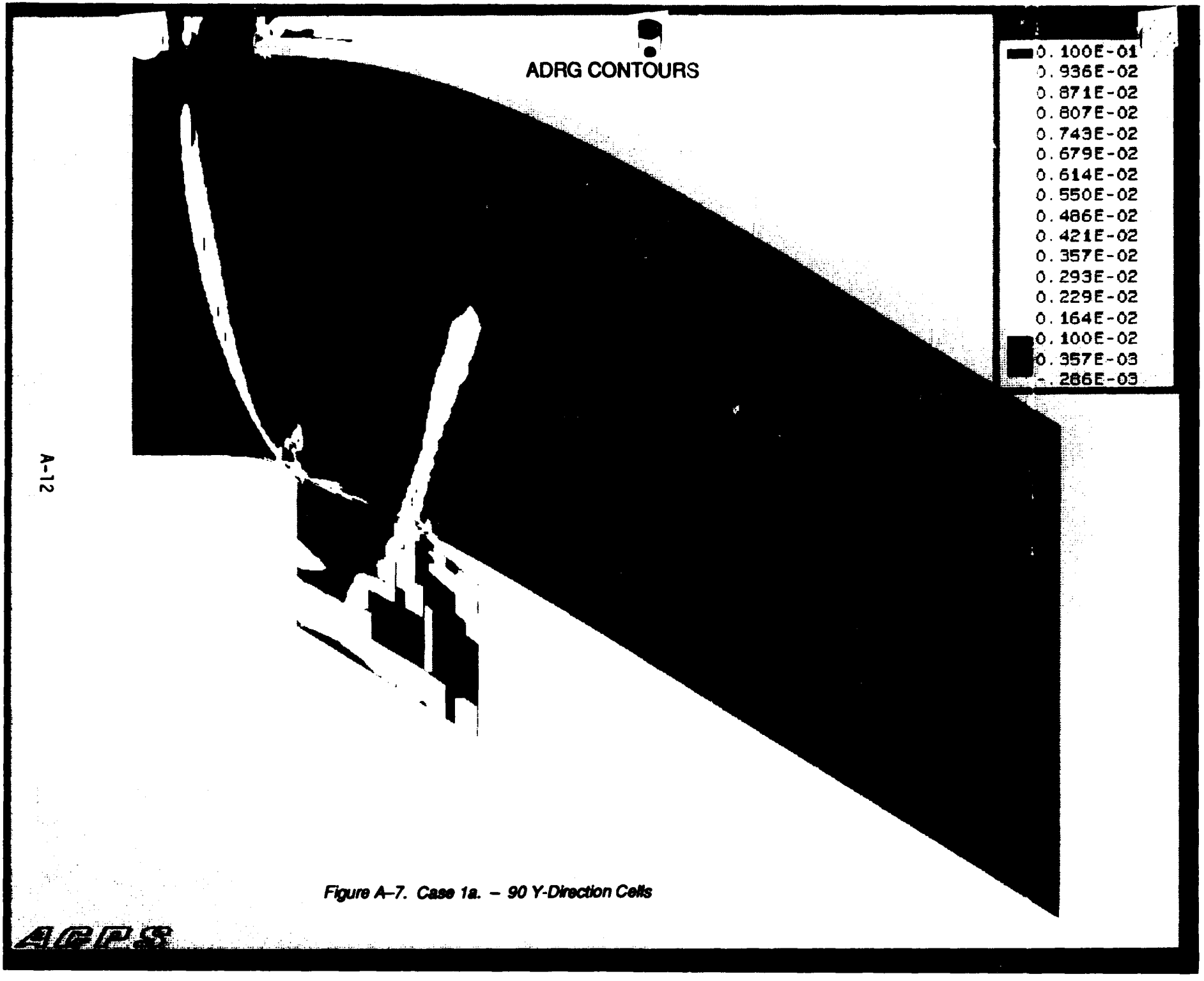

Figure A–7. Case 1a. – 90 Y-Direction Cells

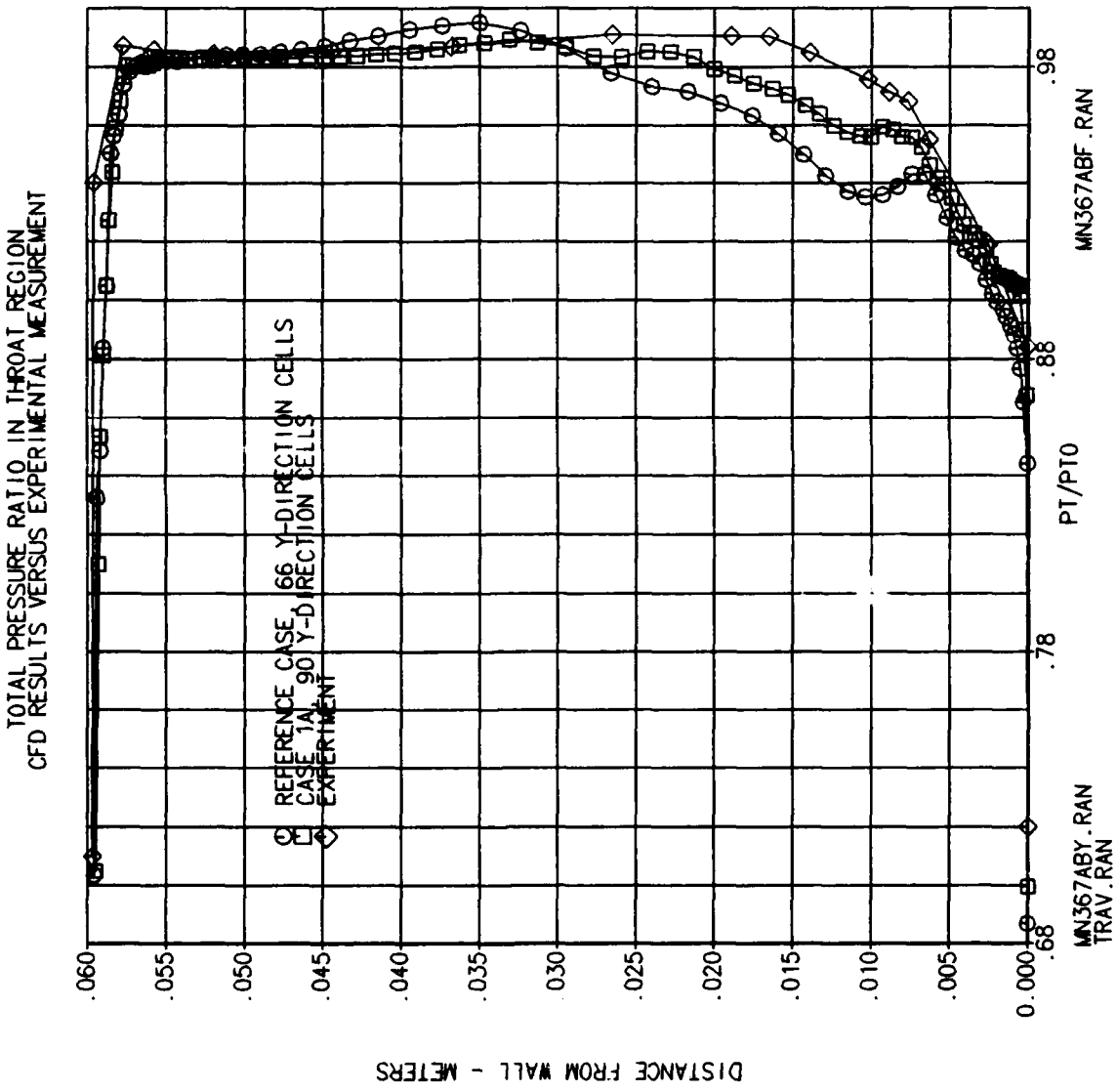

Figure A-8. Total Pressure Comparison – Reference Case and Case 1a.

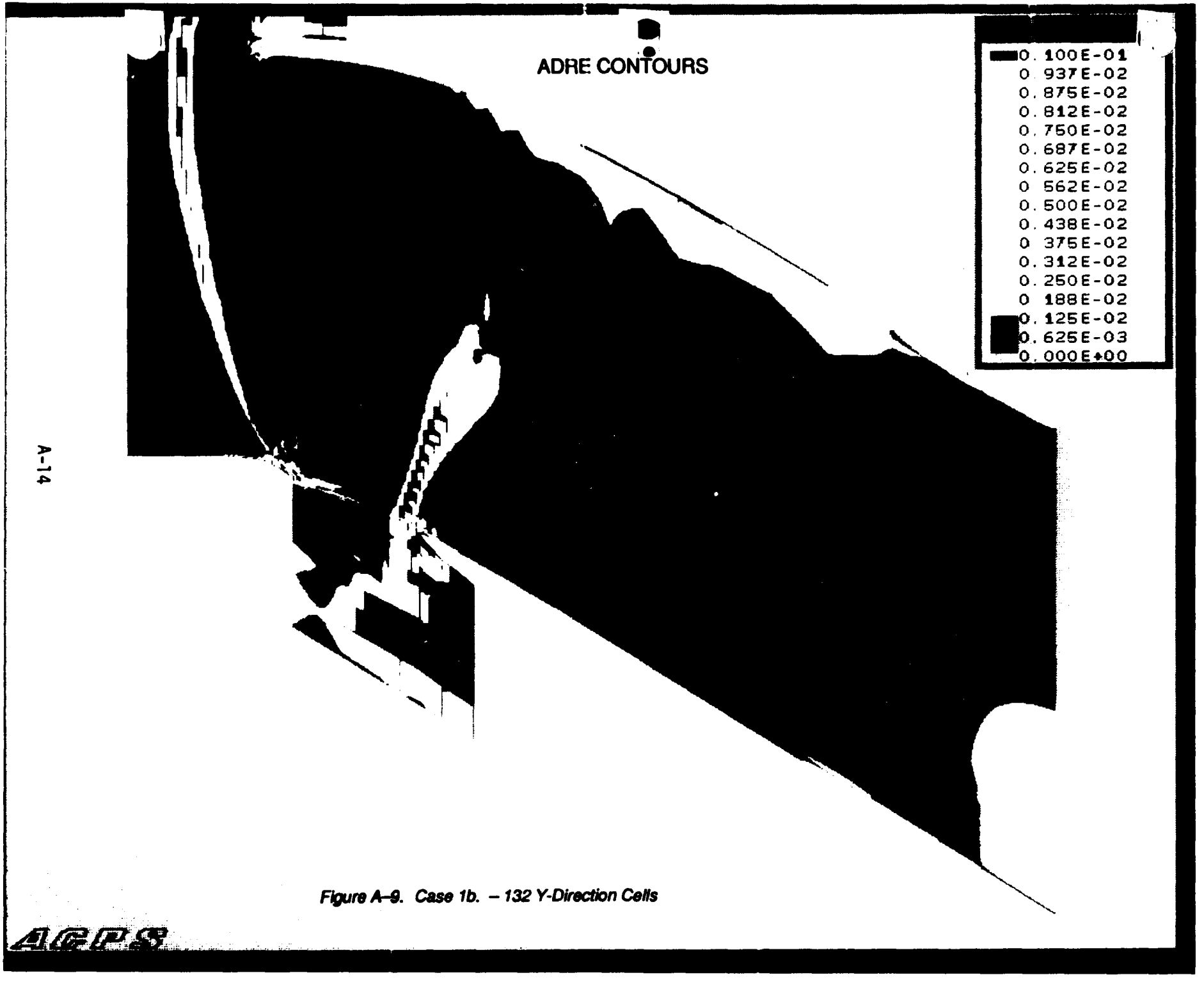

Figure A–9. Case 1b. – 132 Y-Direction Cells

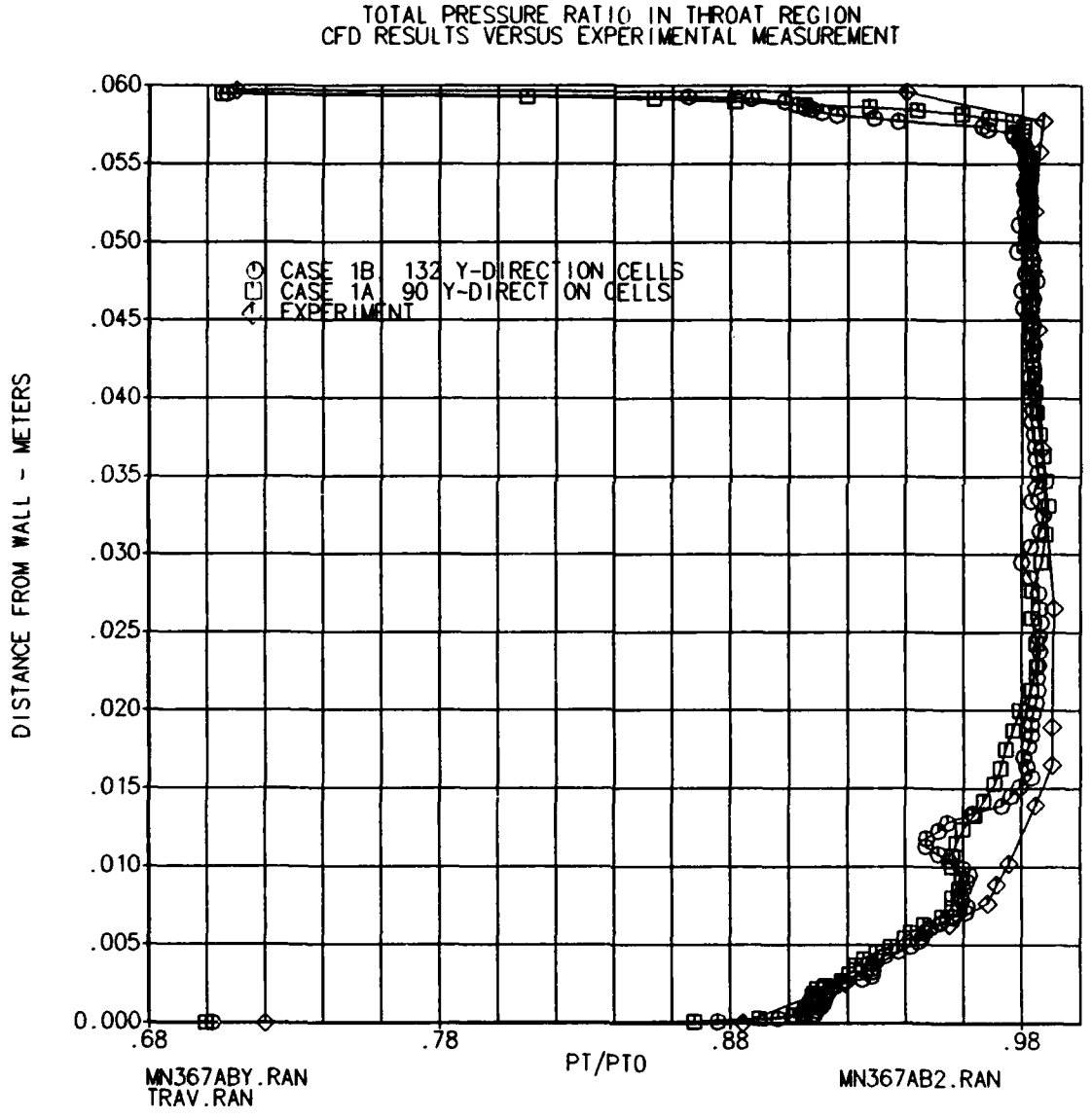

Figure A–10. Total Pressure Comparison – Case 1a. and 1b.

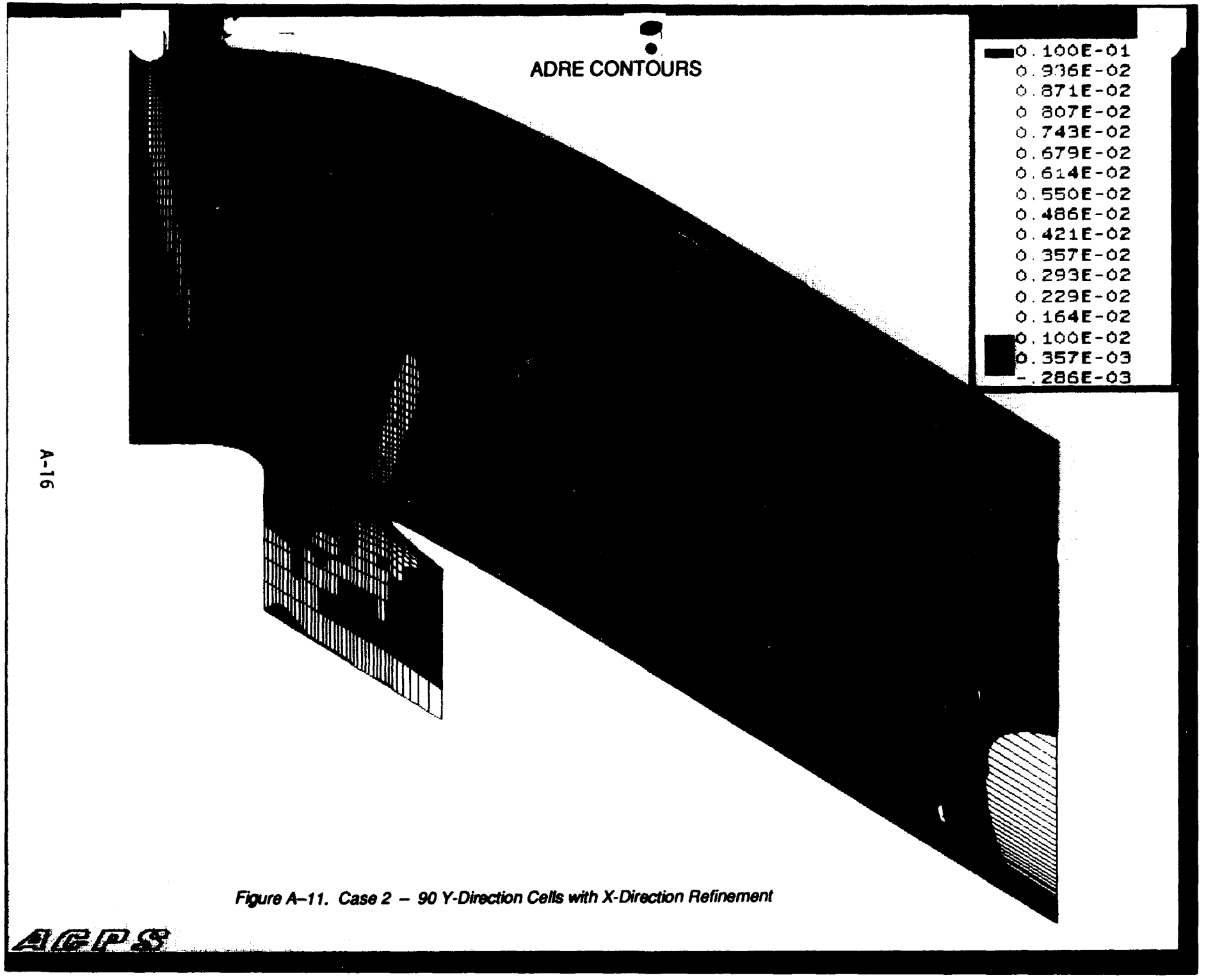

Figure A–11. Case 2 – 90 Y-Direction Cells with X-Direction Refinement

AGPS

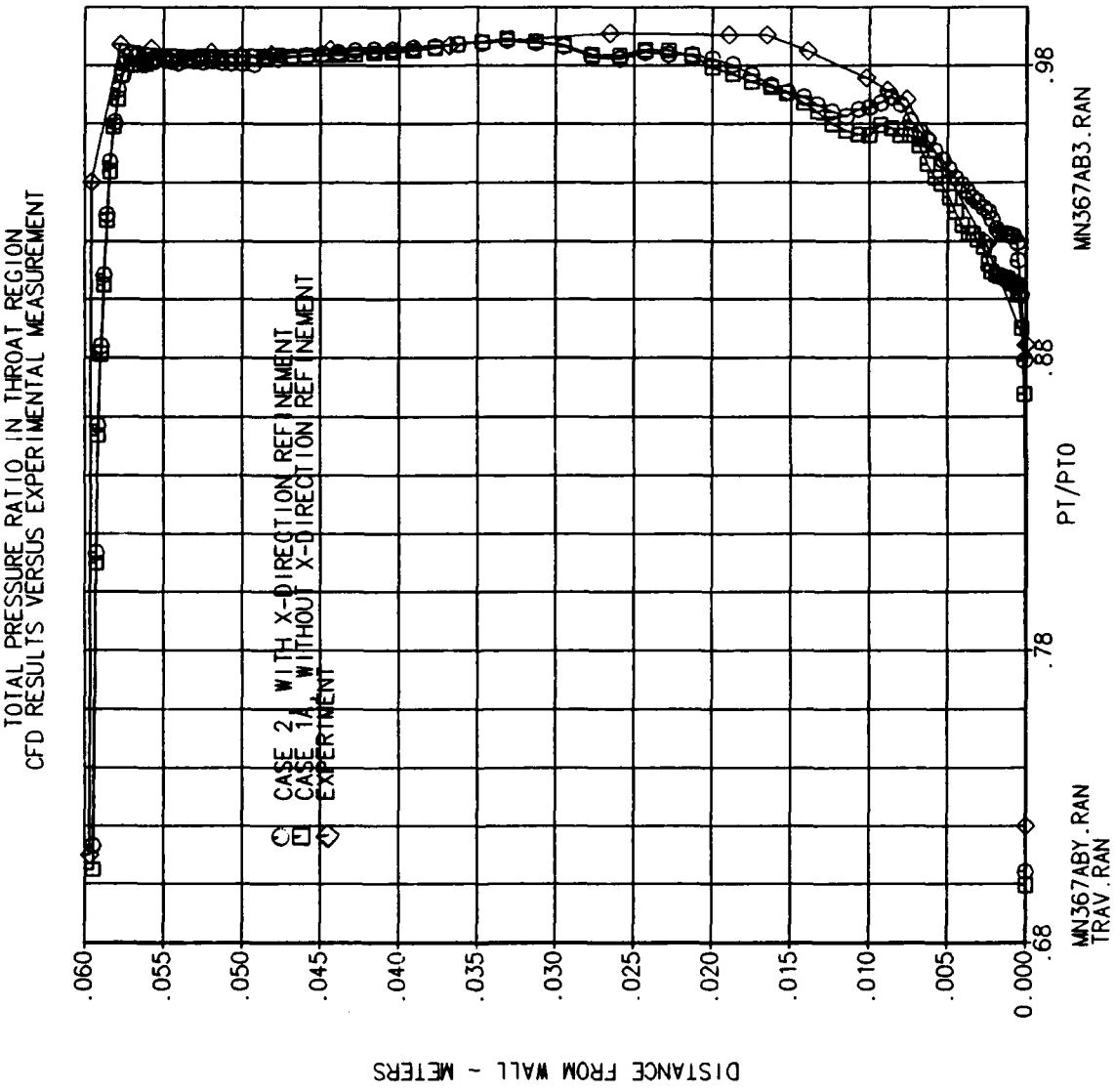

Figure A-12. Total Pressure Comparison – Case 1a. and 2.

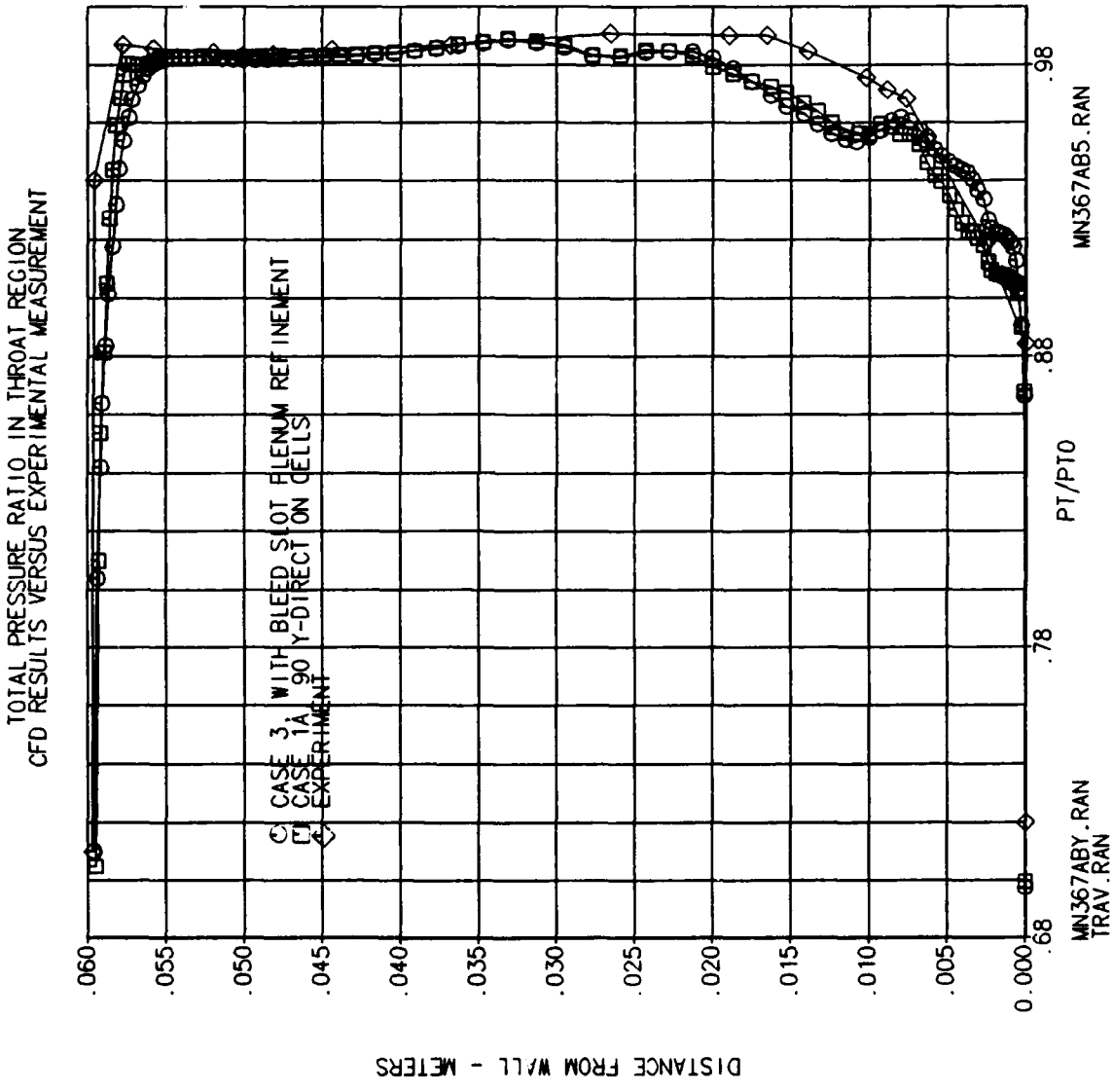

Figure A-13. Total Pressure Comparison – Case 1a. and 3.

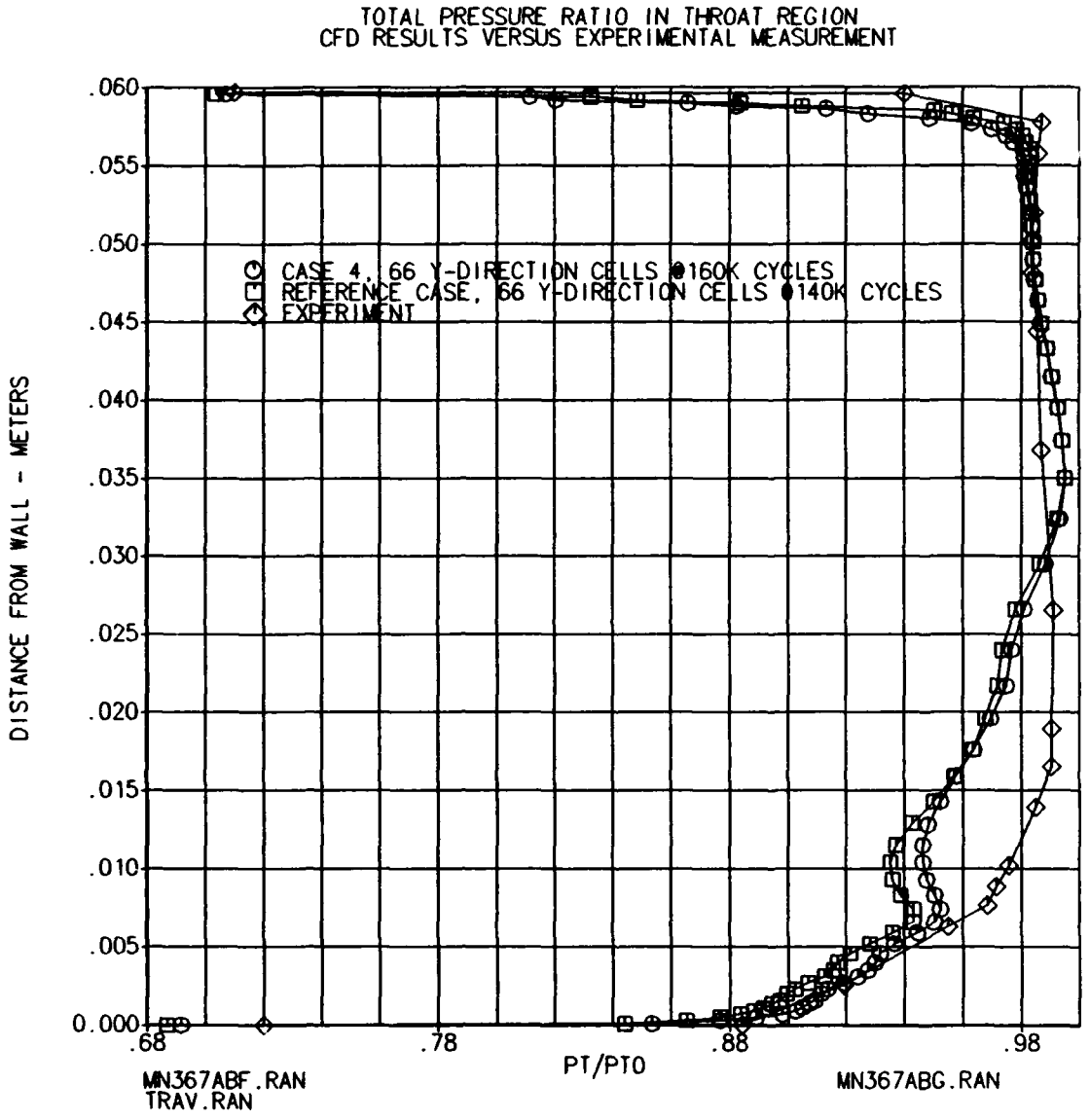

Figure A–14. Total Pressure Comparison – Reference Case and Case 4.

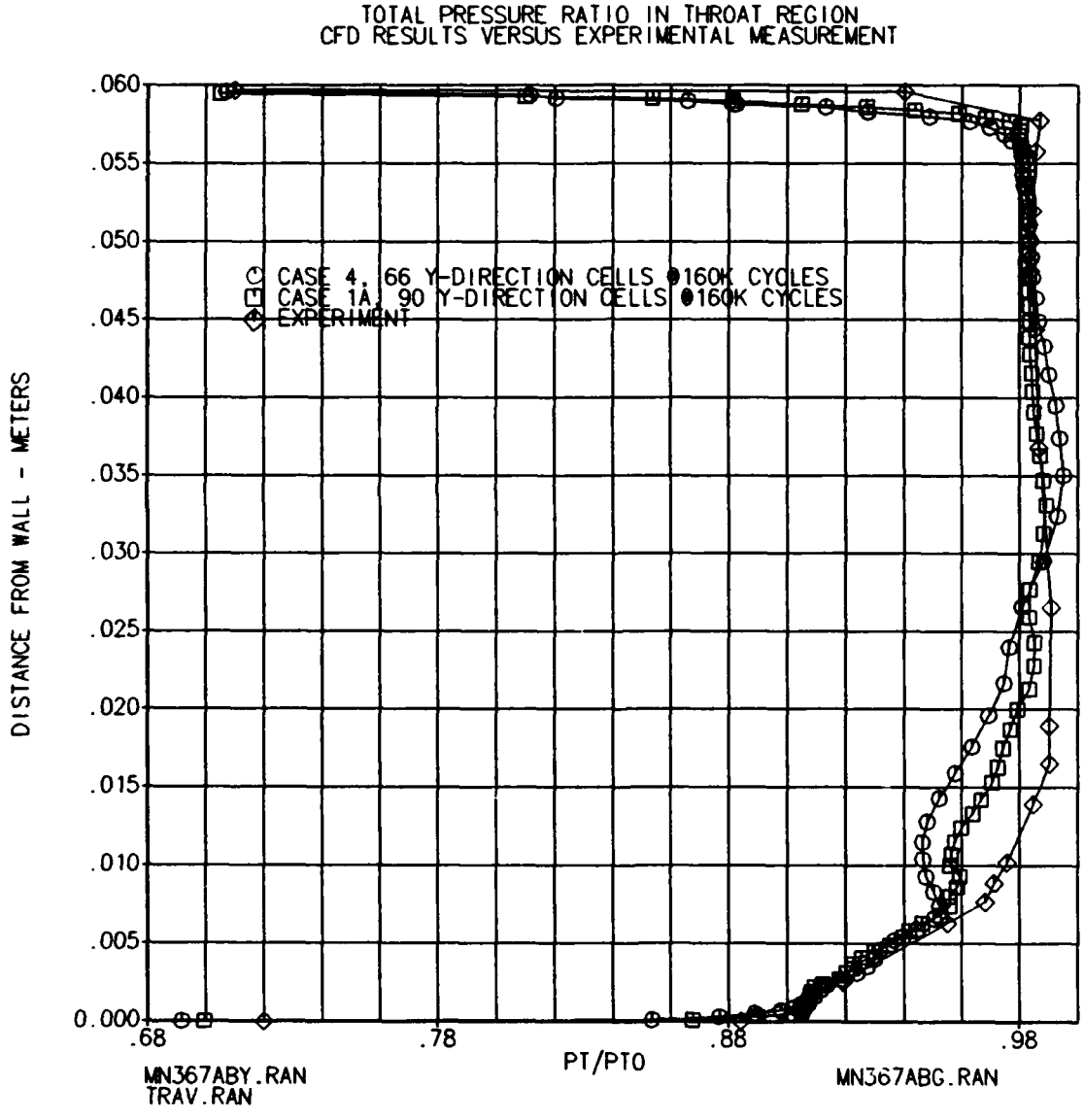

Figure A–15. Total Pressure Comparison – Case 1a. and 4.

APPENDIX B:
Modified Equation Analyses for Spatial Truncation Error Effects in Numerical Solutions of Burgers Equation

by
GC Paynter

1. Summary

The contract effort resulted in the identification of an error monitor, the artificial diffusion ratio, useful for guiding grid adjustment and establishing solution accuracy. A follow-on IRAD study was completed to explore the use of ADR for algorithms other than MacCormack's explicit and to establish a relationship between the ADR level and solution accuracy. The follow-on study used Burgers equation as an analog to the NS equations. As part of this, modified equations were developed for the linear viscous Burgers equation for both the MacCormack explicit and the Beam-Warming implicit algorithms. The modified equation is the finite difference equation written as a sum of the partial differential equation and the truncation error with the lead time derivative terms in the truncation error replaced by spatial derivatives through a manipulation of this equation. The modified equation portion of the follow-on study is reported below. It was found that the lead truncation error term with the MacCormack algorithm is dispersive and that the lead term with the Beam-Warming algorithm is dissipative.

2. Introduction

In Computational Fluid Dynamics (CFD), algebraic approximations to the Navier-Stokes equations (or a subset) are solved for the values of the dependent variables at each point on a grid of points distributed over a flow domain of interest. Defining,

PDE = Partial Differential Equation

FDE = Finite Difference Equation

TE = Truncation Error

Then PDE = FDE + TE

Since it is usually assumed that

FDE = 0,

This implies that we are actually solving,

PDE = TE

Solving the FDE = 0 is thus equivalent to solving the PDE with a nonphysical source term equal to the truncation error.

Truncation error effects can be classified as dissipative, dispersive, or diffusive, as discussed in Anderson, et al. (1984). The truncation

error can be derived from the FDE by substituting Taylor series expansions about a point for the dependent variable values at neighboring points appearing in the FDE. Dissipation, associated with the even derivative terms in the truncation error expression, acts like an "artificial viscosity" to reduce all gradients in dependent variables in the solution. Dispersion, associated with the odd derivative terms in the truncation error, acts to distort the predicted values of dependent variables in the vicinity of wave fronts (like shocks). The combined effects of dissipation and dispersion are referred to as diffusion.

In addition, it is common to introduce explicit "artificial viscosity" into the solution to control dispersive error effects. The problem with this is that adding artificial dissipation to eliminate dispersion introduces a dissipative error of unknown magnitude and thus it has an unknown effect on solution accuracy. The work reported in this appendix addresses the relationship between ADR and solution accuracy through modified equation analyses of the MacCormack and Beam-Warming approximations to the linear Burgers equation.

The remainder of this appendix consists of sections on Burgers equation, the modified equation analyses, a discussion of results, and conclusions. Numerical solutions to Burgers equation using the two algorithms and comparisons between numerical and analytic results to address ADR as a measure of solution accuracy, are reported in Appendix C.

3. Burgers Equation

As noted in Anderson, et al. (1984) Burgers equation is a simple nonlinear analog of the NS equations. Both have an unsteady term, a convective term and a viscous term. The most important difference is that Burgers equation is a scalar equation and the NS equations are a set of vector equations of the same form. Burgers equation is useful for evalution of error monitors because it is recognized as an analog to the NS equations, analytic solutions are available, programming for numerical solutions using a variety of algorithms is simple enough to be feasible, and development of the modified equation for a given algorithm is feasible. The viscous Burgers equation can be written,

$$u_t + E_x = 0 \qquad \text{(B-1)}$$

where,

$$E = F - \mu u_x, \quad F = cu + \frac{bu^2}{2}$$

If $b = 0$, the equation is linear. If $\mu = 0$, the equation is inviscid. If $b = 0$ and $\mu = 0$, the equation becomes the familiar wave equation.

4. Modified Equation Analyses

If the PDE is a function of both space and time, the truncation error associated with an FDE approximation of the PDE is also a function of both space and time. The FDE is an algebraic expression for the value of the dependent variable(s) at a point in the grid at a new time level in terms of the value for the point at the old time level and values at neighboring

points at either old or new time levels. The points involved in the FDE are referred to as the finite difference stencil. An expression for the truncation error of the FDE is obtained by substituting Taylor series expansions for the dependent variable(s) about one of the points in the stencil for the values at the other points into the FDE. As noted in the introduction, this results in an equation of form,

$$PDE - TE = 0$$

When this equation is manipulated to eliminate the lowest order time derivative terms appearing in the truncation error, the resulting equation is called the modified equation. The modified equation suggests the spatial effect of the lead or dominant truncation error terms on the spatial solution.

Because of the complexity, it was impractical to develop modified equations for the nonlinear form of the viscous Burgers equation in the time available for the study. Modified equations are thus reported for the linear form of the viscous Burger's equation, b = 0 in Equation B-1.

4.1 The Modified Equation, MacCormack Algorithm

The MacCormack explicit algorithm, described in Anderson, et al. (1984), uses forward-time forward-space differencing for a predictor step and forward-time backward-space differencing for a corrector step. The values of the dependent variables resulting from the predictor and corrector steps are treated as temporary values at time n and the value of the dependent variable at n+1 is set equal to the average of the values resulting from the predictor and corrector steps. It should be noted that the spatial derivatives in the corrector step are computed using the temporary values of the dependent variable from the predictor step.

With reference to Equation B-1, the predictor step is,

$$\left.\begin{aligned} &\frac{u_j^* - u_j^n}{\Delta t} + \frac{E_{j+1}^n - E_j^n}{\Delta x} = 0 \\ &\text{or,} \\ &U_j^* = U_j^n - \frac{\Delta t}{\Delta x}\left(E_{j+1}^n - E_j^n\right) \end{aligned}\right\} \quad \text{(B-2)}$$

where u* is a temporary value of "u" at n. The corrector step is,

$$\left.\begin{aligned} \frac{u_j^{**} - u_j^n}{\Delta t} + \frac{E_j^* - E_{j-1}^*}{\Delta x} &= 0 \\ u_j^{**} &= u_j^n - \frac{\Delta t}{\Delta x}\left(E_j^* - E_{j-1}^*\right) \end{aligned}\right\} \quad \text{(B-3)}$$

where u** is the temporary value of "u" at n resulting from the corrector step. Averaging the temporary values of "u" resulting from the predictor and corrector steps, the FDE for the value of "u" at n+1 is obtained.

$$u_j^{n+1} = u_j^n - \frac{\Delta t}{2\,\Delta x}\left(E_{j+1}^n - E_j^n\right) - \frac{\Delta t}{2\,\Delta x}\left(E_j^* - E_{j-1}^*\right) \quad \text{(B-4)}$$

Note that E^*_j and E^*_{j-1} are computed using the temporary values of "u" resulting from the predictor step.

Selecting point n,j about which to expand, Taylor series expansions are needed for u^{n+1}_j, E^n_{j+1}, E^*_j, and E^*_{j-1}. When these expansions are substituted into the FDE, Equation B-4, an equation of form PDE - TE = 0 is obtained. As reported by Baldwin, et al. (1977), when this equation is manipulated to eliminate the time derivative terms, the modified equation results.

$$u_t + cu_x - \mu u_{xx} + \frac{c}{6}\left(\Delta x^2 - c^2\Delta t^2\right) u_{xxx} + \ldots \text{HOT} = 0 \quad \text{(B-5)}$$

where HOT = higher order terms

4.2 The Modified Equation, Beam-Warming Algorithm

From Anderson, et al. (1984), the Beam-Warming algorithm for Equation B-1 can be written,

$$\frac{u_j^{n+1} - u_j^n}{\Delta t} + \frac{F_{j+1}^n - F_{j-1}^n}{2\cdot\Delta x} + \frac{A_{j+1}^n\left(u_{j+1}^{n+1} - u_{j+1}^n\right) - A_{j-1}^n\left(u_{j-1}^{n+1} - u_{j-1}^n\right)}{2\cdot\Delta x} \quad \text{(B-6)}$$

$$\cdots = \mu\,\overleftrightarrow{\delta}_x^{\,2}\,u_j^{n+1}$$

where,

$$\overleftrightarrow{\delta}_x^{\,2}\,u_j^{n+1} = \frac{\delta_x^2\,u_j^{n+1}}{(\Delta x)^2} = \frac{u_{j+1}^{n+1} - 2u_j^{n+1} + u_{j-1}^{n+1}}{(\Delta x)^2}\,,\quad A = F_u = C$$

The finite difference stencil thus involves points j-1, j, and j+1 at times n and n+1. Selecting point n,j about which to expand, Taylor series expansions are needed for the remaining points in the stencil.

$$
\left.
\begin{aligned}
u_j^{n+1} &= u_j^n + u_t \Delta t + u_{tt} \frac{\Delta t^2}{2} + u_{ttt} \frac{\Delta t^3}{6} + \text{HOT} \\
u_{j+1}^n &= u_j^n + u_x \Delta x + u_{xx} \frac{\Delta x^2}{2} + u_{xxx} \frac{\Delta x^3}{6} + \text{HOT} \\
u_{j-1}^n &= u_j^n - u_x \Delta x + u_{xx} \frac{\Delta x^2}{2} - u_{xxx} \frac{\Delta x^3}{6} + \text{HOT} \\
u_{j+1}^{n+1} &= u_j^n + u_t \Delta t + u_x \Delta x + u_{tt} \frac{\Delta t^2}{2} + u_{tx} \Delta t \cdot \Delta x + u_{xx} \frac{\Delta x^2}{2} \\
&\quad + u_{ttt} \frac{\Delta t^3}{6} + u_{ttx} \frac{\Delta t^2 \Delta x}{2} + u_{txx} \frac{\Delta t \, \Delta x^2}{2} + u_{xxx} \frac{\Delta x^3}{6} + \text{HOT} \\
u_{j-1}^{n+1} &= u_j^n + u_t \Delta t - u_x \Delta x + u_{tt} \frac{\Delta t^2}{2} - u_{tx} \Delta t \cdot \Delta x + u_{xx} \frac{\Delta x^2}{2} \\
&\quad + u_{ttt} \frac{\Delta t^3}{6} - u_{ttx} \frac{\Delta t^2 \, \Delta x}{2} + u_{txx} \frac{\Delta t \, \Delta x^2}{2} - u_{xxx} \frac{\Delta x^3}{6} + \text{HOT} \\
F_{j+1}^n &= F_j^n + F_x \cdot \Delta x + F_{xx} \frac{\Delta x^2}{2} + F_{xxx} \frac{\Delta x^3}{6} + \text{HOT} \\
F_{j-1}^n &= F_j^n - F_x \Delta x + F_{xx} \frac{\Delta x^2}{2} - F_{xxx} \frac{\Delta x^3}{6} + \text{HOT}
\end{aligned}
\right\} \quad \text{(B-7)}
$$

Restricting the analysis to the linear form of Equation B-1, the FDE can be written,

$$
\begin{aligned}
&\frac{u_j^{n+1} - u_j^n}{\Delta t} + \frac{c \left(u_{j+1}^n + u_{j-1}^n \right)}{2 \cdot \Delta x} + \frac{c \left(u_{j+1}^{n+1} - u_{j+1}^n - u_{j-1}^{n+1} + u_{j-1}^n \right)}{2 \cdot \Delta x} \\
&\quad \ldots = \frac{\mu \left(u_{j+1}^{n+1} - 2 u_j^{n+1} + u_{j-1}^{n+1} \right)}{(\Delta x)^2}
\end{aligned}
\qquad \text{(B-6)}
$$

Substituting the Taylor expansions from Equation B-7 into Equation B-6, an equation of form PDE - TE = 0 is obtained. This may be written,

$$\overbrace{u_t + cu_x - \mu u_{xx}}^{\text{PDE}} + \overbrace{u_{tt}\,\frac{\Delta t}{2} + u_{tx}\,c\,\Delta t + u_{ttt}\,\frac{\Delta t^2}{6}}^{-\text{TE}}$$

$$\underbrace{+ u_{ttx}\,c\,\frac{\Delta t^2}{2} - u_{txx}\,\mu\,\Delta t + u_{xxx}\,c\,\frac{\Delta x^2}{6} + \text{HOT} = 0}_{-\text{TE Continued}} \qquad \text{(B-8)}$$

Note that the TE = 0 (Δt, Δx^2).

The modified equation is obtained for this algorithm by manipulating Equation B-8. This manipulation involves differentiating Equation B-8 with respect to x and/or t and multiplying it by a coefficient such that when it is added to the original equation, a selected time derivative term is eliminated. When this is done in a sequential fashion, time derivative terms up to a selected order are replaced in Equation B-8 by equivalent space derivative terms. Following Anderson (1984) this is done by constructing a table in which the equation across the top of the table is Equation B-8 and the terms listed on the left side are the manipulations performed on a given line of the table to eliminate a time derivative term. When the equations on each line of the table are summed together, the modified equation is the result. Table B-1 shows this manipulation for the Beam-Warming algorithm applied to the linear viscous Burgers equation.

5. DISCUSSION

With rererence to the modified equation for the MacCormack algorithm, the lead truncation error term (the term with the lowest order spatial derivative) involves a third order spatial derivative. This suggests that the dominant truncation error effect should be dispersive. Implicit in this conclusion however is the difficult to prove assumption that the lowest order term is the dominant term. It should be possible to test this assumption for an algorithm by constructing analytic solutions to a model equation with a dispersive error like effect (ringing) near a steep gradient region. This should result in an equation of form,

PDE = SOURCE TERM

as suggested by McDonough (1988). Since the constructed solution represents a solution to the equation,

FDE = 0

This implies that,

PDE = TE and that TE = SOURCE TERM

It should be possible to directly evalute the derivatives of the TE from this equation.

Examination of the modified equation for the linear Burgers equation, approximated using the MacCormack algorithm, reveals that the lowest order term is zero when the Courant number is 1. The numerical results by Mayer, Appendix C, (recall that Mayer solved the nonlinear Burgers equation) indicate that the exact solution is recovered when the Courant number is near 1. The algorithm is unstable when the Courant number is greater than 1.

With reference to the modified equation for the Beam-Warming algorithm, the lead truncation error term involves a second order spatial derivative. This suggests, somewhat suprisingly, that the dominant truncation error effect is dissipative and that the magnitude of this term is a function of the time step. It should be noted, however, that a third order term does exist. Numerical results by Mayer, Appendix C, show that when the grid is coarse an oscillation of the solution (a dispersive error effect) occurs near a steep spatial gradient. This suggests that when the grid is coarse, the third order term becomes the dominant term near a strong spatial gradient.

Artificial dissipation as implemented by Forester (1985), and Mayer, Appendix C, is a viscous like term added to the FDE to control a dispersive error effect in the solution. This term is typically the product of an artifical viscosity and a second derivative of a dependent variable. When artificial dissipation is used, instead of solving,

$$FDE = 0$$

the equation being solved is,

$$FDE = AD$$

where AD = artificial dissipation. This implies that ,

$$PDE - TE - AD = 0$$

Thus AD is in effect a source term added to the PDE. The artificial viscosity as implemented by Forester and Mayer is proportional to the second derivative of a dependent variable. Thus, unless a dispersive error is present in the solution, the artificial viscosity and hence the AD are zero. Although AD is added to the FDE to control dispersive error, some dispersive error must be present in the solution to activate the artificial viscosity model.

The sum of the TE and the AD act as a source term in the PDE being solved. AD is at least a partial measure of solution accuracy because in regions of high dispersive error the source term is "large". Thus a solution with a locally high AD would have a locally high source term. A solution with a high area normalized value of AD would be expected to be less accurate than one with a low value of this parameter. Unfortunately, other error mechanisms may be present. If the algorithm has intrinsic dissipation, the source term of the PDE could be high while the AD is low.

A second problem is that the relationship between the magnitude of the source term and the solution accuracy is highly nonlinear, Oran and Boris, 1987. This relationship may also be very problem dependent.

AD would be expected to be most useful for algorithms where the lead TE terms are dispersive and less useful for algorithms with intrinsic dissipation. This hypothesis is supported by the numerical results of Appendix C. In the numerical results, the relationship between the local and integrated error and ADR is obviously weaker for the Beam-Warming algorithm than for the MacCormack algorithm. This is true if the hypothesis is true because of the intrinsic dissipation of the Beam-Warming algorithm. It does not appear feasible to establish a relationship between solution accuracy and AD that is not problem and algorithm dependent.

It should perhaps be noted that while addressing algorithms with intrinsic dissipation as the primary means of controlling dispersive error was not a goal of the present study, the Beam-Warming algorithm does have intrinsic dissipation. It is clear from consideration of the modified equation for the Beam-Warming algorithm that a truncation error could exist although the dispersive error is zero (and hence the AD needed to control it).

6. CONCLUSIONS

Modified equations were developed for the linear viscous Burgers equation for both the MacCormack explicit and the Beam-Warming implicit algorithms. It was found that the lead truncation error term with the MacCormack algorithm is dispersive and that the lead term with the Beam-Warming algorithm is dissipative. A third order dispersive error term was also present with the Beam-Warming algorithm. AD is in effect a source term added to the PDE being solved and for algorithms with high dispersive error it is thus a qualitative measure of solution accuracy. AD would be less useful for algorithms with high intrinsic dissipation. It is clear that a quantitative relationship between AD and solution accuracy would be algorithm and problem dependent.

The Modified Equation. The modified equation for the linear viscous Burgers equation is obtained by manipulation of equation B-8.

Coef. \ B-8	$u_t + cu_x - \mu u_{xx} + \frac{\Delta t}{2} u_{tt} + c\cdot\Delta t\cdot u_{tx} +$	$0\cdot u_{xx} + \frac{\Delta t^2}{6} u_{ttt} + c\frac{\Delta t^2}{2} u_{ttx} - \mu\cdot\Delta t\cdot u_{txx} + c\frac{\Delta x^2}{6}\cdot u_{xxx} + HOT = 0$
$\frac{-\Delta t}{2}(\ )_t$	$-\frac{\Delta t}{2} u_{tt} - c\cdot\frac{\Delta t}{2} u_{tx} +$	$0 - \frac{\Delta t^2}{4} u_{ttt} - c\frac{\Delta t^2}{2} u_{ttx} + \mu\frac{\Delta t}{2} u_{txx} + 0 + HOT = 0$
$-\frac{c\Delta t}{2}(\ )_x$	$-c\frac{\Delta t}{2} u_{tx} - c^2\frac{\Delta t}{2} u_{xx} + 0$	$-c\frac{\Delta t^2}{4} u_{ttx} - \frac{c^2\Delta t^2}{2} u_{txx} + c\mu\frac{\Delta t}{2} u_{xxx} + HOT = 0$
$\frac{\Delta t^2}{12}(\ )_{tt}$	$+\frac{\Delta t^2}{12} u_{ttt} + c\frac{\Delta t^2}{12} u_{ttx} +$	$0 + 0 + HOT = 0$
$c\frac{\Delta t^2}{6}(\ )_{tx}$	$+c\frac{\Delta t^2}{6} u_{ttx} c^2\frac{\Delta t^2}{6} u_{txx} +$	$0 + HOT = 0$
$\left(\frac{\mu\Delta t}{2} + \frac{c^2\Delta t^2}{3}\right)(\ )_{xx}$	$+\left(\mu\frac{\Delta t}{2} + \frac{c^2\cdot\Delta t^2}{3}\right) u_{txx} + c\left(\mu\frac{\Delta t}{2} + \frac{c^2\cdot\Delta t^2}{3}\right) u_{xxx} +$	$HOT = 0$

Summing, $u_t + cU_x - \mu u_{xx} - c^2\frac{\Delta t}{2} u_{xx} + \left[\frac{c\cdot\Delta x^2}{6} + c\mu\frac{\Delta t}{2} + c^3\cdot\frac{\Delta t^2}{3}\right] u_{xxx} + HOT = 0$

Since the lead truncation error term is of 2nd order, the predominant truncation error effect is dissipative.

Table B-1 Manipulations to Obtain the Beaming-Warming Modified Equation for the Linear Viscous Burgers Equation

APPENDIX C:
Evaluation of the Artificial Diffusion Ratio through Numerical Solutions to Burgers Equation

by
DW Mayer

1. SUMMARY

The contract explored a variety of truncation error monitors as guides to grid selection and solution accuracy. One of these error monitors, the artificial diffusion ratio (ADR) seemed to provide a simple means of guiding grid refinement and establishing solution accuracy. The objective of the present study was to determine if ADR is applicable to other algorithms and determine how the solution accuracy is related to ADR.

During the course of this study it was found that

- o solution accuracy is not simply related to ADR thresholds,
- o ADR is useful for defining grid regions that require refinement, and
- o ADR is less useful in defining regions of high grid error for the Briley-McDonald algorithm than for the MacCormack explicit algorithm.

It is recommended that the usefulness of artificial dissipation for algorithms with intrinsic smoothing be investigated and demonstrated. The computer program developed for the present study may be readily adapted for this purpose. These follow-on studies should include a modified equation analysis to define the lead truncation error terms for the algorithm and model equation. An analytic solution could be used to directly evaluate these terms. A detailed study of these terms relative to the present (or alternate) definitions of ADR should provide valuable insight and guidance to using ADR for assessing solution accuracy.

The objective of the work presented in this appendix was to determine if ADR is applicable to other algorithms and how the solution accuracy is related to ADR. This appendix presents details on Burgers equation including an analytic solution, finite difference formulations of the two solution algorithms, ADR definitions for each algorithm, and results of numerical solutions compared with ADR levels and measures of solution accuracy. The final section discusses the major conclusions of this study and suggests promising avenues for future investigation. The modified equation analysis of the two algorithms is reported in Appendix B.

2. BURGERS EQUATION

Burgers equation is a simple nonlinear analog of the NS equations; it contains an unsteady term, a convective term and a viscous term. Burgers equation is useful for evaluation of error monitors because it is recognized

as an analog to the NS equations, analytic solutions are available, programming for numerical solutions using a variety of algorithms is straightforward, and development of the modified equation for a given algorithm is feasible.

2.1 Generalized Burgers Equation Formulation

The generalized Burgers equation may be written in a form consistent with the usual representation of the NS equations as follows:

$$\frac{\partial U}{\partial t} + \frac{\partial E}{\partial x} = 0 \qquad \text{(C-1)}$$

where,

where

$$U = u, \quad E = F - \mu \frac{\partial u}{\partial x}, \quad F = cu + \frac{bu^2}{2} \qquad \text{(C-2)}$$

u is the velocity, μ is the fluid viscosity, and c and b are free parameters. Note that if b = 0, the linearized Burgers equation results and if c = 0 and b = 1, the nonlinear Burgers equation is obtained. If μ = 0 the equation is inviscid and if b = 0 and μ = 0 the familiar wave equation is recovered.

2.2 Analytic Solution

If the free parameters b and c are set to 0.5 and -1, respectively, the generalized Burgers equation has the stationary solution (Anderson et al., 1984)

$$u_a = - \frac{c}{b} \left[1 + \tanh \frac{c(x - x_o)}{2\mu} \right] \qquad \text{(C-3)}$$

A plot of the analytic solution is shown in Figure C-1 for several values of μ. Note that this forms a stationary wave that approximates a discontinuity (e.g., a shock wave). This analytic solution was therefore felt to be a good choice for investigations of the error monitor identified during the contract.

3. SOLUTION ALGORITHMS

The MacCormack explicit and the Briley-McDonald implicit algorithms were chosen for the present study. The MacCormack explicit algorithm was selected because the 2D NS code used in the contract work is based on the MacCormack method. The Briley-McDonald algorithm was selected since it is equivalent to the popular Beam-Warming method when applied to Burgers

equation. The numerical results from solution of Burgers equation using these two algorithms, provides a link between the results of the AFOSR contract work and extensions to currently popular Navier-Stokes solvers such as the ARC (Pulliam, 1984) and PARC (Cooper, 1987) series of codes.

The next two sections discuss these algorithms in more detail and provide the mathematical formulations used in the 1D Burgers equation studies.

3.1 MacCormack Explicit Method

The finite-difference expression for MacCormack's explicit predictor-corrector method with a "product" smoother is given by (Anderson et al., 1984)

$$U_i^* = U_i^n - \frac{\Delta t}{\Delta x}\left[(E_{i+1}^n - E_i^n) - (S_{i+1}^n - S_i^n)\right] \qquad \text{(C-4)}$$

$$U_i^{n+1} = \frac{1}{2}\left\{U_i^n + U_i^* - \frac{\Delta t}{\Delta x}\left[(E_i^* - E_{i-1}^*) - (S_i^* - S_{i-1}^*)\right]\right\} \qquad \text{(C-5)}$$

where S represents the artificial dissipation flux at a point. For the NS equations S is defined as

$$S_i^n = \varepsilon\,(|u_i^n| + a_i^n)\,\frac{|P_{i+1}^n - 2P_i^n + P_{i-1}^n|}{(P_{i+1}^n + 2P_i^n + P_{i-1}^n)}\,(U_i^n - U_{i-1}^n) \qquad \text{(C-6)}$$

$$S_i^* = \varepsilon\,(|u_i^*| + a_i^*)\,\frac{|P_{i+1}^* - 2P_i^* + P_{i-1}^*|}{(P_{i+1}^* + 2P_i^* + P_{i-1}^*)}\,(U_{i+1}^* - U_i^*) \qquad \text{(C-7)}$$

and $0 \leq \varepsilon \leq 0.5$

Note that when solving Burgers equation, the pressure, P, is not a dependent variable and the speed of sound, a, is not a solution parameter. Therefore, for this study, velocity was used in place of pressure and the wave speed, c, was used in place of a in the definition of the artificial dissipation flux.

An additive artificial viscosity is thus defined as

$$\mu_{a,i} = \varepsilon\,(\Delta x)\,r\,|u_{i+1} - 2u_i + u_{i-1}| \qquad \text{(C-8)}$$

where $$r = \frac{(|u_i| + c)}{(u_{i+1} + 2u_i + u_{i-1})}$$

The Δx is included in the definition of the artificial viscosity so that $S = \mu_a \partial u/\partial x$ and is comparable to the viscous term $\mu \partial u/\partial x$ contained in E. Also note that the sign on the smoothing terms in Equations C-4 and C-5 have been selected so that they have the same sign as the viscous term in E. This smoother is triggered by oscillations in a numerical solution (a third order or dispersive effect). With an appropriate setting for ε the dissipation added by the smoother will damp the third order dispersion error.

For this study u is ≤ 0 for certain regions of the solution domain (refer to Figure C-1). This condition results in negative or zero values for the artificial viscosity computed from Equation C-8 and causes numerical difficulties. This problem is not normally experienced when using MacCormack's smoother for the NS equations since pressure should be greater than zero throughout the flow field. To overcome this difficulty r was assumed equal to 1 for all conditions. An order of magnitude analysis of r indicates this assumption is approximately correct if the solution is shifted far from the origin. For example, if r is evaluated in a region of the flow where u = 100 then $r \approx 0.25$.

3.2 Briley-McDonald Implicit Method

The Briley-McDonald method is an implicit algorithm with the following finite-difference expression for the generalized Burgers equation (Anderson et al., 1984)

$$\frac{u_i^{n+1} - u_i^n}{\Delta t} + \frac{F_{i+1}^n - F_{i-1}^n}{2\Delta x} + \frac{A_{i+1}^n (u_{i+1}^{n+1} - u_{i+1}^n) - A_{i-1}^n (u_{i-1}^{n+1} - u_{i-1}^n)}{2\Delta x} = \mu \frac{u_{i+1}^{n+1} - 2u_i^{n+1} + u_{i-1}^{n+1}}{(\Delta x)^2} \qquad \text{(C-9)}$$

where

$$A = \frac{\partial F}{\partial u} = c + bu \qquad \text{(C-10)}$$

This method is equivalent to the Beam-Warming method when applied to the Burgers equation. Smoothing was added to this algorithm by replacing μ with $\mu + \mu_a$ where μ_a is defined by Equation C-8. To facilitate the programming of the smoother term, lagged values of u were used in the computation of μ_a.

4. ERROR MONITOR DEFINITION

The contract results indicated that the magnitude of the smoothing term for the MacCormack method may be indicative of the error magnitude. This may be true since

- o the lead truncation error term involves a third order spatial derivative and is dispersive in nature (Appendix B), and
- o the MacCormack smoother adds sufficient artificial dissipation to damp the dispersive effect (i.e., ringing or oscillatory solutions).

Therefore, the magnitude of the smoothing term may be of the same order of magnitude as the lead truncation error term. For the contract effort the error monitor was defined as the ratio of the smoothing flux to the total flux through computational cell faces (Forester and Tjonneland, 1988). This error measure was called the artificial diffusion ratio, ADR. The following sections provide mathematical details on computing ADR for the two solution algorithms chosen for this study.

4.1 ADR for the MacCormack Method

The following definition of the artificial diffusion ratio, ADR, was used during this study and is consistent with the definition used in the AFOSR contract report.

$$ADR = \frac{|(S^n_{i+1} - S^n_i)|}{|(E^n_{i+1} - E^n_i)| + |(S^n_{i+1} - S^n_i)|} \qquad \text{(C-11)}$$

Note that the magnitude of the added artificial smoothing term is compared with the $\partial E/\partial x$ term such that ADR must range between 0 and 1. This definition is for the predictor step. A similar definition may be expressed for the corrector step, but studies have shown that both definitions have essentially the same characteristics. ADR based on the predictor step was used for the AFOSR contract work.

4.2 ADR for the Briley-McDonald Method

The definition of ADR used for the Briley-McDonald method is mathematically more complex than the definition used for MacCormack's method. It is comparable from the standpoint that the magnitude of the artificial smoothing term is compared with the $\partial E/\partial x$ term. Defining

$$F_c = \frac{F^n_{i+1} - F^n_{i-1}}{2\Delta x} + \frac{A^n_{i+1}\,(u^{n+1}_{i+1} - u^n_{i+1}) - A^n_{i-1}\,(u^{n+1}_{i-1} - u^n_{i-1})}{2\Delta x} \qquad \text{(C-12)}$$

$$F_v = \mu \frac{u^{n+1}_{i+1} - 2u^{n+1}_i + u^{n+1}_{i-1}}{(\Delta x)^2} \qquad \text{(C-13)}$$

$$F_s = \mu_a \frac{u^{n+1}_{i+1} - 2u^{n+1}_i + u^{n+1}_{i-1}}{(\Delta x)^2} \qquad \text{(C-14)}$$

then

$$ADR = \frac{|F_s|}{|F_c - F_v| + |F_s|} \qquad \text{(C-15)}$$

This definition is equivalent to the definition of ADR used for the MacCormack method.

5. RESULTS

The methods and the definitions of ADR discussed in the previous sections were programmed into a Fortran code that can be rapidly executed on a Digital Equipment Corporation VAX computer. Graphics files were generated and procedures for automatically generating plots were developed. This level of automation allowed rapid investigation of ADR for the two methods.

The first step was to determine grid spacing and fluid properties that would result in a noisy solution (and thereby trigger the smoother). To avoid stability issues, the following stability criteria suggested by Tannehill (Anderson et al., 1984) was satisfied for all numerical studies presented:

$$\Delta t \leq \frac{(\Delta x)^2}{|A|\Delta x + 2\mu} \qquad \text{(C-16)}$$

The solution for three values of viscosity (μ = 1., 0.1, and 0.01) was computed with the MacCormack method. Time and space steps of 0.1 and 0.5, respectively, were used for these calculations. The numerical and analytic solution results are shown in Figure C-1. The largest value of viscosity did not result in any noise. The intermediate viscosity value resulted in negligible noise. The smallest value of viscosity triggered appreciable noise.

The solution was next recomputed with the Briley-McDonald method to check that the smallest value of viscosity would trigger noise with this method. This result is shown in Figure C-2. Since the smallest value of viscosity triggered noise for both methods this value was used for the remainder of the study.

A simple grid refinement study was next performed for both algorithms. The cases were run first with the smoother turned off and then with the smoother turned on. For the cases with smoothing the smoothing coefficient, ε, was fixed at a value of 0.25. The grid spacing was started at $\Delta x = 2.$ and was reduced by factors of 2 until a grid spacing of $\Delta x = 0.03125$ was reached. Thus, the solution was computed on seven grid levels. For brevity detailed results will only be shown for grid spacings of $\Delta x = 1.$, 0.25, and 0.0625 (i.e., representative coarse, medium, and fine grid results). To avoid stability problems it was necessary to reduce the step size for two of the grids ($\Delta x = 0.0625$ and 0.03125). For consistency all the solutions were run to $t = 10$.

During these calculations several measures of solution error were collected. The objective was to look at these error measures relative to ADR and determine if a correlation between error and ADR exists. The values collected were the %error, ADR, Σerror, ΣADR, peak error, and peak ADR defined as

$$\%\text{error} = 100 \frac{u - u_a}{u_{max} - u_{min}} \tag{17}$$

where u_a, u_{max}, and u_{min} are based on the analytic solution.

$$\Sigma\text{error} = \int_{x_{min}}^{x_{max}} |u - u_a| \, dx \tag{18}$$

$$\Sigma\text{ADR} = \int_{x_{min}}^{x_{max}} \text{ADR} \, dx \tag{19}$$

the peak error and peak ADR are simply the maximum values for the absolute error and ADR computed for a given grid density.

The details of these results for each algorithm are summarized in the next two sections.

5.1 MacCormack Explicit Results

The MacCormack explicit results, without smoothing, are shown in Figures C-3 through C-5. These figures show the results in the sequence of coarse, medium and fine grids, respectively. The top plot in each figure compares the analytic and numerical solutions for the velocity. The middle plot shows the %error. The bottom plot shows the ADR values which are identically zero when smoothing is not used. As expected the range and extent of the error is minimized with improved grid density.

The results with the smoother turned on are shown in Figures C-6 through C-8 (in the same sequence as Figures C-3 through C-5). The extent of the high error region is reduced with improved grid density and the ADR values exhibit a similar behavior. The range of the error seems to be nearly the same for the coarse and medium grids, and increases for the fine grid. The range of the ADR values increases with grid refinement.

Figure C-9 shows the peak error (with and without smoothing) and the peak ADR (with smoothing only) as a function of grid spacing for all the grids investigated. Figure C-10 shows the Σerror and ΣADR as a function of grid spacing. Two features may be noted from these results.

1) There is a relationship between the peak error and peak ADR, but it is not a simple one-to-one correlation (compare the middle and bottom plots in Figure C-9). This means the threshold idea proposed during the contract is not supported by these results. That is, the magnitude of ADR is not directly related to the magnitude of the error in the numerical solution.

2) It is apparent that the use of smoothing is beneficial (compare the top and middle plots in Figures C-9 and C-10). The accuracy (whether measured as peak error or Σerror) is significantly improved for coarse grids. Conversely, the use of the smoother does not significantly impair the result for fine grids. The low error observed for the coarsest grid ($\Delta x = 2$), without smoothing, is probably due to a Courant number and diffusion number effect. For these conditions the truncation error is apparently negligible and a nearly exact solution is recovered. This should be checked by performing a modified equation analysis for the nonlinear Burgers equation.

5.2 Briley-McDonald Implicit Results

The Briley-McDonald implicit results, without smoothing, are shown in Figures C-11 through C-13. These figures show the results in the sequence of coarse, medium and fine grids, respectively. The top plot in each figure compares the analytic and numerical solutions for the velocity. The

middle plot shows the %error. The bottom plot shows the ADR values which are identically zero when smoothing is not used. As expected the range and extent of the error is minimized with improved grid density. This trend is consistent with the trend noted for the MacCormack algorithm.

The results with the smoother turned on are shown in Figures C-14 through C-16 (in the same sequence as Figures C-11 through C-13). The extent of the high error region is reduced with improved grid density and the ADR values exhibit a similar behavior. The results differ somewhat from the MacCormack results since the extent of the high ADR regions are greater for the Briley-McDonald method. The range of the error increases with grid refinement (differing from the trend noted for the MacCormack method where the coarse and medium grid results have nearly the same range of error). The range of the ADR values is nearly the same for the coarse and medium grids, and increases for the fine grid (differing from the trend noted for the MacCormack method where the range of ADR values increased with grid refinement).

Figure C-17 shows the peak error (with and without smoothing) and the peak ADR (with smoothing only) as a function of grid spacing for all the grids investigated. Figure C-18 shows the Σerror and ΣADR as a function of grid spacing. The following features may be noted from these results:

1) A simple relationship between the peak error and peak ADR does not exist (compare the middle and bottom plots in Figure C-17). That is, the magnitude of ADR is not directly related to the magnitude of the error in the numerical solution. Therefore, an ADR threshold is not supported for either the MacCormack or Briley-McDonald method.

2) A weaker relationship exists between the peak ADR and the peak error for the Briley-McDonald algorithm than is observed for the MacCormack algorithm (compare the middle and bottom plots of Figures C-9 and C-17). Similarly, the relationship is weaker between the ΣADR and Σerror (compare the middle and bottom plots of Figures C-10 and C-18).

3) It is apparent that the use of smoothing is beneficial (compare the top and middle plots in Figure C-17 and Figure C-18). The accuracy (whether measured as peak error or Σerror) is significantly improved for coarse grids. Conversely, the use of the smoother does not significantly impair the result for fine grids. The low error observed for the coarsest grid ($\Delta x = 2$), without smoothing, is probably due to a Courant number and diffusion number effect. For

these conditions the truncation error is apparently negligible and a nearly exact solution is recovered. This should be checked by performing a modified equation analysis for the nonlinear Burgers equation.

6. CONCLUSIONS AND RECOMMENDATIONS

In summary, the following conclusions have been drawn from the 1-D Burgers equation results:

- o The ADR threshold as a measure of solution accuracy has not been established. There does exist a correlation between ADR and solution accuracy, but the correlation is more complex than a simple one-to-one relationship. Achieving a given level of ADR does not guarantee a given accuracy level.

- o The use of ADR to pinpoint grid problems has been demonstrated. Regions of the flow where the grid is too coarse to accurately capture gradients results in noise or ringing in the solution. This noise is dispersive in nature, activates MacCormack type smoothers, and results in correspondingly high values of ADR. Therefore, regions of the flow that have relatively high levels of ADR are candidates for further grid refinement.

- o ADR does not pinpoint regions of grid error as well for the Briley-McDonald method. The regions of high ADR cover a greater extent than the regions of relatively high solution error. This means that ADR for the Briley-McDonald method exaggerates the extent of regions that require grid refinement.

This investigation could be readily extended to other algorithms using techniques similar to those describe in this coordination sheet.

The usefulness of ADR for solution algorithms that use intrinsic smoothing (i.e., not added explicitly) has not been demonstrated. The computer program written for the present study may be readily adapted to explore the use of ADR for these and other algorithms.

The results of the modified equation analysis of the MacCormack explicit and Briley-McDonald implicit algorithm (Appendix B) makes it feasible to directly evaluate the lead truncation error terms for an analytic solution. A detailed study of these terms relative to the present (or alternate) definitions of ADR may provide valuable insight and guidance to using ADR for assessing accuracy.

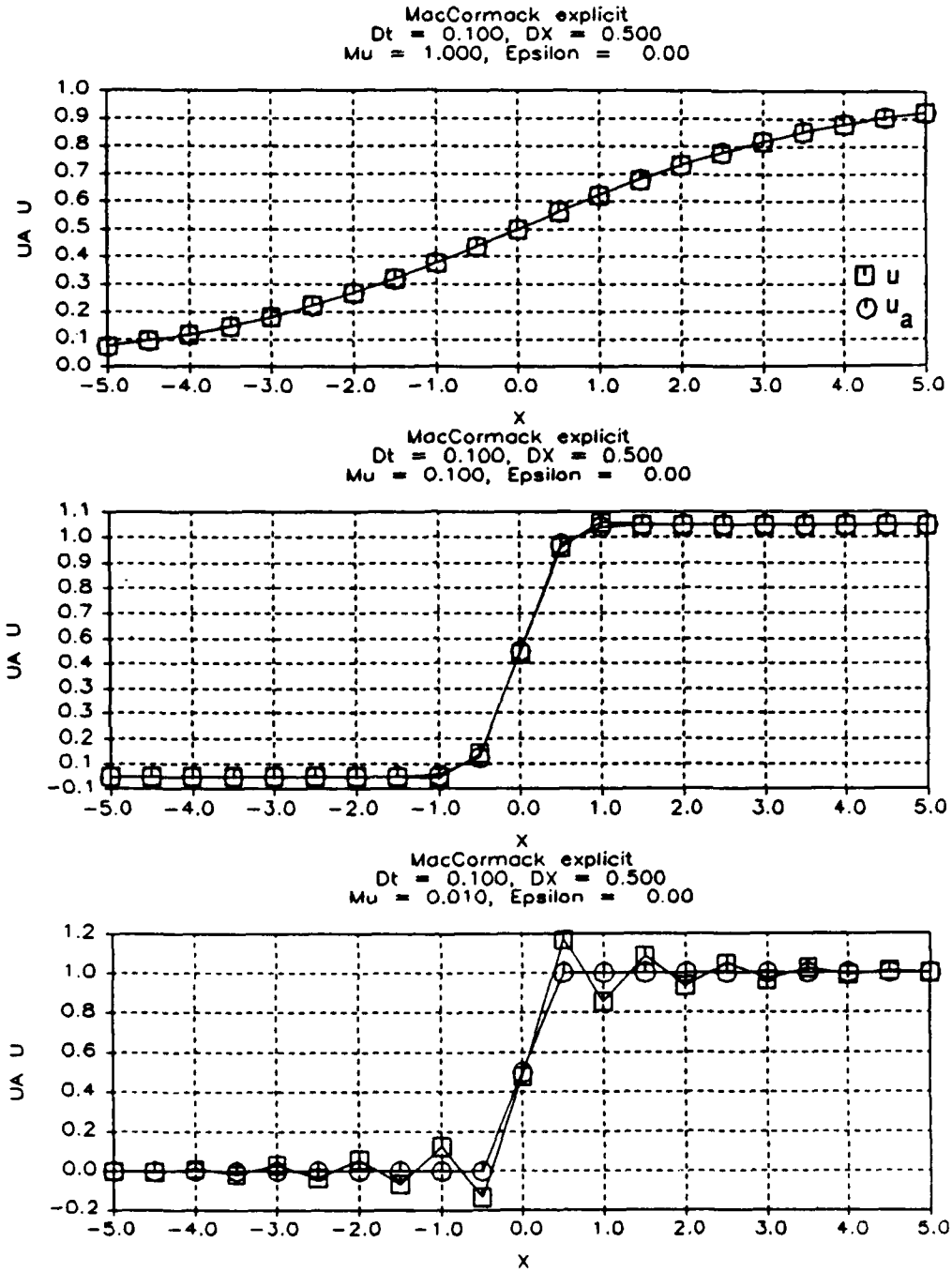

Figure C–1. MacCormack Explicit Results Compared With Analytic Velocity Profiles

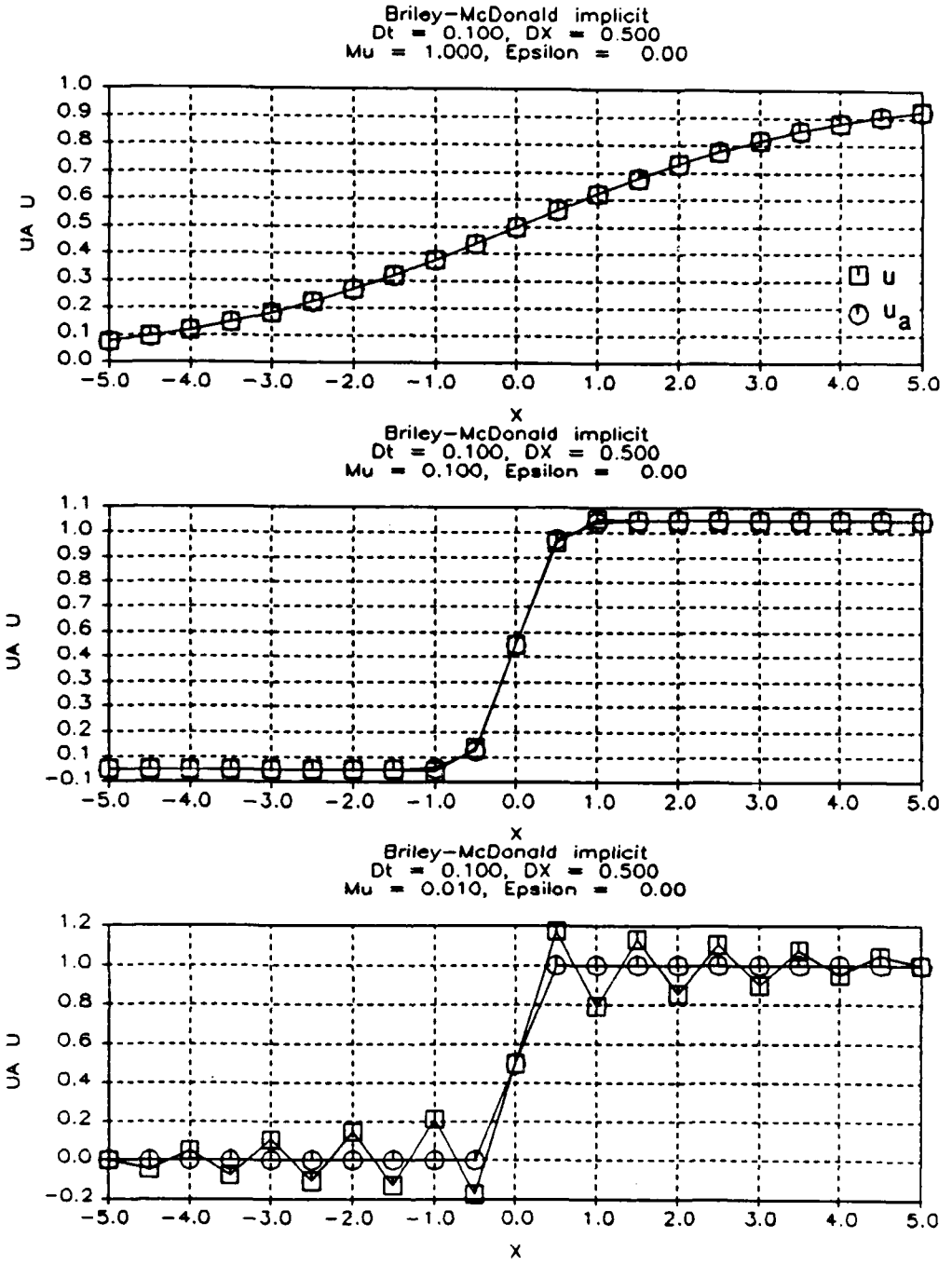

Figure C–2. Briley-McDonald Implicit Results Compared With Analytic Velocity Profiles

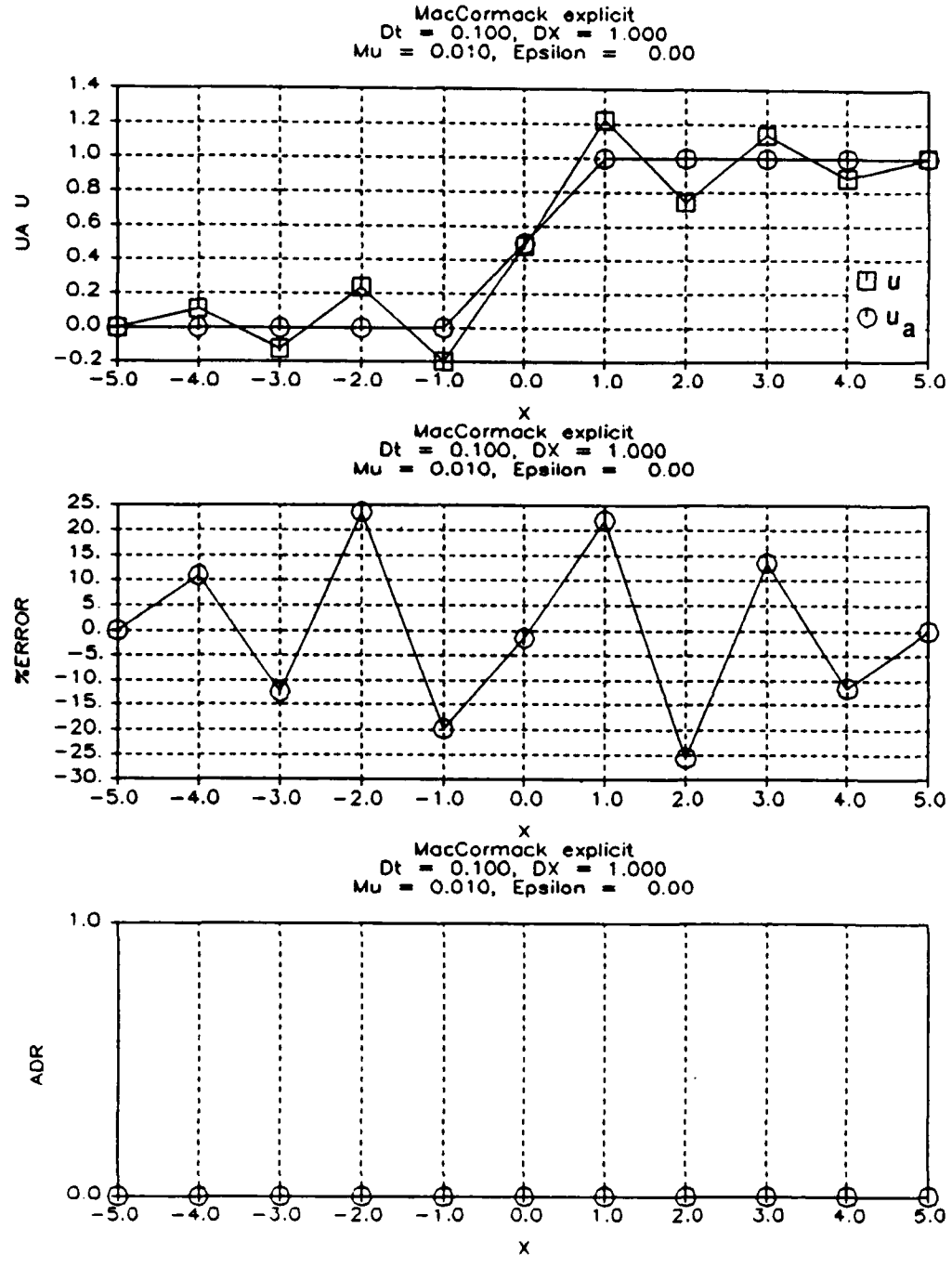

Figure C–3. MacCormack Explicit Results: Coarse Grid, No Smoothing

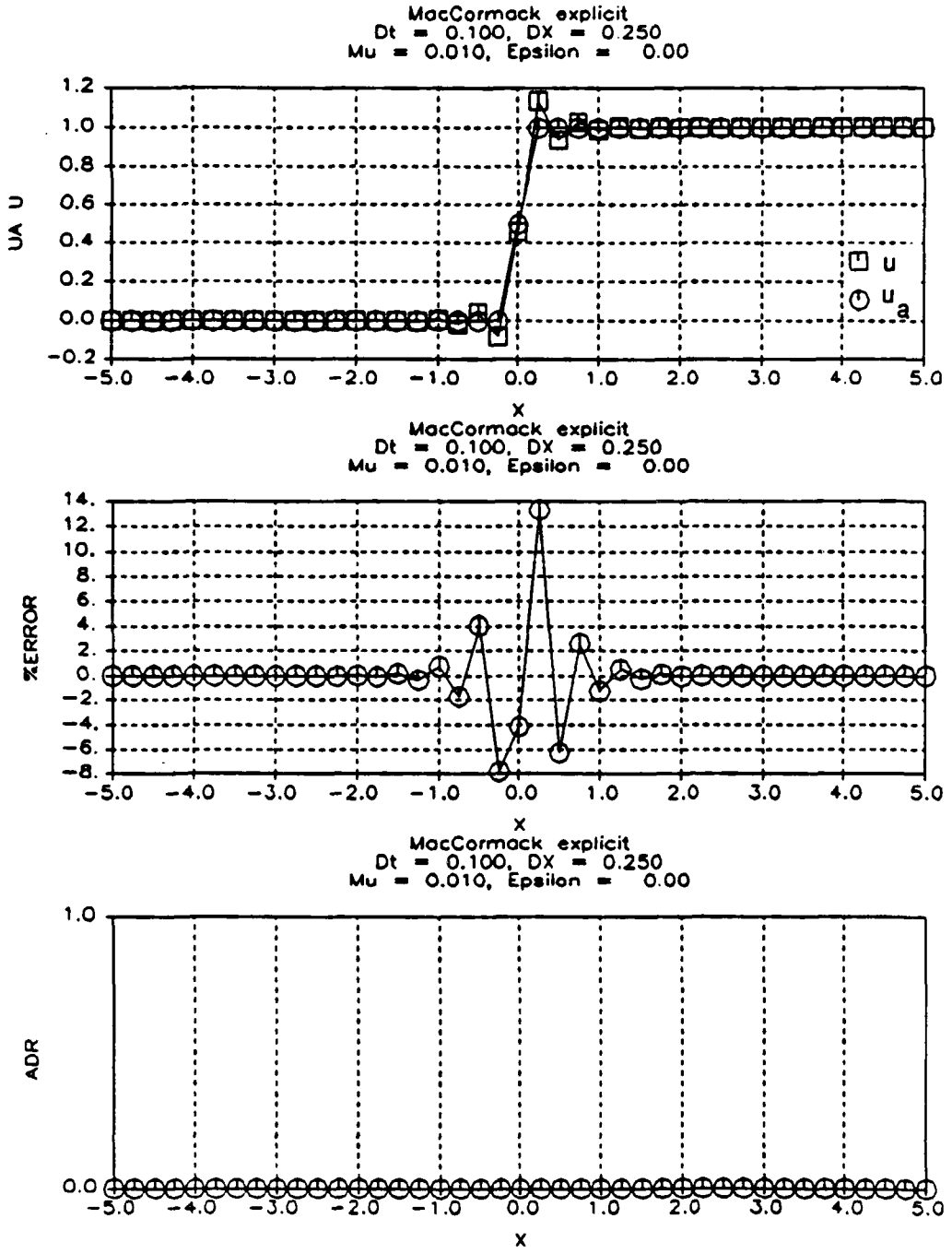

Figure C–4. MacCormack Explicit Results: Medium Grid, No Smoothing

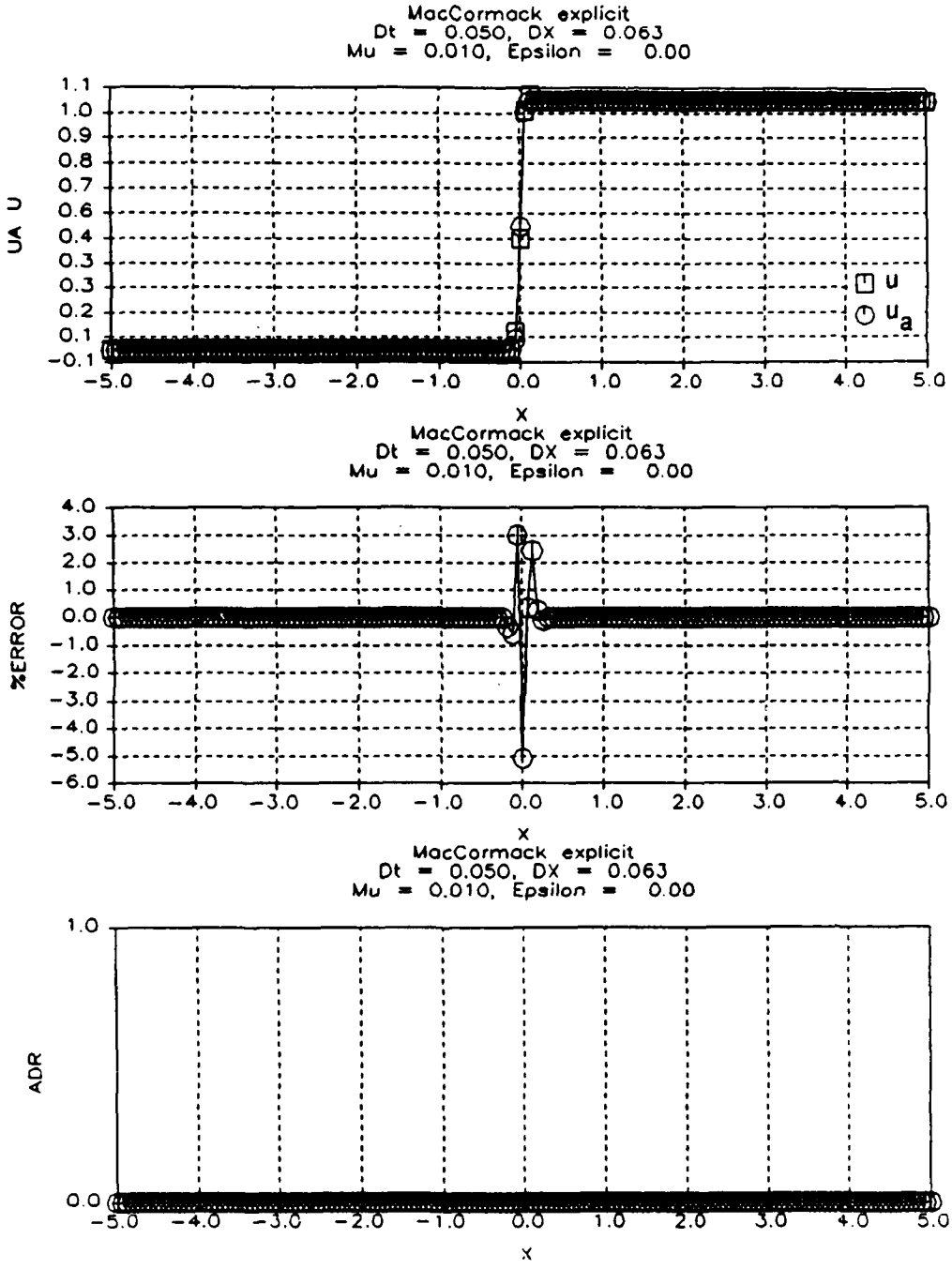

Figure C–5. MacCormack Explicit Results: Fine Grid, No Smoothing

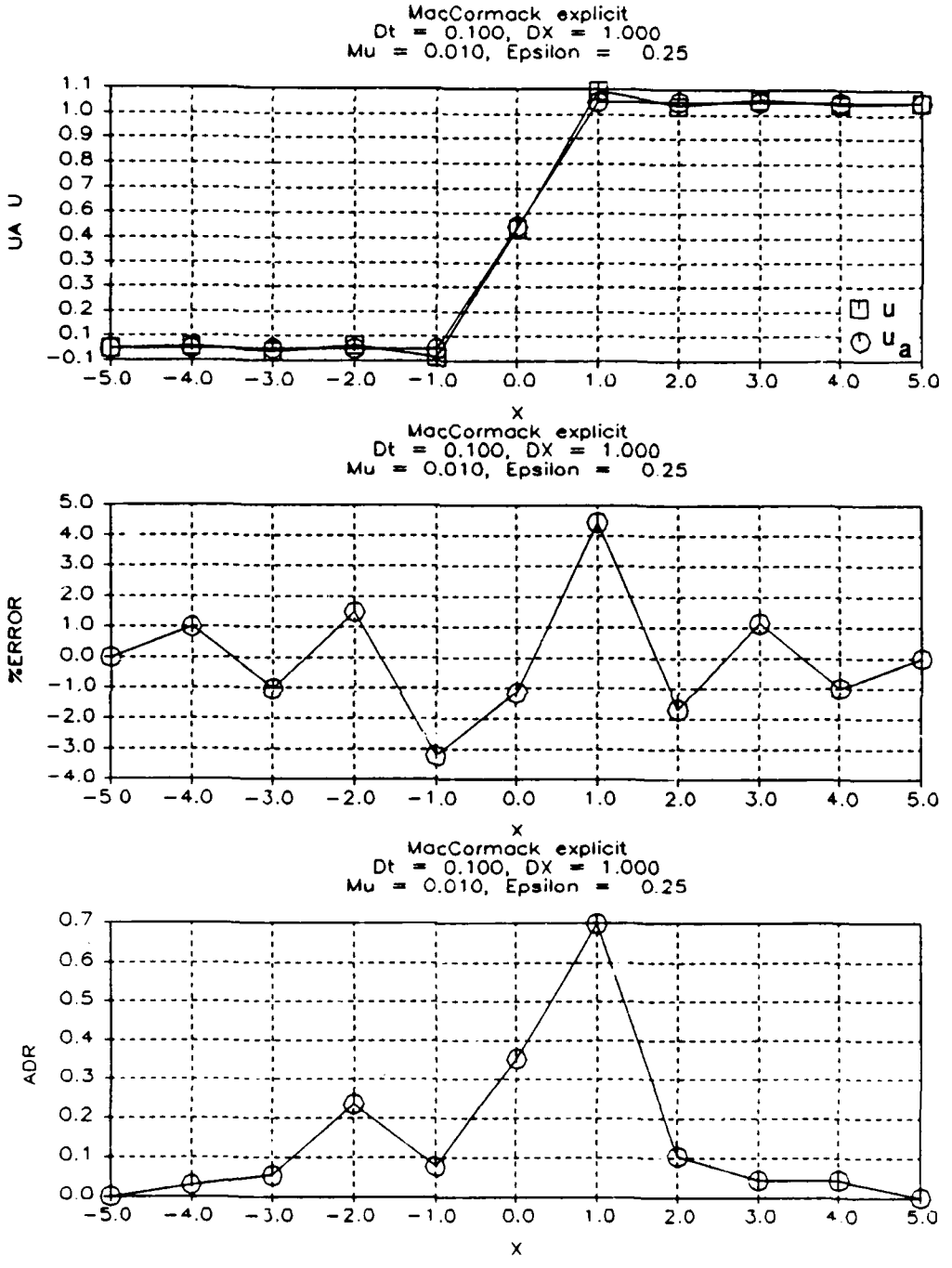

Figure C–6. MacCormack Explicit Results: Coarse Grid, With Smoothing

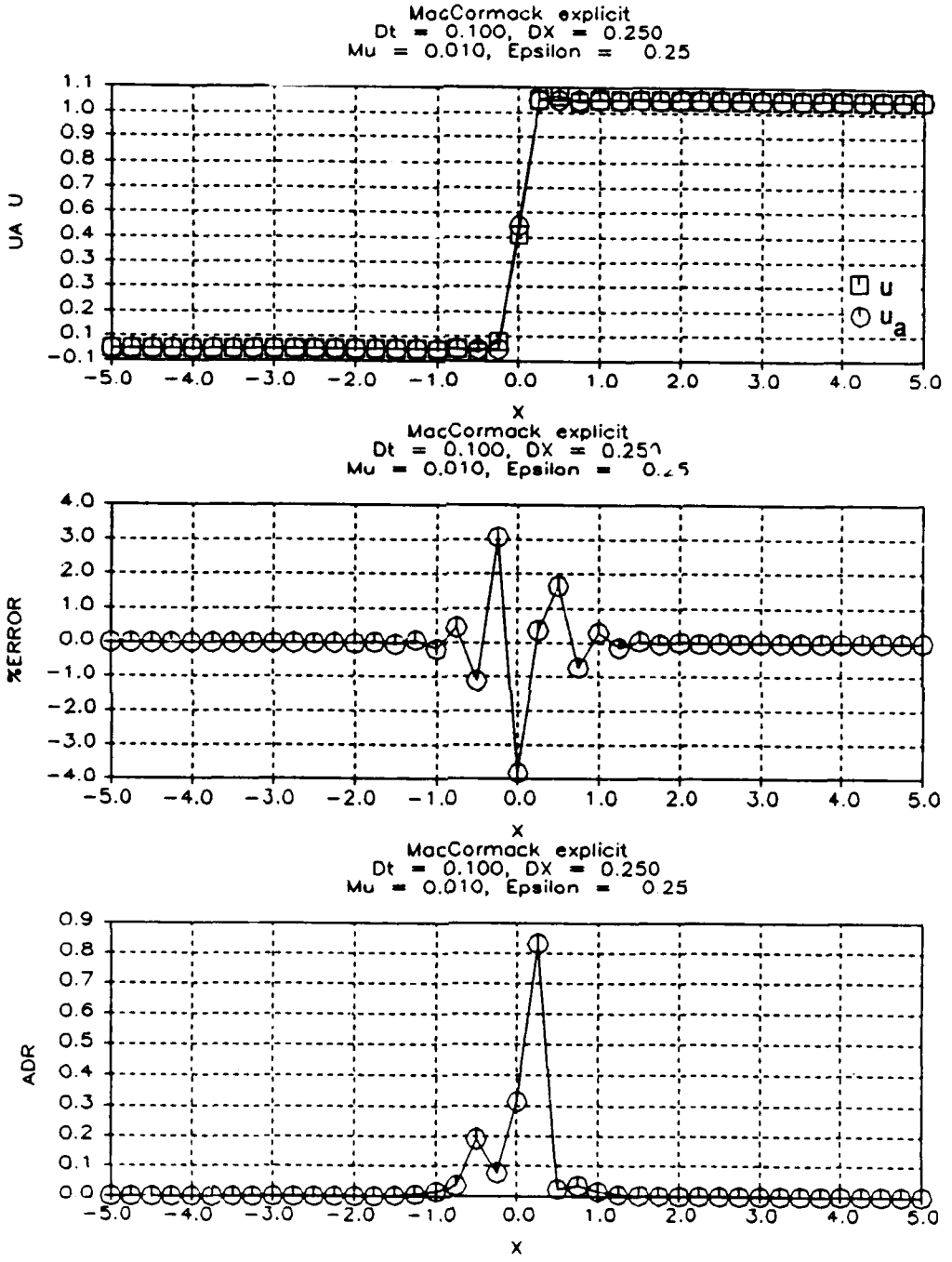

Figure C–7. MacCormack Explicit Results: Medium Grid, With Smoothing

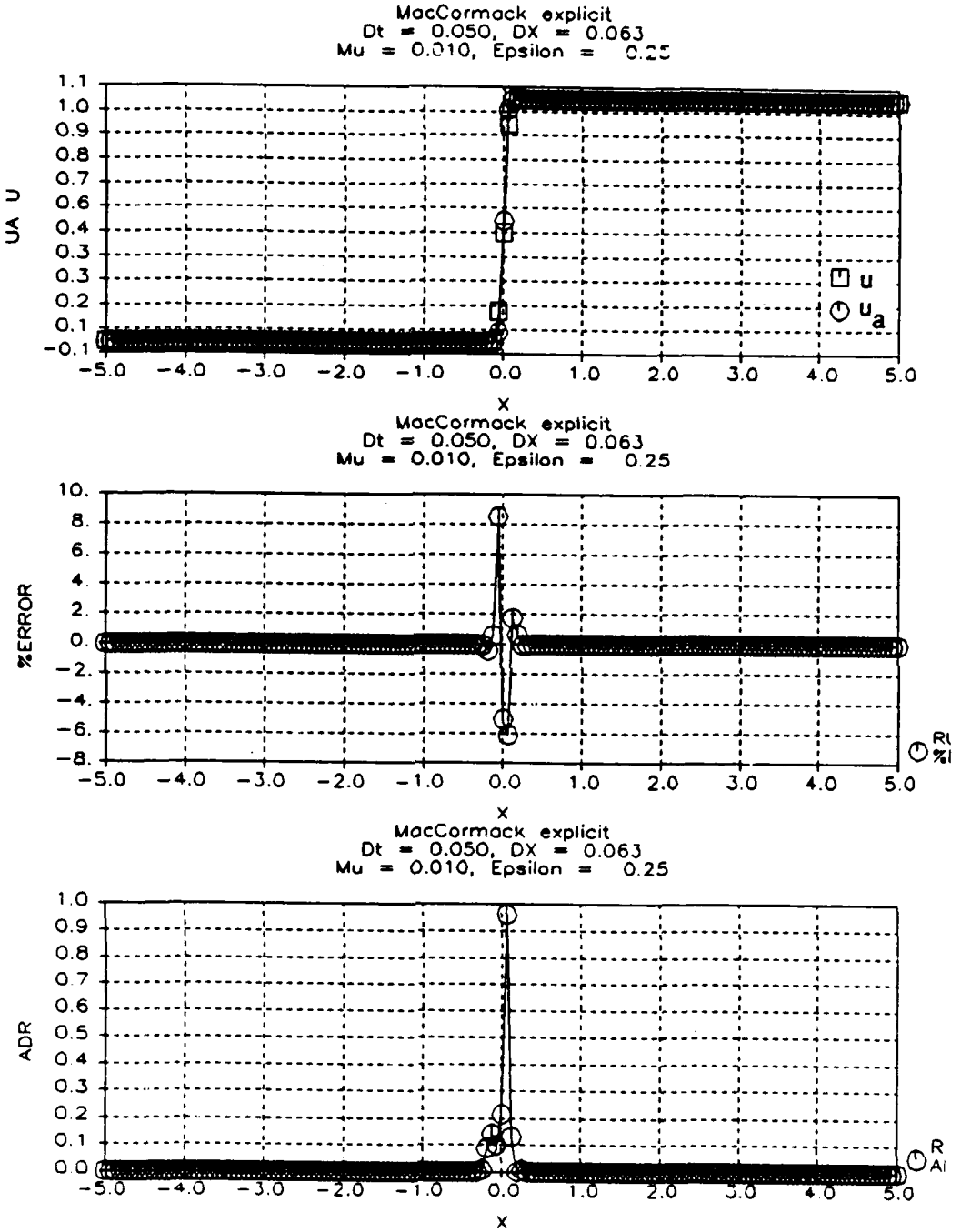

Figure C–8. MacCormack Explicit Results: Fine Grid, With Smoothing

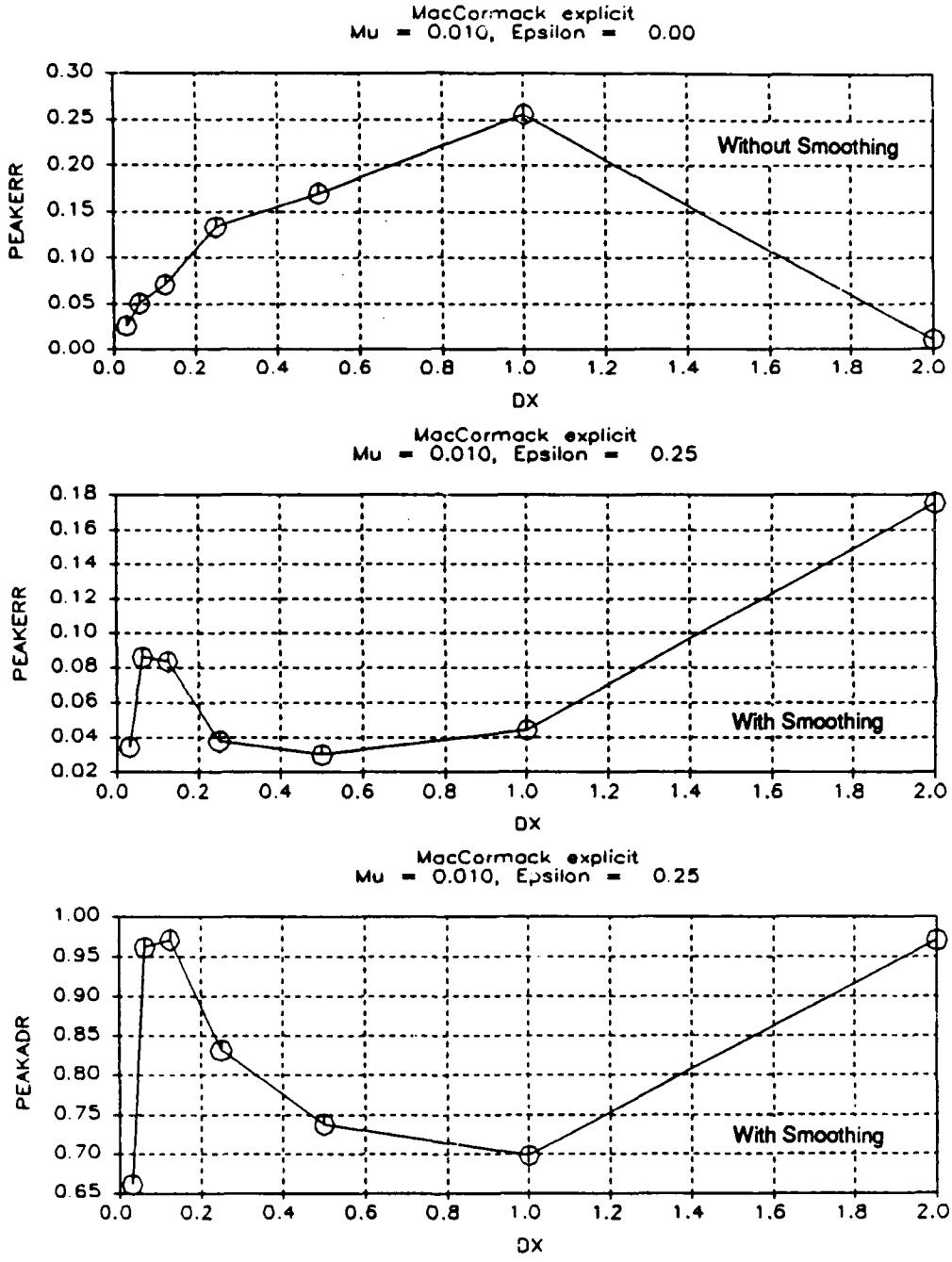

Figure C–9. MacCormack Explicit Results: Peak error and Peak ADR

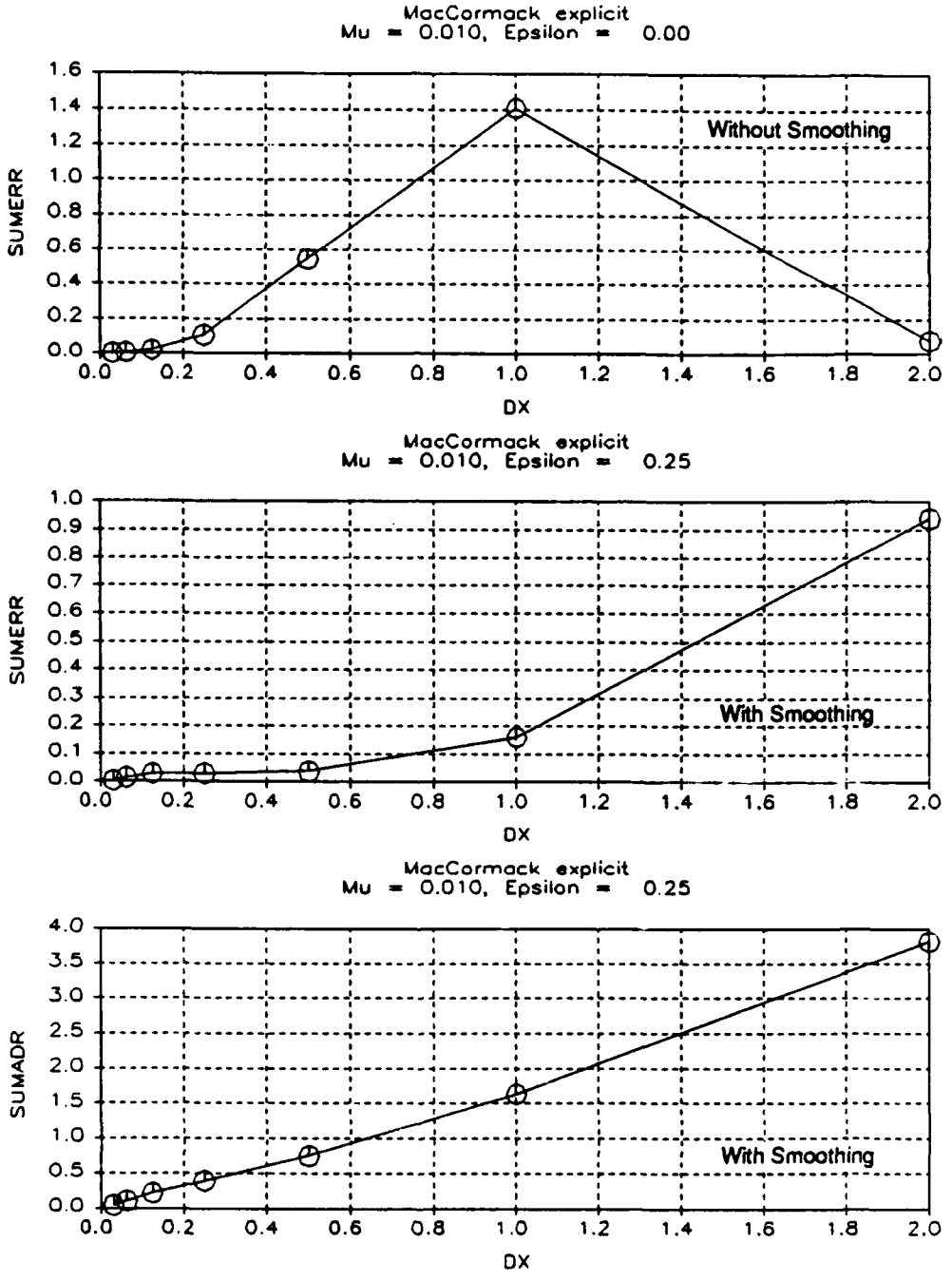

Figure C–10. MacCormack Explicit Results: Σerror and ΣADR

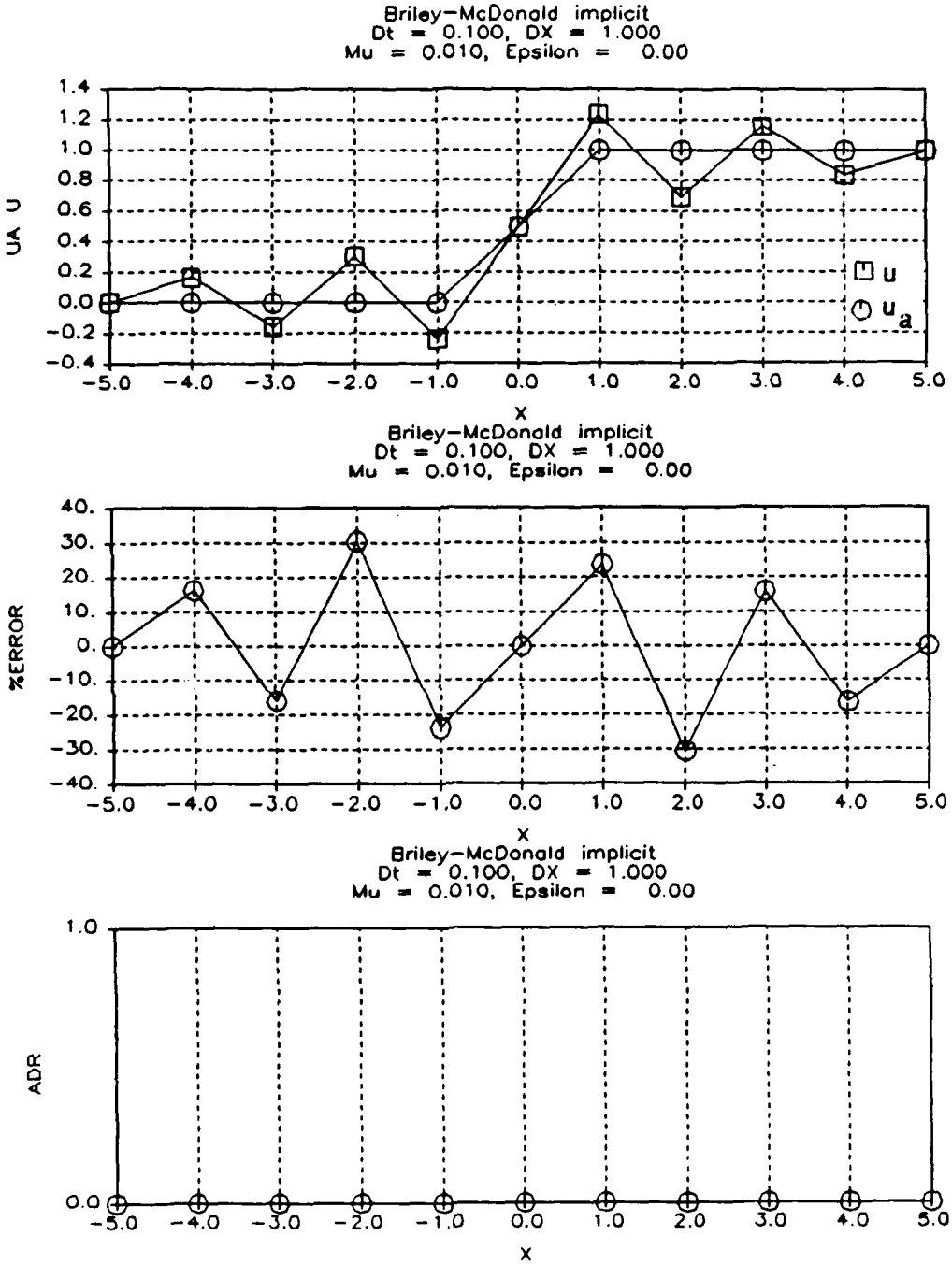

Figure C–11. Briley-McDonald Implicit Results: Coarse Grid, No Smoothing

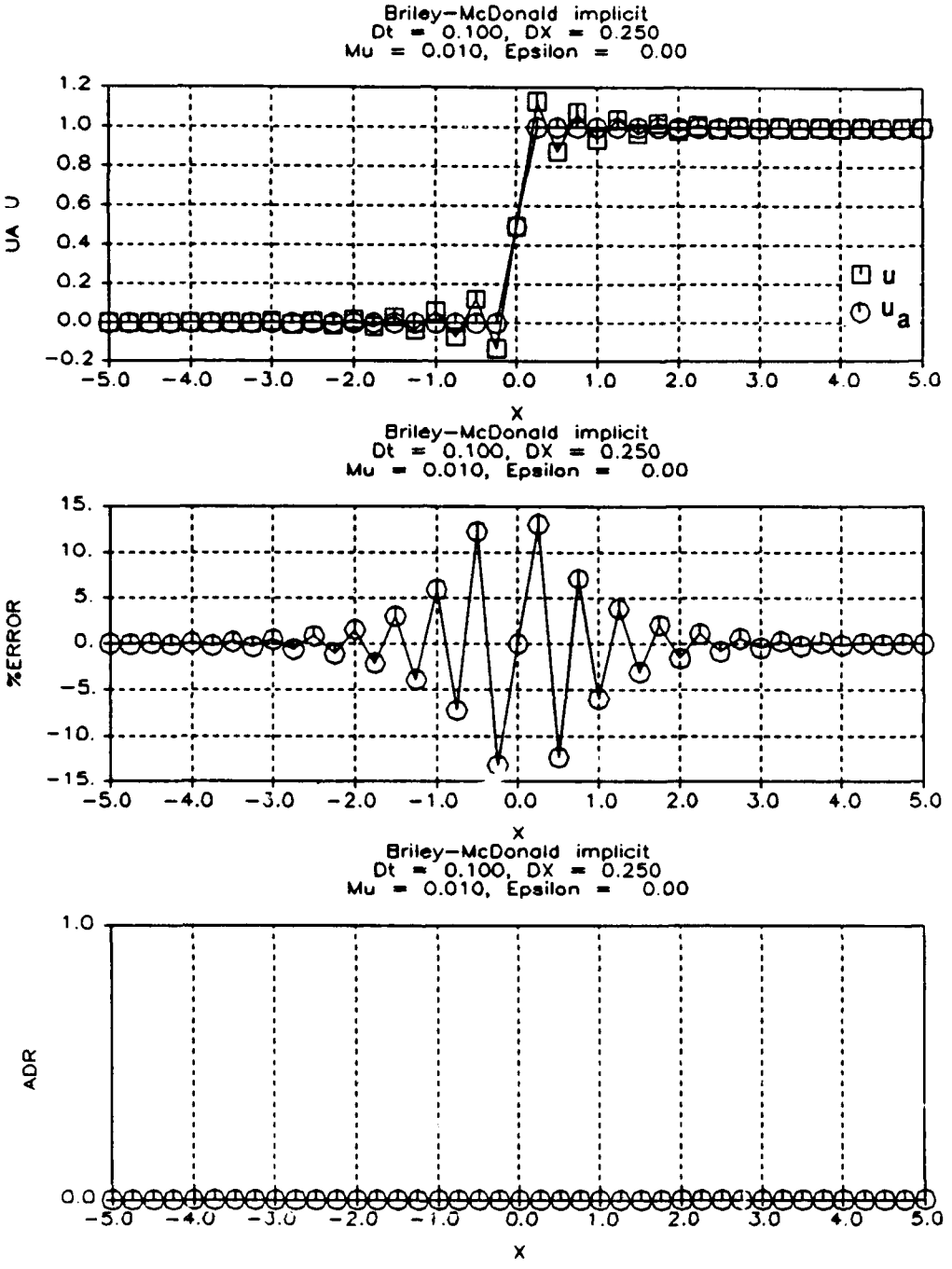

Figure C–12. Briley-McDonald Implicit Results: Medium Grid, No Smoothing

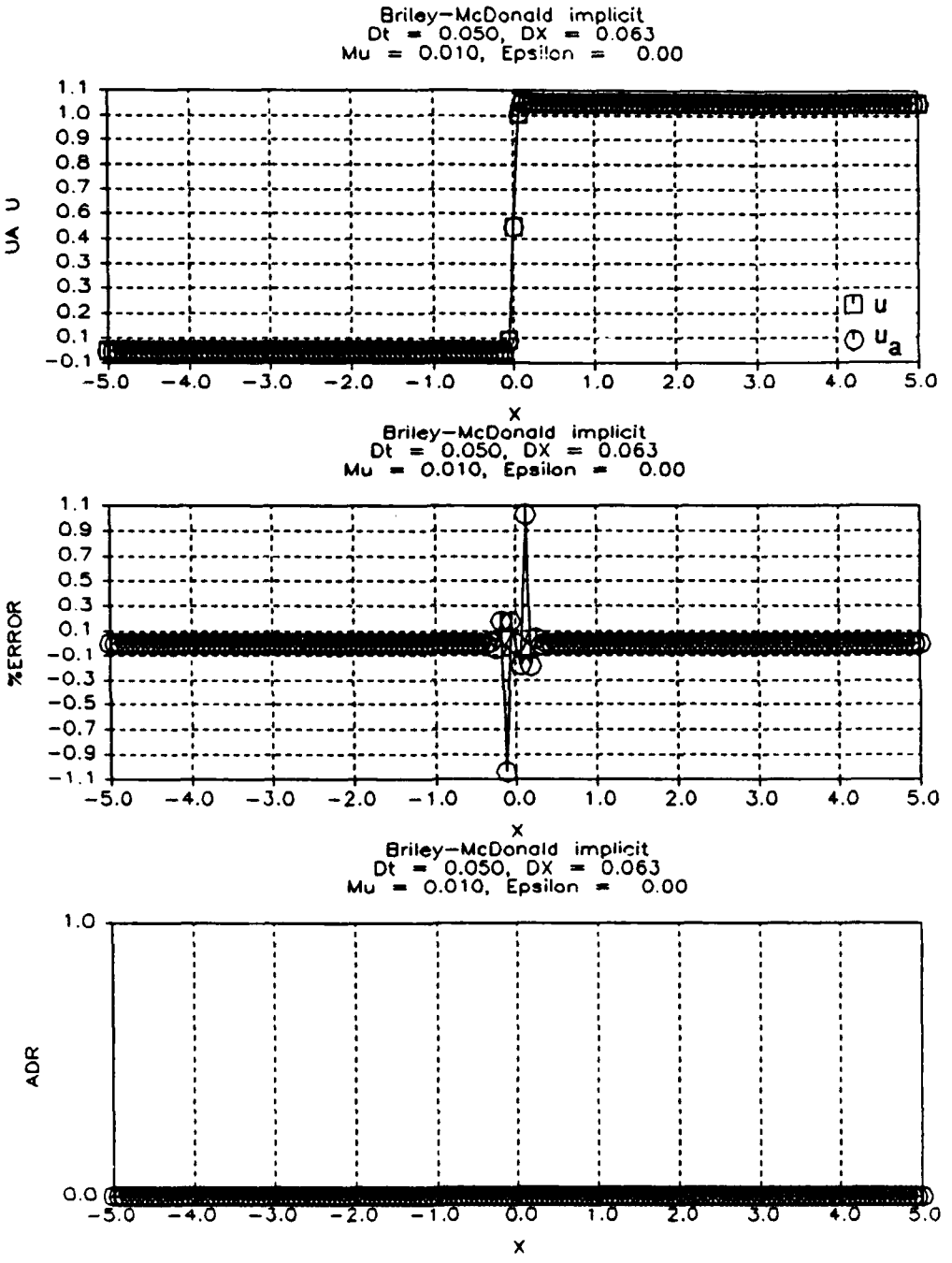

Figure C–13. Briley-McDonald Implicit Results: Fine Grid, No Smoothing

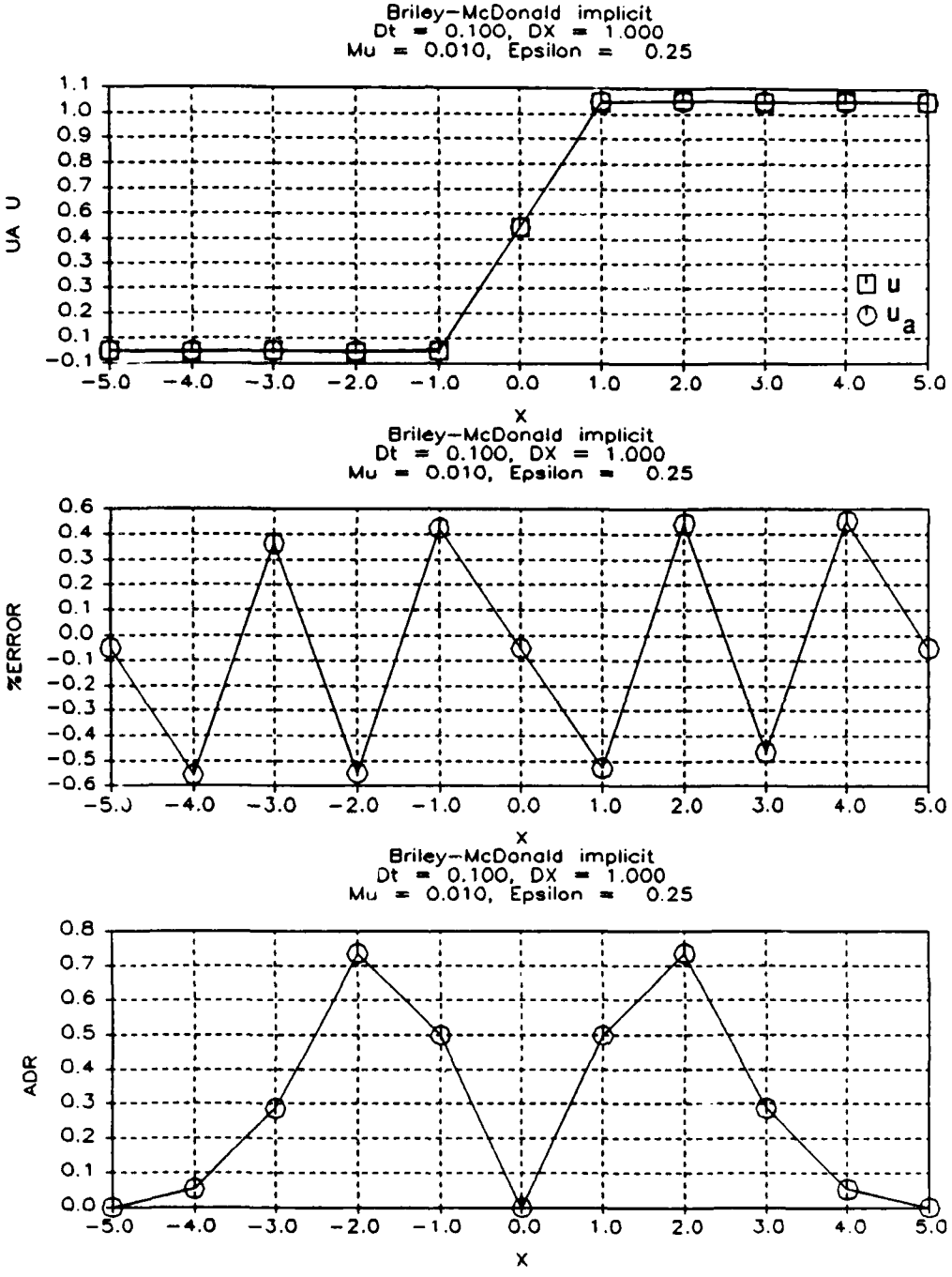

Figure C–14. Briley-McDonald Implicit Results: Coarse Grid, With Smoothing

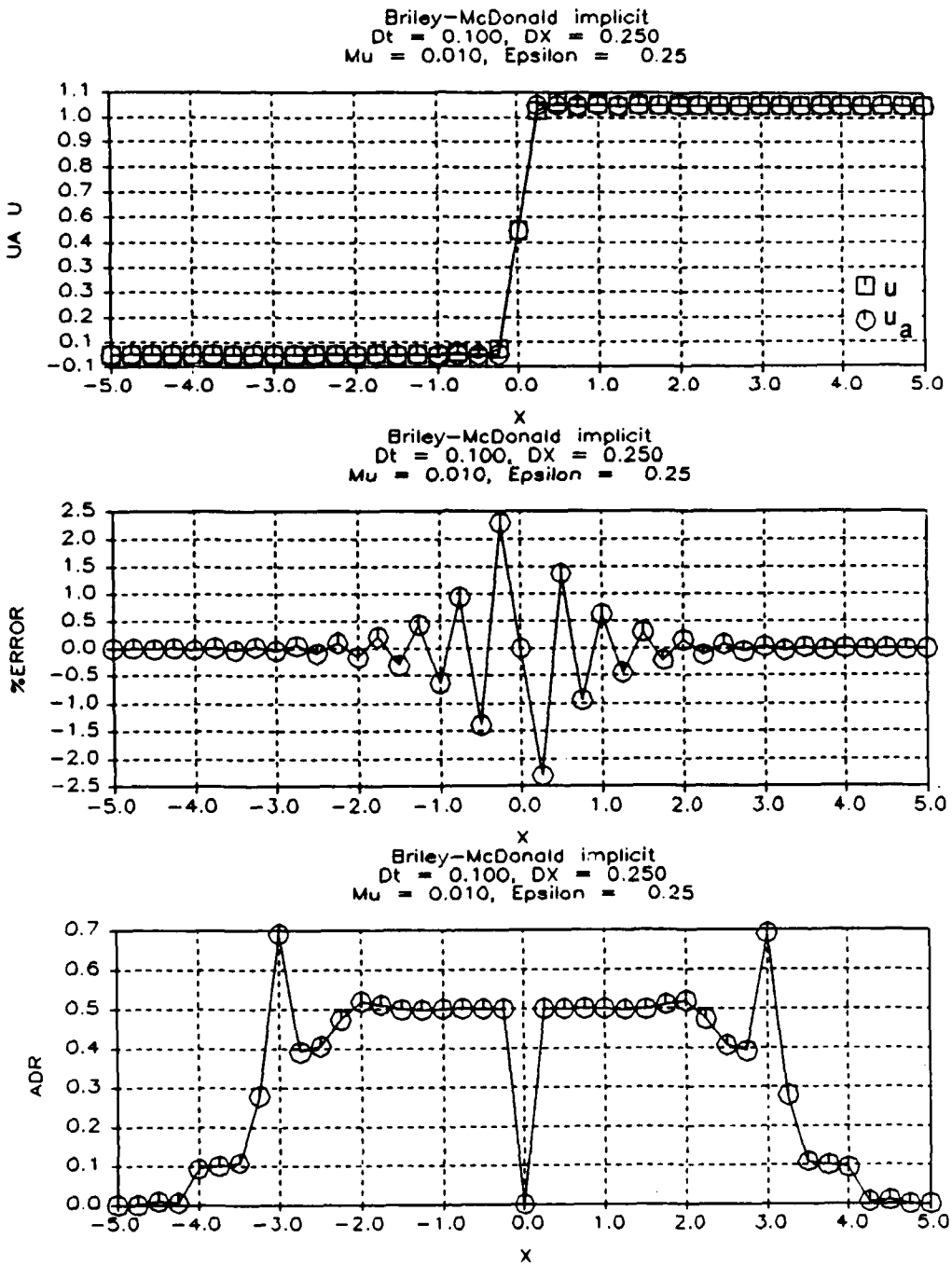

Figure C–15. Briley-McDonald Implicit Results: Medium Grid, With Smoothing

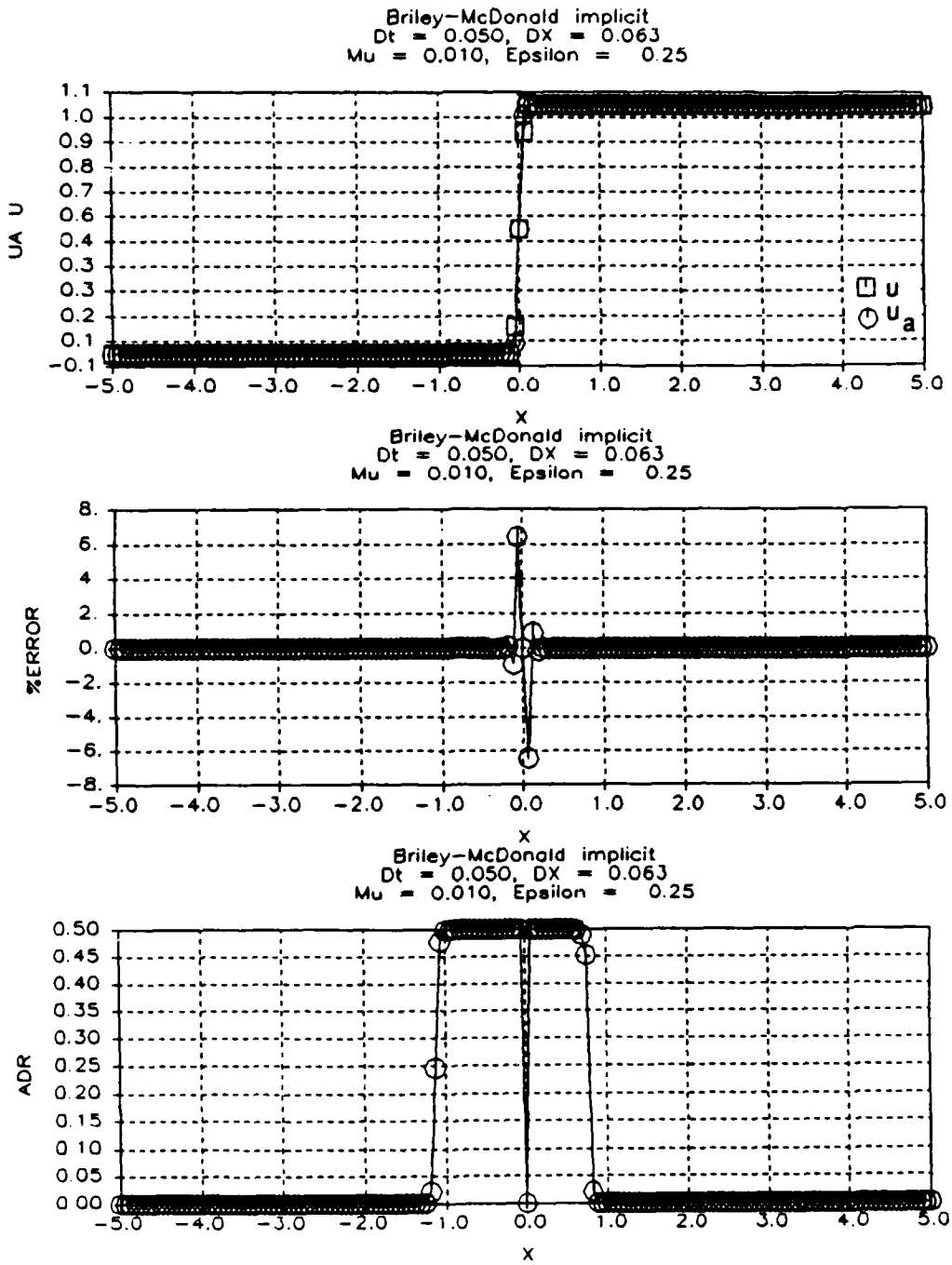

Figure C–16. Briley-McDonald Implicit Results: Fine Grid, With Smoothing

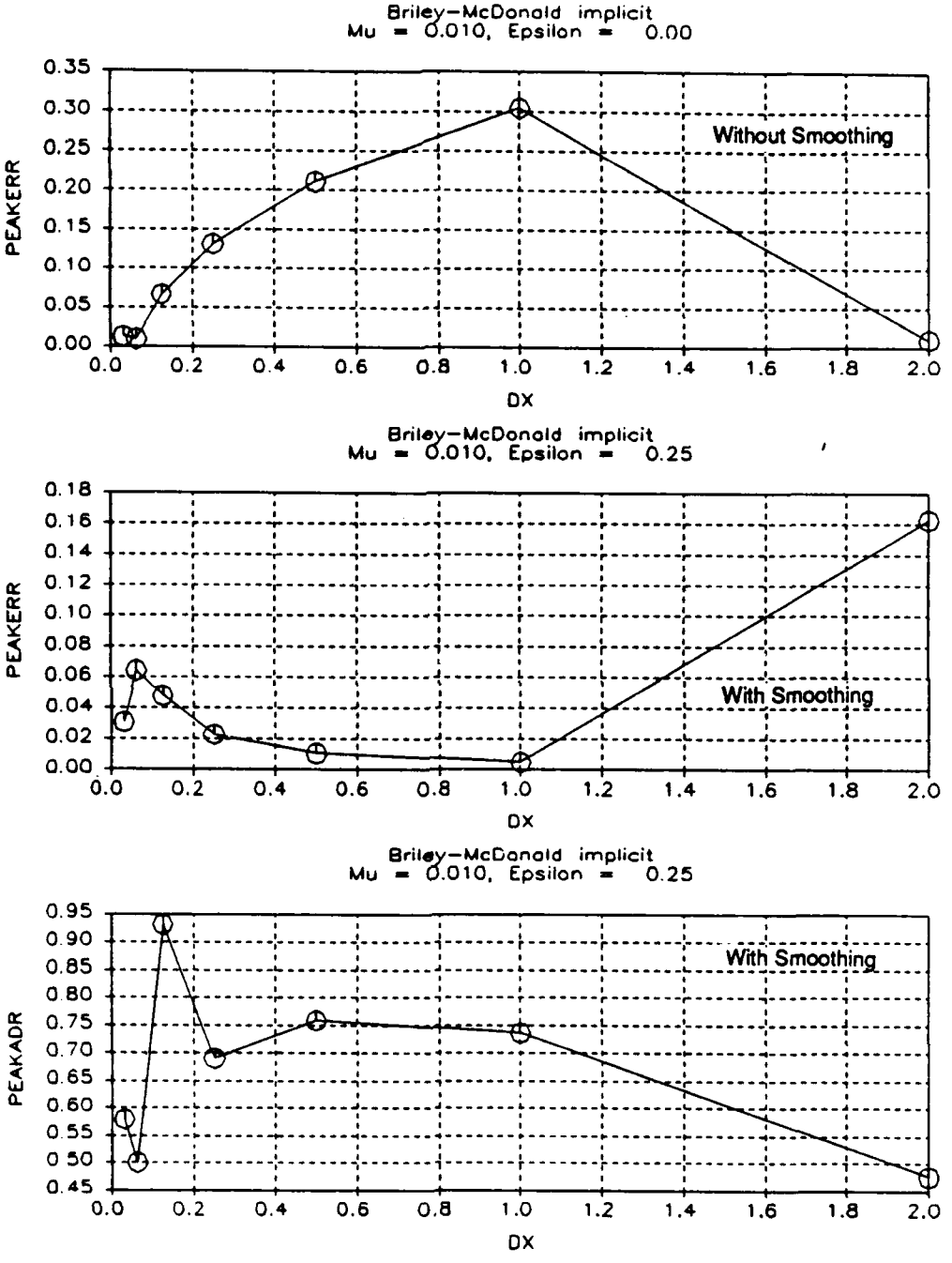

Figure C–17. Briley-McDonald Implicit Results: Peak error and Peak ADR

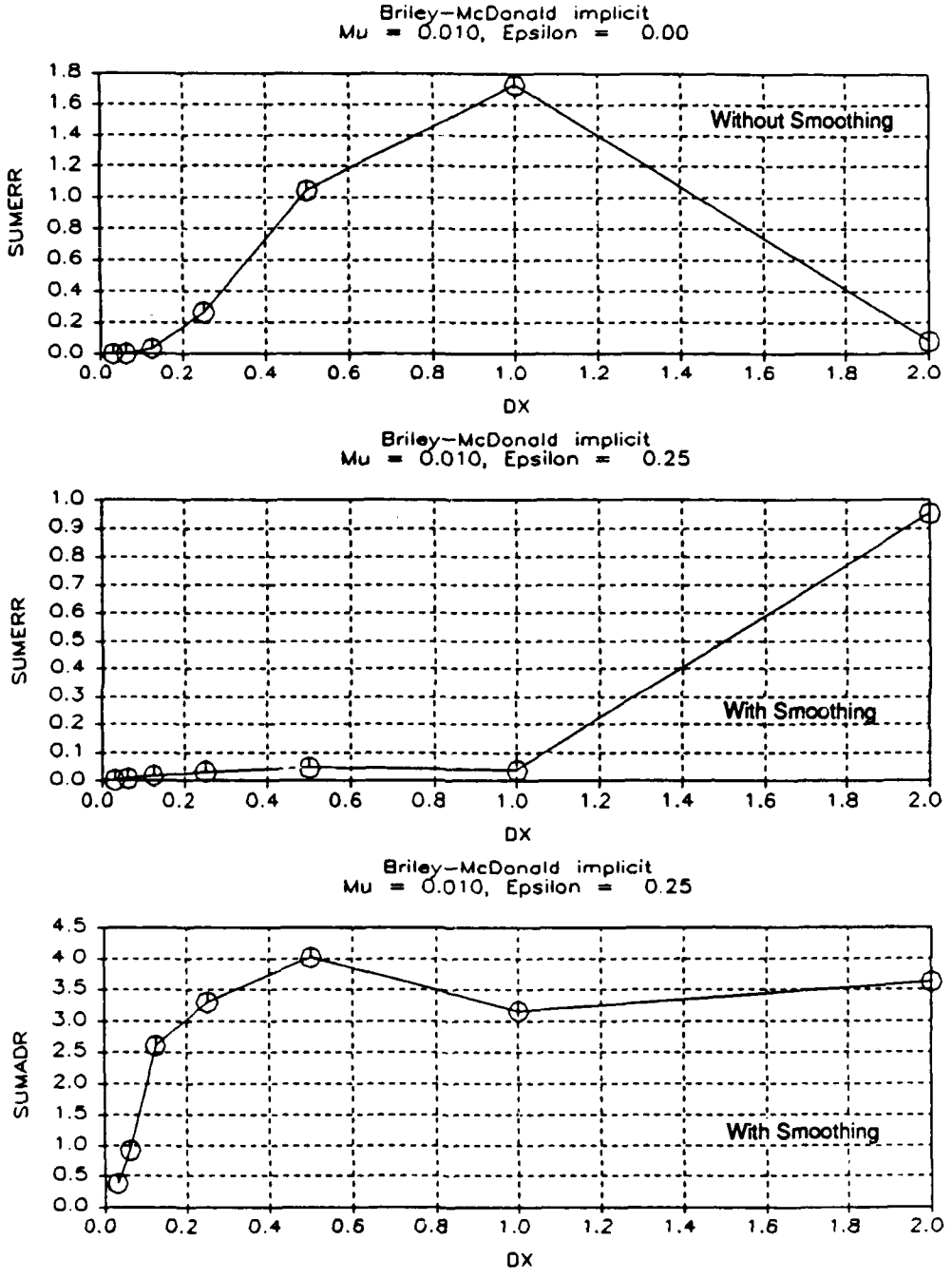

Figure C–18. Briley-McDonald Implicit Results: Σerror and ΣADR

APPENDIX D:
Source Code Listing for Burgers Equation Study

```
      PROGRAM BURGER
C**   Author: Dave Mayer
C**           Boeing Advanced Systems
C**           PO Box 3703, M/S 33-14
C**           Seattle, WA 98124
C**           (206) 241-4403

      INCLUDE 'BURGER.INC/LIST'
      IMPLICIT REAL*8 (A-H,O-Z)
      PARAMETER (MAXN=500+1, MAXI=500+1)
      COMMON /IOUNITS/
     $       LUE, LUI, LUO, LUP
      COMMON /VAR/
     $       TITLE, ISCHEME
     $     , X(MAXI), XMIN, DX, NDX, IMAX, ISKIP, XO
     $     , T(MAXN), TMIN, DT, NDT, NMAX, NSKIP
     $     , VIS, EPSILON
     $     , ADR1(MAXI,MAXN), ADR2(MAXI,MAXN), ADR3(MAXI,MAXN)
     $     , F(MAXI), A(MAXI)
     $     , PHI(MAXI,MAXN), PHIB(MAXI,MAXN)
     $     , B, C, PHIA(MAXI,MAXN)
     $     , PHII, PHIS1, PHIS2
      COMMON /STATS/
     $       AMERR(MAXN), SIGMA(MAXN), RMSERR(MAXN)
     $     , SUMPHI(MAXN), SUMERR(MAXN)
     $     , SUMADR1(MAXN), SUMADR2(MAXN), SUMADR3(MAXN)
     $     , PEAKERR(MAXN)
     $     , PEAKADR1(MAXN), PEAKADR2(MAXN), PEAKADR3(MAXN)
      CHARACTER*60 TITLE

      CALL IO
100   CALL INPUT
      CALL INIT
      CALL ANALYTIC
      IF(ISCHEME .EQ. 1) THEN
C**     Solve using MacCormack explicit procedure
        CALL MAC
      ELSE IF(ISCHEME .EQ. 2) THEN
C**     Solve using the Briley-McDonald implicit procedure
        CALL BRILEY
      ENDIF
      CALL STATS
      CALL EGG
      CALL EGGS
      CALL LP
      GO TO 100
      END
```

```
      SUBROUTINE ANALYTIC
C**   Compute the analytic solution.

      INCLUDE 'BURGER.INC'

      IF(B .EQ. -1. .AND. C .EQ. 0.5) THEN
C**     Compute analytic solution
        PI = ACOS( -1. )
        DO 300 N=1,NMAX,NSKIP
          DO 200 I=1,IMAX,ISKIP
            PHIA(I,N) = -C / B
     $                * (1. + TANH( C * ( X(I) - XO ) / (2. * VIS) ) )
200       CONTINUE
300     CONTINUE
      ENDIF
      RETURN
      END
```

```
      SUBROUTINE BRILEY
C**   Solve using the Briley-McDonald implicit solution procedure

      INCLUDE 'BURGER.INC'
      DIMENSION AA(MAXI), BB(MAXI), CC(MAXI), DD(MAXI)
      DO 400 N=1,NMAX-1
C**     Load coefficients for boundary at I=1 (Dirichlet condition)
        DD(1) = 1.
        AA(1) = 0.
        CC(1) = PHIS1
C**     Compute A and F
        DO 100 I=1,IMAX
          A(I) = C + B * PHI(I,N)
          F(I) = C * PHI(I,N) + B * PHI(I,N)**2 / 2.
100     CONTINUE
C**     Load coefficients for interior points
        CN = DT / DX
        DO 200 I=2,IMAX-1
C**       Note that the smoothing viscosity is based on lagged values
          DN = ( VIS + VISA(I,N) ) * DT / DX**2
          BB(I) = - CN / 2. * A(I-1) - DN
          DD(I) = 1. + 2. * DN
          AA(I) = CN / 2. * A(I+1) - DN
          CC(I) = ( - CN / 2. * A(I-1) ) * PHI(I-1,N)
     $          + PHI(I,N)
     $          + ( CN / 2. * A(I+1) ) * PHI(I+1,N)
     $          - CN / 2. * ( F(I+1) - F(I-1) )
200     CONTINUE
C**     Load coefficients for boundary at I=IMAX (Dirichlet condition)
        BB(IMAX) = 0.
        DD(IMAX) = 1.
        CC(IMAX) = PHIS2
        CALL TRIDIAG(1,IMAX,BB,DD,AA,CC)
        DO 300 I=1,IMAX
          PHI(I,N+1) = CC(I)
300     CONTINUE
        DO 400 I=2,IMAX-1
C**       Compute ADR
          FLUXC = 0.5 * ( F(I+1) - F(I-1)
     $                + A(I+1) * ( PHI(I+1,N+1) - PHI(I+1,N) )
     $                - A(I-1) * ( PHI(I-1,N+1) - PHI(I-1,N) ) )
          FLUXV = VIS
     $          * ( PHI(I+1,N+1) - 2.*PHI(I,N+1) + PHI(I-1,N+1) ) / DX
          FLUXS = VISA(I,N)
     $          * ( PHI(I+1,N+1) - 2.*PHI(I,N+1) + PHI(I-1,N+1) ) / DX
          ADR1(I,N+1) = ABS( FLUXS )
     $                / ( ABS( FLUXC - FLUXV ) + ABS( FLUXS ) + 1.E-24 )
          ADR2(I,N+1) = ABS( FLUXS )
     $                / ( ABS( FLUXC ) + ABS( FLUXV ) + ABS( FLUXS )
     $                  + 1.E-24 )
          ADR3(I,N+1) = ABS( FLUXS )
     $                / ( ABS( FLUXC ) + ABS( FLUXS ) + 1.E-24 )
400   CONTINUE
      RETURN
      END
```

```
      SUBROUTINE EGG
C**   Generate plot file for the Boeing Engineering Graphics
C**   Generator program.

      INCLUDE 'BURGER.INC'

      WRITE(LUE,8000)
8000  FORMAT('(F5.0,7E11.0)')
      WRITE(LUE,8005) TITLE, DT, DX
     $               , VIS, EPSILON
8005  FORMAT('*DUPT'/
     $       '$'A60/
     $       '$Dt ='F6.3', DX ='F6.3/
     $       '$Mu ='F6.3', Epsilon ='F6.2)
      DO 200 N=1,NMAX,NSKIP
        K = K + 1
        WRITE(LUE,8010) DX, SUMERR(N), SUMADR1(N)
     $                , PEAKERR(N), PEAKADR1(N)
8010    FORMAT('*PAR DX'1PE11.3/
     $         '*PAR SUMERR'E11.3/
     $         '*PAR SUMADR1'E11.3/
     $         '*PAR PEAKERR'E11.3/
     $         '*PAR PEAKADR1'E11.3)
        WRITE(LUE,8020) K
8020    FORMAT('RUN'I2)
        WRITE(LUE,8030)
8030    FORMAT(T5'I'T9'X'T20'Ua'T31'U'T42'%Error'
     $         T53'ADR1'T64'ADR2'T75'ADR3')
        DO 100 I=1,IMAX,ISKIP
          PHIMIN = PHIS1
          PHIMAX = PHIS2
          PCTERR = 100. * ( PHI(I,N) - PHIA(I,N) ) / ( PHIMAX - PHIMIN )
          WRITE(LUE,8040) I, X(I), PHIA(I,N), PHI(I,N)
     $                  , PCTERR, ADR1(I,N), ADR2(I,N), ADR3(I,N)
8040      FORMAT(I5,1P7E11.3)
100     CONTINUE
        WRITE(LUE,8050)
8050    FORMAT('*EOF')
200   CONTINUE
      RETURN
      END
```

```
      SUBROUTINE EGGS
C**   Generate plot file of statistical error measures
C**   for use with the Boeing Engineering Graphics Generator program.

      INCLUDE 'BURGER.INC'

      LU = 9
      K = K + 1
      IF( K .EQ. 1 ) THEN
        WRITE(LU,8000)
8000    FORMAT('(10E11.0)')
        WRITE(LU,8010) TITLE, VIS, EPSILON
8010    FORMAT('$'A60/
     $         '$Mu ='F6.3', Epsilon ='F6.2)
        WRITE(LU,8020)
8020    FORMAT('RUN 1')
        WRITE(LU,8030)
8030    FORMAT(T4'DX'T15'SUMPHI'T26'SUMERR'
     $         T37'SUMADR1'T48'SUMADR2'T59'SUMADR3'
     $         T70'PEAKERR'
     $         T81'PEAKADR1'T91'PEAKADR2'T102'PEAKADR3')
      ENDIF
      WRITE(LU,8040) DX, SUMPHI(NMAX), SUMERR(NMAX)
     $             , SUMADR1(NMAX), SUMADR2(NMAX), SUMADR3(NMAX)
     $             , PEAKERR(NMAX)
     $             , PEAKADR1(NMAX), PEAKADR2(NMAX), PEAKADR3(NMAX)
8040  FORMAT(1P10E11.3)
      RETURN
      END
```

```
      SUBROUTINE INIT
C**   Initialize variables

      INCLUDE 'BURGER.INC'

C**   Set indices
      NMAX = NDT + 1
      IMAX = NDX + 1

C**   Set time and space grid coordinates
      T(1) = TMIN
      DO 100 N=2,NMAX
        T(N) = T(N-1) + DT
100   CONTINUE
      X(1) = XMIN
      DO 200 I=2,IMAX
        X(I) = X(I-1) + DX
200   CONTINUE

C**   Set initial conditions
      DO 300 I=1,IMAX
        PHI(I,1) = -C / B
     $           * (1. + TANH( C * ( X(I) - XO ) / (2. * VIS) ) )
300   CONTINUE

C**   Set boundary conditions
      PHIS1 = PHI(1,1)
      PHIS2 = PHI(IMAX,1)

      RETURN
      END
```

```
      SUBROUTINE INPUT
C**   Read input data

      INCLUDE'BURGER.INC'

C**   Input values for
C**     Title,
C**     Ischeme: 1 --> MacCormack explicit
C**              2 --> Briley-MacDonald implicit
C**     Minimum value for X, Delta X, Number of Delta X, Output skip factor
C**     Minimum value for t, Delta t, Number of Delta t, Output skip factor
C**     Output skip factor
C**     Viscosity, Artificial viscosity coefficient
C**     B, C --> The coefficients in the generalized Burger's eq.
C**              Ut + (C + B * U) * Ux = VIS * Uxx

      READ(LUI,5000,END=100) TITLE
5000  FORMAT(A60)
      READ(LUI,*) ISCHEME
      READ(LUI,*) XMIN, DX, NDX, ISKIP
        XMAX = XMIN + NDX * DX
        XO = (XMAX + XMIN) / 2.
      READ(LUI,*) TMIN, DT, NDT, NSKIP
        TMAX = TMIN + NDT * DT
      READ(LUI,*) VIS, EPSILON
      READ(LUI,*) B, C
      RETURN
100   STOP 'End of input data detected'
      END
```

```
      SUBROUTINE IO
C**   Initialize logical units and files for Input/Output

      INCLUDE 'BURGER.INC'

      LUI = 5
C      OPEN(UNIT=LUI, FILE='BURGER.DAT', STATUS='UNKNOWN')
      LUO = 6
C      OPEN(UNIT=LUO, FILE='BURGER.OUT', STATUS='UNKNOWN')
      LUP = 7
C      OPEN(UNIT=LUP, FILE='BURGER.PLT', STATUS='UNKNOWN')
      LUE = 8
C      OPEN(UNIT=LUE, FILE='BURGER.GGP', STATUS='UNKNOWN')
      RETURN
      END
```

```
      SUBROUTINE LP
C**   Generate lineprinter output

      INCLUDE 'BURGER.INC'

      DO 200 N=1,NMAX,NSKIP
        WRITE(LUO,6000) TITLE
6000    FORMAT('1'/
     $         ' 'A60)
        WRITE(LUO,6010) T(N), DT, DX, VIS, EPSILON
6010    FORMAT(T5't ='1PE11.3', Dt ='E11.3', DX ='E11.3
     $           ', Mu ='E11.3', Epsilon ='E11.3)
        WRITE(LUO,6020)
6020    FORMAT(T5'I'T9'X'T20'Ua'T31'U'T42'%Error'
     $         T53'ADR1'T64'ADR2'T75'ADR3')
        DO 100 I=1,IMAX,ISKIP
          PHIMIN = PHIS1
          PHIMAX = PHIS2
          PCTERR = 100. * ( PHI(I,N) - PHIA(I,N) ) / ( PHIMAX - PHIMIN )
          WRITE(LUO,6030) I, X(I), PHIA(I,N), PHI(I,N), PCTERR
     $                  , ADR1(I,N), ADR2(I,N), ADR3(I,N)
6030      FORMAT(I5,1P7E11.3)
100     CONTINUE
        WRITE(LUO,6040) AMERR(N), SIGMA(N), RMSERR(N)
     $                , SUMERR(N), SUMADR1(N)
     $                , PEAKERR(N), PEAKADR1(N)
6040    FORMAT(T5'Arithmetic mean error ='1PE11.3
     $           ', Standard deviation ='E11.3', RMS error ='E11.3/
     $         T5'Integrated ABS(error) ='E11.3
     $           ', Integrated ADR1 ='E11.3/
     $         T5'Peak ABS(error) ='E11.3
     $           ', Peak ADR1 ='E11.3)
200   CONTINUE
      WRITE(6,6050)
6050  FORMAT('1')
      RETURN
      END
```

```
      SUBROUTINE MAC
C**   Solve using the MacCormack explicit method

      INCLUDE 'BURGER.INC'

      DO 600 N=1,NMAX-1
C**     First check stability criteria
        DO 100 I=1,IMAX
          A(I) = C + B * PHI(I,N)
          CRITERIA = DX**2 / ( ABS(A(I)) * DX + 2. * VIS )
          IF ( DT .GT. CRITERIA ) THEN
C**         Write a warning message and halt execution
            WRITE(LUO,6000) DT, CRITERIA, N, I, PHI(I,N)
6000        FORMAT(' Dt exceeds stability criteria'/
     $             ' Dt ='1PE11.3', criteria ='E11.3
     $             ', N ='I3', I ='I3', U ='E11.3)
            STOP ' Program execution stopped'
          ENDIF
100     CONTINUE

C**     Predictor step
        DO 200 I=1,IMAX
          F(I) = C * PHI(I,N) + B * PHI(I,N)**2 / 2.
200     CONTINUE
C**     Set boundary condition at I = 1 (Dirichlet condition)
        PHIB(1,N+1) = PHIS1
        DO 300 I=2,IMAX-1
C**       Solve interior points
          FLUXC = F(I+1) - F(I)
          FLUXV = VIS         * ( PHI(I+1,N) - PHI(I,N) ) / DX
     $          - VIS         * ( PHI(I,N) - PHI(I-1,N) ) / DX
          FLUXS = VISA(I+1,N) * ( PHI(I+1,N) - PHI(I,N) ) / DX
     $          - VISA(I,N)   * ( PHI(I,N) - PHI(I-1,N) ) / DX
          PHIB(I,N+1) = PHI(I,N)
     $                - DT / DX * ( FLUXC - FLUXV - FLUXS )
          ADR1(I,N+1) = ABS ( FLUXS )
     $                / ( ABS( FLUXC - FLUXV ) + ABS( FLUXS ) + 1.E-24 )
          ADR2(I,N+1) = ABS( FLUXS )
     $                / ( ABS( FLUXC ) + ABS( FLUXV ) + ABS( FLUXS )
     $                  + 1.E-24 )
          ADR3(I,N+1) = ABS ( FLUXS )
     $                / ( ABS( FLUXC ) + ABS( FLUXS ) + 1.E-24 )
300     CONTINUE
C**     Set boundary condition at I = IMAX (Dirchlet condition)
        PHIB(IMAX,N+1) = PHIS2

C**     Corrector step
        DO 400 I=1,IMAX
          F(I) = C * PHIB(I,N+1) + B * PHIB(I,N+1)**2 / 2.
400     CONTINUE
C**     Set boundary condition at I = 1 (Dirichlet condition)
        PHI(1,N+1) = PHIS1
        DO 500 I=2,IMAX-1
C**       Solve interior points
          FLUXC = F(I) - F(I-1)
          FLUXV = VIS           * ( PHIB(I+1,N+1) - PHIB(I,N+1) ) / DX
```

```
     $          - VIS           * ( PHIB(I,N+1) - PHIB(I-1,N+1) ) / DX
          FLUXS = VISB(I,N+1)   * ( PHIB(I+1,N+1) - PHIB(I,N+1) ) / DX
     $          - VISB(I-1,N+1) * ( PHIB(I,N+1) - PHIB(I-1,N+1) ) / DX
          PHI(I,N+1) = 0.5 * ( PHI(I,N) + PHIB(I,N+1)
     $               - DT / DX * ( FLUXC - FLUXV - FLUXS ))
C          ADR3(I,N+1) = ABS ( FLUXS )
C     $                / ( ABS( FLUXC - FLUXV ) + ABS( FLUXS ) + 1.E-24 )
500       CONTINUE
C**       Set boundary condition at I = IMAX (Dirchlet condition)
          PHI(IMAX,N+1) = PHIS2
600     CONTINUE
        RETURN
        END
```

```
      SUBROUTINE STATS
C**   Compute statistical error measures

      INCLUDE 'BURGER.INC'
      DIMENSION ERROR(MAXI), TMP1(MAXI), TMP2(MAXI)

      DO 400 N=1,NMAX,NSKIP
C**     Compute arithmetic mean and RMS error
        SUM1 = 0.
        SUM2 = 0.
        DO 100 I=1,IMAX
          ERROR(I) = PHI(I,N) - PHIA(I,N)
          SUM1 = SUM1 + ERROR(I)
          SUM2 = SUM2 + ERROR(I)**2
100     CONTINUE
        AMERR(N) = SUM1 / IMAX
        RMSERR(N) = SQRT( SUM2 ) / IMAX
C**     Compute variance and standard deviation of the error
        SUM3 = 0.
        DO 200 I=1,IMAX
          SUM3 = SUM3 + ( ERROR(I) - AMERR(N) )**2
200     CONTINUE
        VAR = SUM3 / IMAX
        SIGMA(N) = SQRT( VAR )
C**     Compute the integrals of the absolute error and ADR
C**     Compute the peak values of absolute error and ADR
        PEAKERR(N) = 0.
        PEAKADR1(N) = 0.
        PEAKADR2(N) = 0.
        PEAKADR3(N) = 0.
        DO 300 I=1,IMAX
          ERROR(I) = ABS( ERROR(I) )
          TMP1(I) = ABS( PHI(I,N) )
          PEAKERR(N) = MAX( ERROR(I), PEAKERR(N) )
          PEAKADR1(N) = MAX( ADR1(I,N), PEAKADR1(N) )
          PEAKADR2(N) = MAX( ADR2(I,N), PEAKADR2(N) )
          PEAKADR3(N) = MAX( ADR3(I,N), PEAKADR3(N) )
300     CONTINUE
        CALL TRAPZ(ERROR(1), IMAX, DX, SUMERR(N))
        CALL TRAPZ(TMP1(1), IMAX, DX, SUMPHI(N))
        CALL TRAPZ(ADR1(1,N), IMAX, DX, SUMADR1(N))
        CALL TRAPZ(ADR2(1,N), IMAX, DX, SUMADR2(N))
        CALL TRAPZ(ADR3(1,N), IMAX, DX, SUMADR3(N))
400   CONTINUE
      RETURN
      END
```

```
      SUBROUTINE TRAPZ(F, IMAX, DX, SUM)
C**   Perform trapezoidal rule integration of a function defined
C**   by a table of equispaced values.

C**   Parameters:
C**     F     Array of values of the function
C**     IMAX  Number of values
C**     DX    Uniform spacing between values
C**     SUM   Estimate of the integral

      IMPLICIT REAL*8 (A-H,O-Z)
      DIMENSION F(IMAX)

      SUM = 0.
      DO 100 I=1,IMAX-1
        SUM = SUM + DX / 2. * ( F(I) + F(I+1) )
100   CONTINUE
      RETURN
      END
```

```
      SUBROUTINE TRIDIAG(IL,IU,B,D,A,C)
C**   Tri-diagonal matrix solver (using the Thomas algorithm)

      IMPLICIT REAL*8 (A-H,O-Z)
      DIMENSION A(IU-IL+1), B(IU-IL+1), C(IU-IL+1), D(IU-IL+1)

C**   Reference:
C**     Anderson, DA, JC Tannehill, and RH Pletcher.  "Computaional
C**     Fluid Mechanics and Heat Transfer."  McGraw-Hill Book Company,
C**     1984.  pp. 549-550.

C**   IL = subscript of first equation
C**   IU = subscript of last equation
C**   B  = coefficient behind (to left of) diagonal
C**   D  = coefficient on diagonal
C**   A  = coefficient ahead (to right of) diagonal
C**   C  = element of constant vector (right hand side)

C**   Establish upper triangular matrix
      LP = IL + 1
      DO 100 I=LP,IU
        R = B(I) / D(I-1)
        D(I) = D(I) - R * A(I-1)
        C(I) = C(I) - R * C(I-1)
100   CONTINUE

C**   Back substitution
      C(IU) = C(IU) / D(IU)
      DO 200 I=LP,IU
        J = IU - I + IL
        C(J) = ( C(J) - A(J) * C(J+1) ) / D(J)
200   CONTINUE

C**   Solution has now been stored in C
      RETURN
      END
```

```
      FUNCTION VISA(I,N)
C**   Compute artificial viscosity due to fourth order smoothing

      INCLUDE 'BURGER.INC'

      IF( I .EQ. 1 ) THEN
C**     Use first order forward difference
        PIM1 = PHI(I,N)
        PI = PHI(I+1,N)
        PIP1 = PHI(I+2,N)
      ELSE IF( I .GT. 1 .AND. I .LT. IMAX ) THEN
C**     Use second order centered difference
        PIM1 = PHI(I-1,N)
        PI = PHI(I,N)
        PIP1 = PHI(I+1,N)
      ELSE IF( I .EQ. IMAX ) THEN
C**     Use first order backward difference
        PIM1 = PHI(I-2,N)
        PI = PHI(I-1,N)
        PIP1 = PHI(I,N)
      ENDIF
      R = 1.
C      R = ( ABS( PHI(I,N) ) + C ) / ( PIP1 + 2. * PI + PIM1 )
      VISA = EPSILON * DX * R * ABS( PIP1 - 2. * PI + PIM1 )
      RETURN
      END
```

```
      FUNCTION VISB(I,N)
C**   Compute artificial viscosity due to fourth order smoothing

      INCLUDE 'BURGER.INC'

      IF( I .EQ. 1 ) THEN
C**     Use first order forward difference
        PIM1 = PHIB(I,N)
        PI = PHIB(I+1,N)
        PIP1 = PHIB(I+2,N)
      ELSE IF( I .GT. 1 .AND. I .LT. IMAX ) THEN
C**     Use second order centered difference
        PIM1 = PHIB(I-1,N)
        PI = PHIB(I,N)
        PIP1 = PHIB(I+1,N)
      ELSE IF( I .EQ. IMAX ) THEN
C**     Use first order backward difference
        PIM1 = PHIB(I-2,N)
        PI = PHIB(I-1,N)
        PIP1 = PHIB(I,N)
      ENDIF
      R = 1.
C      R = ( ABS( PHIB(I,N) ) + C ) / ( PIP1 + 2. * PI + PIM1 )
      VISB = EPSILON * DX * R * ABS( PIP1 - 2. * PI + PIM1 )
      RETURN
      END
```